



**HAL**  
open science

## Resveratrol-mediated glycemic regulation is blunted by curcumin and is associated to modulation of gut microbiota

Navin Sreng, Serge Champion, Jean-Charles Martin, Saber Khelaifia, Jeffrey Christensen, Roshan Padmanabhan, Vincent Azalbert, Vincent Blasco-Baque, Pascale Loubières, Laurent Pechere, et al.

### ► To cite this version:

Navin Sreng, Serge Champion, Jean-Charles Martin, Saber Khelaifia, Jeffrey Christensen, et al. Resveratrol-mediated glycemic regulation is blunted by curcumin and is associated to modulation of gut microbiota. *Journal of Nutritional Biochemistry*, 2019, 72, pp.108218. 10.1016/j.jnutbio.2019.108218 . hal-02487542

HAL Id: hal-02487542

<https://amu.hal.science/hal-02487542>

Submitted on 20 Jul 2022

**HAL** is a multi-disciplinary open access archive for the deposit and dissemination of scientific research documents, whether they are published or not. The documents may come from teaching and research institutions in France or abroad, or from public or private research centers.

L'archive ouverte pluridisciplinaire **HAL**, est destinée au dépôt et à la diffusion de documents scientifiques de niveau recherche, publiés ou non, émanant des établissements d'enseignement et de recherche français ou étrangers, des laboratoires publics ou privés.



Distributed under a Creative Commons Attribution - NonCommercial 4.0 International License

**Resveratrol-mediated glyceic regulation is blunted by curcumin and is associated to modulation of gut microbiota.**

**Navin Sreng<sup>1,2,3</sup>, Serge Champion<sup>4</sup>, Jean-Charles Martin<sup>3</sup>, Saber Khelaifia<sup>5</sup>, Jeffrey E. Christensen<sup>1,2,6</sup>, Roshan Padmanabhan<sup>1,2</sup>, Vincent Azalbert<sup>1,2</sup>, Vincent Blasco-Baque<sup>1,2</sup>, Pascale Loubieres<sup>1,2</sup>, Laurent Pechere<sup>7</sup>, Jean-François Landrier<sup>3,§</sup>, Rémy Burcelin<sup>1,2,§,#</sup>, and Eric Séréé<sup>3,§,#</sup>**

<sup>1</sup>Institut National de la Santé et de la Recherche Médicale (INSERM), Toulouse, France.

<sup>2</sup>Université Paul Sabatier (UPS), Unité Mixte de Recherche (UMR) 1048, Institut des Maladies Métaboliques et Cardiovasculaires (I2MC), Team 2 : 'Intestinal Risk Factors, Diabetes, Dyslipidemia, Heart Failure' F-31432 Toulouse Cedex 4, France.

<sup>3</sup>Aix Marseille Univ, INSERM, INRA, C2VN, Marseille, France

<sup>4</sup>IMBE-UMR CNRS 7263/IRD 237, Mutagenèse Environnementale, Faculté de Pharmacie, Aix-Marseille Université, 27 boulevard Jean Moulin, 13385 Marseille, France

<sup>5</sup>Unité de Recherche sur les Maladies Infectieuses et Tropicales Emergentes, UM 63, CNRS 7278, L'Institut de Recherche pour le Développement 198, Inserm 1095, Institut Hospitalo-Universitaire Méditerranée-Infection, Faculté de Médecine, Aix-Marseille Université, 27 Boulevard Jean Moulin, 13385 Marseille Cedex 5, France

<sup>6</sup>VAIOMER SAS, 516 Rue Pierre et Marie Curie, 31670 Labège, France

<sup>7</sup>Laboratoire YVERY sarl, 134 rue Edmond Rostand, 13008 Marseille, France

<sup>§</sup> These three authors equally contributed to the manuscript.

<sup>#</sup> Corresponding authors: [sereee.eric@gmail.com](mailto:sereee.eric@gmail.com) and [remy.burcelin@inserm.fr](mailto:remy.burcelin@inserm.fr)

Telephone: +33 05 61 32 56 14

## **Abstract**

The polyphenols resveratrol (RSV) and curcumin (Cur) are phytoalexins and natural antibiotics with numerous pharmacological functions and metabolic impacts. Recent evidences show a broad control of gut microbiota by polyphenols which could influence glycemic regulation. The aim of this work is to estimate the respective effect of resveratrol (RSV) and curcumin (Cur) alone or in association on the control of glycaemia and on gut microbiota. A five-week chronic treatment of hyperglycemic mice with RSV and/or Cur, resulted in a differential effect on glucose tolerance test, and modified gut microbiome. We precisely identified groups of bacteria representing a specific signature of the glycemic effect of RSV. Inferred metagenomic analysis and metabolic pathway prediction showed that the sulfur and branched chain amino-acid (BCAA) metabolic activities are tightly correlated with the efficacy of RSV for the control of glycaemia. The impact on BCAA metabolism was further validated by serum metabolomics analysis. Altogether, we show that polyphenols specifically impact gut microbiota and corresponding metabolic functions which could be responsible for their therapeutic role.

## Introduction

Dietary polyphenols have been of great interest in recent decades due to their therapeutic activities. Resveratrol (3,5,4'-trihydroxy-*trans*-stilbene; RSV) and Curcumin (1,7-bis-(4-hydroxy-3-methoxyphenyl)-hepta-1,6-diene-3,5-dione; Cur) are natural polyphenols which have numerous pharmacological properties. RSV is a phytoalexin with anti-inflammatory activity that is found in various plants, such as grape skin [1]. This anti-inflammatory activity of RSV is supportive of a role in the control of disease where the etiology involves an inflammatory process. Indeed, low grade chronic inflammation is characteristic of the etiology of for metabolic diseases such as diabetes and obesity [2]. In response to a prolonged period of fat-enriched diet, the metabolic organs, liver, adipose, and pancreatic islets are infiltrated by immune cells such as macrophages and lymphocytes [3]. These cells secrete cytokines which inhibit insulin secretion and action and, leading to obesity and type 2 diabetes (T2D). A leading hypothesis regarding the origin of inflammation in metabolic disease is the gut microbiota [4]. Type 2 diabetic patients [5] and high-fat diet-fed mice [6] are characterized by a gut microbiota dysbiosis which is causal to the disease as demonstrated in gut microbiota transfer to germ free mice [6]. One of the corresponding mechanisms is the gastrointestinal translocation of bacterial components from the gut, across the intestinal epithelial barrier, to the tissues. Bacterial fragments such as lipopolysaccharides [7], and even full bacteria [8], can trigger the proliferation of macrophages and preadipocytes within the tissues leading to a chronic inflammation [4]. This translocation process is due to an impaired intestinal immune defense [6]. Therefore, control of metabolic inflammation by targeting the intestinal inflammatory activity could be a therapeutic strategy for metabolic diseases. Whether polyphenols are involved in this mechanism remains unknown, but the possibility is supported by published data. Indeed, RSV controls gut microbiota in different animal models such as dextran sulfate sodium-induced colitis [9] or in response to a fat-enriched diet [10-12], and even in humans [13]. As a result of the modulation of gut microbiota dysbiosis, insulin secretion and sensitivity were improved and hyperglycemia was corrected [14, 15]. Other polyphenols such as Cur, an extract of *Curcuma longa*, have shown similar health benefits such as anti-infectious, anti-tumor, and anti-inflammation effects [16]. The anti-inflammatory effect of Cur has been demonstrated in several cell type, and in different physiopathological context, including type 2 diabetes [17]. Altogether there is a need to precisely study changes

in gut microbiota in response to different polyphenols in order to decipher the specific changes, notably in terms of metabolic activities, which could be at play in the control of glycaemia.

To this aim a cohort of mice was fed a high-fat diet to induce hyperglycemia, and were treated with polyphenols alone or in combination to evaluate their impact on gut microbiota and correlate metagenomics parameters with glycaemia. Importantly, we aimed at isolating the impact of hyperglycemia from the impact on body weight change, and therefore used a dedicated fat-enriched diet as described [18, 19]. We aimed at studying the impact of polyphenols on microbiota and the subsequent effect on glycaemia, rather than the impact of a drastic glycemic change on gut microbiota. Therefore, we studied the effect polyphenol treatments on early onset glycemic conditions. We show that the polyphenols specifically affect gut microbiota, and notably sulfur and branched chain amino-acid metabolic pathways, which correlate with glycaemia. Serum metabolomic analyses further supported this result.

## **Materials and methods**

### **1. Polyphenol formulation**

The RSV (Omnipharm, Chambéry, France) and Cur (Omnipharm, Chambéry, France) were mixed at the dose of 60mg/Kg/day and 30mg/Kg/day, respectively, with a specific formulation (Yvery, Marseille, France). This formulation contains 100mg of RSV and 50mg of Cur with 125 mg of polysorbate 20 (Sigma, France) and 2.25g of polyglyceryl-3Diolate (Sigma, France) as described [20]. This formulation enables the polyphenols to be absorbed with a 10 time increased efficacy and to last up to 5 hours into the blood [20]. The RSV, Cur or RSV and Cur within their formulation were daily mixed with the High-fat Diet (HFD) diet.

### **2. Animals and treatments**

Eight week-old male C57Bl/6J wild type mice (Charles River, L'Arbresle, France) were housed in SOPF (Specific and Opportunistic Pathogen Free) conditions with a 12-/12-hour light (10 p.m.)/dark (10 a.m.) cycle and had free access to water and food. After one week of acclimatization, mice were divided to five groups. One group (n=7) was maintained on normal chow diet (NC, energy content: 12% fat, 28% protein, and 60% carbohydrate) and another group (n=8) was fed a high-fat diet (HFD, energy content: roughly 72% fat comprising corn oil and lard, 28% protein, and <1% carbohydrate, SAFE, Augy, France). Additional groups of HFD-fed mice (n=8 per group) were supplemented with RSV, Cur, or both. Mice were maintained on these diets for five weeks. The high-fat diet was used specifically to induce hyperglycemia for study at early onset of diabetes, and therefore considered pre-diabetic. This procedure prevented from the direct effect of hyperglycemic control which could secondarily impact gut microbiota. This time course allows changes in gut microbiota before the development of long term chronic disease where gut microbiota dysbiosis could be a secondary effect to metabolic impairments. Altogether, gut microbiota dysbiosis occurs within less than 4 weeks, i.e. before the onset of obesity, which allows the study of a direct effect of the polyphenols on the regulation of glycemia without the confounding impact of obesity, as described in numerous instances [6, 8, 18]. All animal experimental procedures were approved by the local animal ethical committee of the Ranguel hospital under the

authorization number '31-278' and were in accordance with the institutional animal care and use committee guidelines.

#### ***Oral glucose tolerance test***

An oral glucose tolerance test (OGTT, 2g/kg of glucose) was performed in 6h-fasted mice after five weeks of treatment as described [6].

#### ***Statistical Analyses***

Results are presented as means  $\pm$  SEM. One-way ANOVA followed by Tukey-Kramer post-test was used to assess the statistical significance between groups. A two-sided p-value  $<0.05$  was considered statistically significant. Statistical analyses were performed using GraphPad Prism version 6.0g for Mac OS X (GraphPad Software, San Diego, CA).

### **3. Analysis of the microbiota**

#### ***DNA extraction and 16S rDNA targeted metagenomic sequencing***

The bacterial population present in the samples has been determined using next generation high throughput sequencing of variable regions of the 16S rRNA bacterial gene, with a specific protocol established by Vaiomer. The metagenomics workflow was used to classify organisms from a metagenomic sample by amplifying specific regions in the 16S ribosomal RNA gene and was exclusive to bacteria. Total DNA bacteria from the ceacum was extracted, as previously described [21]. The V3-V4 hyper-variable regions of the 16S rDNA gene were amplified from the DNA extracts during a first PCR step using Vaiomer universal 16S primers V2 [21]. The joint pair length was set to encompass 476 base pairs amplicon and included specificity for the 16S rDNA gene of 95% of the bacteria in the Ribosomal Database Project. For each sample, a sequencing library was generated by addition of sequencing adapters and multiplexing indexes during a second PCR step. The pool was denatured, diluted and loaded onto the Illumina MiSeq cartridge according to the manufacturer's instructions using MiSeq Reagent Kit v3 (2x300 bp Paired-End Reads). (Illumina, San Diego, CA, USA).

#### ***Bioinformatic analyses of metagenomics data***

The targeted metagenomic sequences from microbiota were analyzed using the bioinformatics pipeline established by Vaiomer [21]. After demultiplexing of the bar coded Illumina paired reads, single read sequences were cleaned and paired for each sample independently into longer fragments. After alignment against a 16S reference database, sequences were clustered into operational taxonomic units (OTU) with a 97% identity threshold. Remaining sequencing errors were filtered out by eliminating the OTU with less than 3 sequences, and a taxonomic assignment was performed in order to determine community taxonomic profiles against the RDP database using the RDP Classifier tool. To estimate individual sample microbial alpha diversity, rarefaction curves were generated based on metrics and the number of OTUs present in the samples was determined (Shannon diversity index). t-Distributed Stochastic Neighbor Embedding (t-SNE) was used for dimensionality reduction for the visualization of the OTU dietary group datasets.

### ***Differential analysis of bacterial taxa and inferred metagenomics***

The taxonomic output matrix containing the count data for OTUs per sample was processed with the online Galaxy interface for LEfSe (linear discriminant analysis effect size) algorithm using an alpha parameter significance threshold for the Kruskal-Wallis (KW) test among classes set to 0.05 and the logarithmic LDA score cut-off was set to 2.0 [22]. The functional metagenome was inferred from the clustered 16S sequences using the PICRUSt software (version 1.0.0) as per the instructions provided for the Genome Prediction Tutorial for PICRUSt ([http://picrust.github.io/picrust/tutorials/genome\\_prediction.html#genome-prediction-tutorial](http://picrust.github.io/picrust/tutorials/genome_prediction.html#genome-prediction-tutorial)) with recommended scripts and default settings. As described in the PICRUSt tutorial, the sequences previously grouped into OTU were processed through the QIIME closed reference OTU picking tool with a 97% similarity threshold to obtain a set of OTU IDs from the Greengenes reference collection (gg\_otus\_13\_5.tar.gz) as input for prediction of corresponding metagenomes by PICRUSt. Through this inference process, the abundance values of each OTU were normalized to their respective predicted 16S rRNA copy numbers and then multiplied by the respective gene counts for metagenome prediction. The resulting core output was a list of Kyoto Encyclopedia of Genes and Genomes (KEGG) orthologues and predicted gene count data for each sample. We used in house scripts to parse the output into KEGG module categories for functional pathways and structural complex hierarchies using the KEGG database (<http://www.genome.jp/kegg/module.html>). The output matrix

containing the relative abundance of KEGG orthologous groups (KO) per sample was processed with the online Galaxy interface for LEfSe using an alpha parameter significance threshold for the Kruskal-Wallis (KW) test among classes set to 0.05 and the logarithmic LDA score cut-off was set to 2.0. Respective cladograms were generated with modules at the lowest level. Quantitative plots of differential features were generated from normalized module level predicted gene data showing means with standard deviation using GraphPad Prism 6 software (GraphPad Software, La Jolla, CA, USA).

### ***Statistical Analyses***

For statistical analyses of gut microbiota related data, nonparametric Mann-Whitney tests and nonparametric Kruskal-Wallis tests followed by Dunn's multiple comparison tests and Spearman's correlations were conducted using computer software (PRISM, Version 6.05, GraphPad, Inc., La Jolla, CA) and a software environment (R, Version 3.1.2, <https://cran.r-project.org/bin/windows/base/old/3.1.2/>).

### ***Denaturing gradient gel electrophoresis (DGGE)***

Total DNA was isolated from caecum was amplified by PCR, targeting the V3 region of the 16S rRNA gene using the universal bacterial primers HDA1-GC and HDA2 (**Supplementary Table 1**) as described <sup>13</sup>.

### ***Bacterial culture***

Seven bacterial strains chosen from 16S rDNA analyses were included in this study: *Alistipes shahii*, *Alistipes putredinis*, *Bacteroides fragilis*, *Bacteroides irregular*, *Clostridium butiricum*, *Clostridium nordii*, and *Odoribacter splanchnicus*. All strains were cultured using a 5% sheep blood-enriched Columbia agar (COS) and incubated 48-hours at 37°C in anaerobic condition generated by GENbag anaer systems (BioMérieux).

### ***In vitro bacterial sensitivity to polyphenol***

The in vitro susceptibility testing of RSV and Cur against clinical strains of *Alistipes shahii*, *Alistipes putredinis*, *Bacteroides fragilis*, *Bacteroides irregular*, *Clostridium butiricum*, *Clostridium nordii*, and *Odoribacter splanchnicus* was performed on Mueller-Hinton-2 agar by diffusion method as previously described [23] by depositing following solutions: 100 µM of RSV, 50 µM Cur, or 100 µM RSV + 50 µM of Cur solutions in a 0.5 mm diameter well dug into the MH2 agar medium. Beforehand, 1mL of bacterial suspension calibrated at  $10 \times 10^7$  cells / mL was spread on agar to obtain a homogeneous bacterial culture. All petri dishes were incubated in an

anaerobic condition for 48 h at 37°C. The diameters of the zones of growth inhibition for the tested bacteria were measured and photographed using a Scan 1200 (Interscience, St-Nom-la-Bretèche, France) to determine the antimicrobial activity of RSV, Cur or RSV+Cur.

#### **4. Analysis of the metabolites in plasma**

##### ***Plasma sample processing***

Ten µL of plasma aliquoted from each sample were mixed to set the quality control (QC) samples and prepared as previously described [24]. Briefly, after drying under a stream of nitrogen, the protein free methanol extract was derivatized with O-methoxylamine hydro-chloride in pyridine. Then, index marker solution was added (0.3 mg mL<sup>-1</sup> docosane, nonadecane, decane, dodecane, and pentadecane in pyridine) prior to centrifugation at 15,800g for 15 min. The resulting supernatant (90µL) was immediately transferred to GC/MS vials for analysis to prevent any sample decay.

##### ***GC/MS***

Analyses were carried out on a Agilent gas-chromatography 6890-mass spectrometer 5973N fitted with a split/splitless injector, connected to HP5 column, 30 m length, 0.25 mm ID and 0.25µm film thickness. The injector was set at 260°C in splitless mode. The analytes were eluted using a temperature gradient (injection at 50°C, +10°C/min to 70°C, 2 min hold, +5°C/min to 110°C, +30°C/min to 290°C, and +20°C/min to 325°C). The mass spectrometer interface was heated at 300°C and the electron impact ionization was performed at 70eV at 230°C. Data was acquired at 2.8 scan/min.

##### ***Data post-processing***

MS files were processed by the Shimadzu GCMS postrun analysis® software. During runs the intensity values were normalized to tryptophan-d4 or cholesterol-d4 added as internal standard as previously described [25]. The web interface Workflow4Metabolomics was then used to extract results [26]. MS features displaying more than 30% of relative standard deviation in the QC samples were discarded, resulting in retention of 60 different features. Metabolite annotation was performed using the National Institute of Standards and Technology (NIST) and Gölm databases for fragment matching patterns and ECLs.

### ***Statistics for metabolomics***

Statistical analyses were performed using SIMCA P+12 (Umetrics, Umea, Sweden). Partial least square-discriminant analyses (PLS-DA) were used to calculate the statistical distance among the study group metabolomes and to select the most relevant variables attached to group discrimination [27]. After PLD-DA, variables selection was performed on the variable importance in projection (VIP) score calculated by the SIMCA algorithm, plotted in a normal probability plot distribution and selected with 80% confidence interval. For all statistical significant PLS-DA models, the P values obtained after variables selection and cross-validation ANOVA were lower than 0.001, with a low residual (regression/residual less than 4), a class variance explained (R2Y) over 88%, and class variance predicted (after cross-validation) over 81%, and a variables variance explained (R2X) over 71%. Permutation tests (200 hundred permutations) ascribing false class assignment to observations gave bad R2Y and Q2Y values, indicating that model predictions were not due to chance.

## Results

### Resveratrol improves glucose tolerance of high-fat diet-fed pre-diabetic mice

To explore the therapeutic effect of polyphenols on glycemic parameters and gut microbiota ecology we fed the mice with a high-fat diet for 5 weeks with RSV, Cur, or the combination of RSV and Cur. RSV improved the glycemic control of the HFD-fed mice following an oral glucose challenge (**Fig. 1A and 1B**). In contrast, Cur had a less significant impact on glycaemia (**Fig. 1C and 1D**). Interestingly, the combination had no effect on the glycaemia of the HFD-fed treated mice (**Fig. 1E and 1F**). Plasma triglycerides, cholesterol, and insulin were not impacted by any of the treatments (data not shown).

### Effect of polyphenols on gut microbiota in high-fat diet-fed pre-diabetic mice

We hypothesized that polyphenols could impact hyperglycemia via a modulation of the gut microbiota dysbiosis. Thus gut microbiota samples were sequenced. The sequencing of the 16S rDNA genes followed by taxonomic classification (**Fig. 2A**) and dimensional reduction analyses (**Fig. 2B**) demonstrated first that the fat-enriched diet dramatically changed the ecology of the gut microbiota at the phylum, family, and genus taxonomic levels when compared to the NC-fed mice. Compared to the NC-fed mice, the HFD-fed mice were characterized by an increased abundance in the phyla Proteobacteria and Deferribacteres (**Fig. 2A**). At the family level the proportion of Rikenellaceae, Bacteroidaceae, Peptostreptococcaceae, and Deferribacteraceae were increased in HFD-fed mice (**Fig. 2A**). In contrast, the proportion of Lactobacillaceae family were notably absent from the HFD mouse cecal samples. The HFD also decreased the abundance of the families Lachnospiraceae and Porphyromonadaceae. At the genus level, the HFD increased the proportion of Alistipes, Bacteroides, and Odoribacter (**Fig. 2A**). The appearance of Mucispirillum and Clostridium XI were also promoted by HFD treatment, while Lactobacillus was diminished greatly compared to the NC-fed mice. A dimensional reduction plot depicting the relationships between the microbiota for each cecal content sample, with respect to the five dietary groups, shows that the high-fat diet treatment had a strong impact (**Fig. 2B**). The treatment of the HFD-fed mice with either RSV or Cur further and similarly modifies the microbiota ecology. Interestingly, the Cur and RSV association treatment of HFD-fed mice had a strong impact on gut microbiota ecology. Changes of the gut

microbiota ecologies were also observed at the level of the taxonomic diversity as calculated using the Shannon index (**Fig. 2C**). The mice fed a HFD had an increased Shannon diversity at both taxonomic levels. The RSV and Cur treatments or combination reversed the increased bacterial diversity.

To more precisely identify the differential taxons at all taxonomic levels, we performed LEfSe analyses followed by a linear discriminant analysis of the taxonomic count data (**Fig. 3**). The impact of a HFD generated numerous differences at all taxonomic levels (**Fig. 3A**). Among them the proportion of Deferibacteraceae, Peptostreptococcaceae, and Desulfovibrionaceae was increased by the HFD while the proportion of Lactobacillaceae, Coriobacteriaceae, and Anaeroplasmataceae was reduced.

Focusing on the comparison of the HFD group to the HFD+RSV group, we showed that when RSV was consumed by the mice the ratio between Firmicutes/Bacteroidetes phyla increased while the proportion of Proteobacteria reduced (**Fig. 2A and 3B**). At the family level RSV increased the proportion of Ruminococcaceae while reducing that of Rikenellaceae and Peptostreptococcaceae (**Fig. 2A and 3B**). Cur treatment impacted different taxa and mostly reduced Rikenellaceae while increasing Bacteroidaceae. Importantly, combination of RSV and Cur inhibited the impact of RSV by further reducing the proportion of Ruminococcaeae and Porphyromonadaceae (**Fig. 2A and 3C**). At the level of genus, RSV reduced the proportion of Alistipes and Clostridium XI whereas increasing Anaerotruncus (**Fig. 2A**). We then precisely identified the taxa increased by the HFD-treatment and reversed by the RSV and masked by the Cur (**Supplementary Table 2 and Fig 3D**). Out of 14 taxonomic elements showing differences between groups 10 were characterized by an increased abundance in NC compared to HFD. We then compared which of the taxon had its frequency reduced by HFD (difference between NC and HFD), reversed by the RSV treatment (Difference between HFD and HFD-RSV and that the impact of RSV was reversed by Cur (difference between HFD-RSV and HFD-CUR). Only one taxon (S24-7 family) was identified using a Venn analysis (**Supplementary Table 2, Fig. 3E**). Altogether the S24-7 family could be considered as an important target of the RSV treatment which could explain the improved glycemic control induced by the polyphenol. The linear regression analysis showed a negative correlation between the glycemic index of glucose intolerance and the proportion of the bacteria (**Fig. 3I**). Conversely, we analyzed the taxons which frequency were increased by the HFD treatment but reduced by the RSV, and that the reduction was blunted by the Cur (**Supplementary**

**Table 2, Fig. 3F).** We identified *Bifidobacterium pseudolongum* and a member of the Peptostreptococcaceae family (**Fig. 3G and 3H**).

To identify all taxa impacted in response to a single diet (different treatments) we performed linear regression analyses for the HFD groups only (HFD, HFD+RSV, HFD+Cur, and HFD+RSV+Cur) between the relative abundance of the bacteria and the glycemic index (AUC). In addition to the Bacteroidales S24-7 family (as above), we also identified Prevotellaceae family (Bacteroidales order) and *Akkermansia muciniphila* as having a negative correlation with glycemic index of glucose intolerance (**Fig. 3J and 3K**). In contrast, we identified the Peptococcaceae family (Clostridiales order), Lachnospiraceae *Dorea* genus (Clostridiales order), and *Mucispirillum schaedleri* as having a positive correlation with glycemic index of glucose intolerance (**Fig. 3L, 3M, and 3N**).

To investigate the impact of RSV alone within the context of a HFD (i.e. HFD+RSV), on glycemia we performed linear regression analyses between the relative abundance of bacterial taxons and the glycemic index within only the HFD+RSV treated group. As for the Bacteroidales S24-7 family, a negative correlation was shown for the genus *Lactobacillus* (Lactobacillales order) and *Prevotella* (Bacteroidales order) (**Fig. 3O and 3P**). As for the impact of HFD, the Peptococcaceae family (Clostridiales order) and *Mucispirillum schaedleri* demonstrated a positive correlation with the glycemic index of the glucose tolerance test (**Fig. 3Q and 3R**). We hypothesized that the lack of effect of RSV and Cur combination on glycemia might be due to differential effect of the two polyphenols on gut microbiota. Based on the 16S rDNA data (**Supplementary Table 2**) and DGGE analysis results (**Fig 3S**), several bacteria strains were selected according to the gut microbiota analysis and cultured in the presence or absence of polyphenols. We selected 4 bacterial strains according to their capacity to grow and with respect to the differential results induced by the polyphenol treatments (*Alistipes*, *Bacteroides*, *Clostridium*, *Odoribacter*). The results show that only *Alistipes putredinis* was sensitive to the antibiotic action of RSV while Cur counteracted this effect (**Fig. 3T**).

To investigate potential microbial mechanisms of glycemic control, we used the PICRUSt computational approach to predict the functional composition of the bacterial metagenomes derived from each dietary group.

The 16S targeted metagenomics profiling information for the cecal contents of each mouse were used to assign KEGG orthologies based on bacterial genomic content, and then combined to predict the composite metagenomes. The composite metagenomes were then parsed into KEGG derived modules for pathway and structural complex prediction. Pathway modules represent tight functional units in KEGG metabolic pathway maps (e.g. glycan metabolism) and structural complexes often form molecular machineries. The pathway and structural complex data were then analyzed by LEfSe for predicted gene enrichment using the same dietary group comparisons as for the taxonomic evaluations (**Fig. 4**).

Predicted microbial genes in cecal contents impacted by the HFD-treated mice were the most numerous and diverse, including many assigned to pathways involved in carbohydrate and amino acid utilization (**Fig. 4A**). The group receiving the NC diet showed enrichment in pathways for glycan, glycosaminoglycan, and other carbohydrate metabolism. This could be expected given the fact that the amount of complex carbohydrate is substantially higher in NC compared to HFD. Similarly, the NC diet appears to enrich for branched chain amino acid and purine/pyrimidine metabolism, as well as degradation of aromatic compounds. In contrast, the HFD diet shows enrichment for genes involved in nitrogen and sulfur metabolism, and biosynthesis of secondary metabolites including amino-acids. Out of the numerous pathways which were different between NC and HFD-fed mice, only some were reversed by the RSV treatment. These include the sulfur metabolism and the biosynthesis of secondary metabolites (**Fig. 4B and Supplementary Table 3**). Others, that we did not focus on since out of the scope, were impacted by Cur alone (**Fig. 4C**). Two of the pathways impacted by RSV, notably the dissimilatory sulfur pathway, were antagonized by Cur (**Fig. 4D and Supplementary Table 3**). A linear regression analysis showed that the proportion of the predicted dissimilatory sulfate reduction pathway was positively correlated with glycemia in the HFD-fed mice (**Fig. 4G**). Venn diagram show that none of the pathways which were reduced by HFD and reversed by RSV while prevented by Cur were identified (**Fig. 4E**). Conversely, we identified two pathways which were increased by the HFD and reversed by the RSV while prevented by Cur (**Fig. 4F**). The first one was related to energy metabolism (i.e. sulfur metabolism) and the second was related to aromatic amino acid metabolism (i.e. tyrosine metabolism; **Supplementary Table 3**).

Similar to the predicted metabolic pathways, the predicted structural complex modules had the most significant differences for NC diet mice compared to HFD mice (**Fig. 5A**). Modules pertaining to energy metabolism, such as ATP synthesis and ABC type II transporter systems, are predicted to be depleted by HFD while components related to environmental signaling such as bacterial secretion systems were enriched. The impact of RSV on predicted gene enrichment compared to HFD alone was more limited (**Fig. 5B**). The effect of RSV on the predicted metagenome was to reduce the genes related to sulfur metabolism and biosynthesis of metabolites. In comparison, the predicted impact of Cur on RSV was to reduce the HFD induced changes in glycan, glycosaminoglycan, and other carbohydrate metabolism as well as reduce contributions to nitrogen metabolism and biosynthesis of secondary metabolites (**Fig. 5C**). An additional interesting feature of the Cur supplemented diet is the predicted reduction of lipopolysaccharide metabolism (**Fig. 5C**). The HFD with RSV and Cur combination altered only three predicted pathway modules compared to HFD with RSV supplementation alone (**Fig. 5D**). We then analyzed the global impact of RSV on predicted structural complex modules (**Supplementary Table 4**). The impact of RSV supplementation with the HFD is less deep rooted in the predicted hierarchies, but includes a shift in various PTS (phosphotransferase system) carbohydrate specific transporters and a reduction of amino acid transport systems. The effect of Cur on the HFD is again broader ranging, but also includes PTS carbohydrate specific transporters a reduction of amino acid transport systems. In addition, the supplementation of Cur is predicted to reduce the abundance of pathogenicity related genes of gram negative bacteria, namely those of type III and type VI secretion systems.

Altogether, our data show that the polyphenol treatments improved the gut microbiota dysbiosis induced by the HFD by putatively impacting bacterial metabolic pathways.

### **Polyphenols regulate plasma metabolomics**

To identify whether the polyphenols could have a systemic impact, we performed metabolomics studies on plasma. The impact of the polyphenols was examined by projection of latent structure-discriminant analysis (PLS-DA) (**Fig. 6A**). Three significant components could be calculated after 7 fold cross-validation, explaining 57.7% of total observation variance ( $R^2(X)$ ), 40% of group variance ( $R^2(Y)$ ), and 23.2 % of predicted group

variance ( $Q^2(Y)$ ). The classes (dietary groups) were significantly heterogeneous ( $P=0.003$  after cross-validation ANOVA). Class assignment ranged from 12.5 to 100% confidence ( $P=7.7e-012$ , fisher probability test), as reported in the confusion matrix (**Supplementary Table 5**). Finally, a permutation test assessing overfitting indicated that the discriminant model was not spurious ( $Q^2$  values being negative at the intercept after 20 permutations) (**Supplementary Table 6**). The metabolic distance among the dietary groups were best displayed using the “c” vectors of the PLS-DA, correlating the class variables with the observations scores. It indicates the “barycentric” coordinates of each class in the loading space, and summarizes a metabolome score for each dietary group (**Fig. 6B**). Strikingly, figure 6B clearly showed that both HFD+RSV and HFD+Cur metabolomes clustered together with a low degree of dissimilarity (dissimilarity index values on the ordinate axis), and exhibited more proximity to the normal low fat chow diet than did the metabolome of both HFD alone or HFD+RSV+Cur. This representation also clearly showed that adding both RSV and Cur to a high-fat diet almost completely abrogated the biological effect induced by each component separately. To get into more details, we then compared the metabolic impact of the diets pairwise, e.g. HFD vs HFD+RSV, and HFD+RSV vs HFD+RSV+Cur. In both cases, the PLS-DA models were robust, using 4 to 5 components describing over 98% and 83% of the explained ( $R^2Y$ ) and predicted ( $Q^2Y$ ) variances, respectively, and  $Q^2Y$  values at the intercept being negative in the permutation test. A further improvement was obtained on the P values after CV-ANOVA (all  $P < 0.0007$ ) after selection of the most discriminating variables (variable importance score criteria over 1.3, selected from a threshold over 80% confidence interval in a normal probability distribution) (**Fig. 6C and 6D**).

Twelve metabolites were found discriminant among the HFD and the HFD+RSV (among them 4 could not be annotated), or HFD and HFD+Cur (among them 3 could not be annotated). When comparing the metabolites that shifted away from the HFD with either the addition of RSV or Cur, we identified metabolites involved in amino acid metabolism, including branched chain amino acid isoleucine strongly increased in RSV treatment over HFD, and aromatic amino acid proline (**Fig. 6E**). Importantly, numerous short chain fatty acids were quantified in the blood of polyphenol treated mice, suggesting a strong impact on gut microbiota dietary fiber fermentation.

We also analysed the metabolites which were impacted by the RSV and Cur combination treatment, parallel to the observations for hyperglycemia. As anticipated we identified glucose, glucitol, and originally isoleucine which is tightly linked to gut microbiota dysbiosis (**Fig. 6E**). These data suggest the impact of gut polyphenols on gut microbiota dysbiosis at the intersection with metabolism.

## Discussion

In this study we identified predicted pathways of gut microbiota impacted by a chronic treatment with two different polyphenols in mice at their early onset of chronic hyperglycemia. Specific sulfur metabolism, short chain fatty acid metabolism, and branched chain amino-acids were mechanisms potentially responsible for the impact of resveratrol on glycaemia. Interestingly, the Cur treatment was found to antagonize the action of RSV. The role of polyphenols on the control of metabolism has been reported the last few decades. Numerous modes of action, including anti-inflammatory and anti-oxidant activities, have been demonstrated to be responsible for the metabolic impact [28]. However, a novel mode of action has emerged recently which reconciles the anti-inflammatory/oxidant mode of action, the impact on metabolism, and the antibiotic activity of polyphenols [29]. The role of gut microbiota on metabolic disease is now considered the leading hypothesis [30]. Gut microbiota dysbiosis characterizes type 2 diabetes [4, 5] which, upon the induction of metabolic endotoxemia [31] (i.e. a raise in the blood concentration of the pro-inflammatory bacterial molecule lipopolysaccharides) triggers the TLR4/CD14 pathway, increases inflammation, and induces insulin resistance [9]. Other microbiota related mechanisms are currently being studied which abrogate inflammation, such as the production of short chain fatty acids acetate, propionate, and butyrate. Fermentative bacteria such as the Bifidobacterium produce significant amounts of SCFA from dietary fibers. Butyrate has been shown to reduce intestinal inflammation in studies of inflammatory bowel disease [32-34], notably through a mechanism implying the activation of the anti-inflammatory IL10-producing TReg lymphocytes [35]. Finally, the role of branched chain amino-acids are emerging as associated with the control of glycemia and hepatic steatosis [36, 37].

Our present data are in agreement with this line of evidence since we show that the glycemic control by RSV is associated with a specific change in gut microbiota ecology. We previously have reported that RSV controls glucose metabolism and modulates gut microbiota ecology [10]. We here demonstrate that the S24-7, Prevotellaceae, Peptostreptococaceae, and Verucomicrobiaceae families are associated with diabetes protection, irrespective of the mouse treatment. Conversely, the Bifidobacteriaceae were positively associated with hyperglycemia. Since then, numerous data have confirmed our observations [38, 39]. In addition to the

bacterial taxons we have now added the knowledge that RSV impacts some microbial pathways controlling carbohydrate and amino-acid metabolism, as well as numerous phosphorylation systems, as shown by metabolic pathway enrichment prediction. We have focused on the pathways which are associated with the glycemic control through linear regression. The most significant pathway correlation was related to the microbial sulfur metabolism. This pathway is related to the metabolism of bile acids [40] and has been previously shown in humans to be a signature of type 2 diabetes [41]. Sulfur can accept electrons in the respiratory chain instead of oxygen and allowing the growth of strict anaerobes such as Bifidobacterium, and therefore prevent from the oxidative stress generated by oxygen. Our data here present a change in Bifidobacterium induced by RSV and is prevented by Cur, which fits with the anti-diabetic effect of RSV. These first set of analyses reveal that RSV impacts the gut microbiota dysbiosis, notably sulfur metabolism, and favors the growth of Bifidobacteria. A clear demonstration of the role played by Bifidobacterium has been proposed on glycemia. The chronic treatment with a strain of Bifidobacterium improves the glycemic control through a mechanism reducing inflammation, metabolic endotoxemia, and insulin resistance [8, 42]. These bacteria are important fermenters of dietary fibers that could be responsible for the metabolic control. This hypothesis is supported by our data which show through metabolomics studies that SCFA are increased in the blood of polyphenol fed mice. SCFA are important molecules to prone an anti-inflammatory effect on gut immune system [35]. Recent data from our laboratory have causally demonstrated the role of an impaired intestinal immune defense and the development of type 2 diabetes [6]. We identified that a reduced TReg lymphocyte frequency in the *lamina propria* of the small intestine was causally induced by the gut microbiota dysbiosis and could contribute to the development of hyperglycemia [6]. Through a microbiota related vaccination strategy we could improve intestinal defense and immune system, thereby preventing the development of type 2 diabetes [43]. Importantly, in addition to the impact by RSV on sulfur and short chain fatty acid metabolism, we also observed changes in amino-acid and phosphorylation transport systems (PTS) of different amino-acids and carbohydrates. This suggests that even without changing the fat-enriched diet, the RSV treatment strongly impacts the bacterial predisposition to modify the energy metabolism and consequently interaction with the host. To validate the metagenomics hypotheses, we performed metabolomics on blood samples and observed that isoleucine we increased uniquely

in RSV and not in Cur-treated mice, while glucose and glucitol concentrations were reduced in RSV mice only. This observation parallels the glucose control suggesting a causal relationship. Isoleucine has been reported, in large meta-analyses, as associated with the type 2 diabetes [44], and derivatives such as hydroxyl-isoleucine were even characterized with hypoglycemic properties [45]. This conclusion is consistent with our observation of the glucose lowering effect of RSV. We observed that the combined RSV and Cur treatment reversed the glycemic control of RSV. We here notice as well that the relative distribution of Bifidobacteriaceae, S24-7, and Peptostreptococaceae were impacted by the HFD, reversed by the RSV, and the RSV effect was also masked by Cur.

Subsequently, the reciprocal effect of RSV and Cur on gut microbiota was examined. Four bacteria strains, the abundance of which were modified in the presence of polyphenols, were selected and tested using a culture plate inhibition assay with their polyphenols. We observed significant inhibition of the growth of *Alistipes putredini* by RSV, which was antagonized by Cur. In a previous study [10], we have also found that the abundance of this species was increased by HFD, which was normalized following the treatment with RSV. Therefore, *Alistipes putredinis* may have a leading role in T2D pathogenesis and the inhibition effect of Cur on RSV of glucose homeostasis.

Altogether, we here precisely correlated the efficacy of RSV on the glycemic control with changes in gut microbiota. We added to the knowledge the observation that several bacterial taxons were tightly impacted by the high fat diet, while RSV reversed this impact. Finally, the Cur treatment could reverse the impact of RSV. Our data can be used as the basis of novel therapeutic strategies associating polyphenols to probiotics for the control of glycaemia.

## References

- [1] Park EJ, Pezzuto JM. The pharmacology of resveratrol in animals and humans. *Biochim Biophys Acta*. 2015;1852:1071-113.
- [2] Gregor MF, Hotamisligil GS. Inflammatory mechanisms in obesity. *Annu Rev Immunol*. 2011;29:415-45.
- [3] Bouloumie A, Casteilla L, Lafontan M. Adipose tissue lymphocytes and macrophages in obesity and insulin resistance: makers or markers, and which comes first? *Arterioscler Thromb Vasc Biol*. 2008;28:1211-3.
- [4] Burcelin R, Garidou L, Pomie C. Immuno-microbiota cross and talk: the new paradigm of metabolic diseases. *Semin Immunol*. 2012;24:67-74.
- [5] Qin J, Li Y, Cai Z, Li S, Zhu J, Zhang F, et al. A metagenome-wide association study of gut microbiota in type 2 diabetes. *Nature*. 2012;490:55-60.
- [6] Garidou L, Pomie C, Klopp P, Waget A, Charpentier J, Aloulou M, et al. The Gut Microbiota Regulates Intestinal CD4 T Cells Expressing ROR $\gamma$  and Controls Metabolic Disease. *Cell Metab*. 2015;22:100-12.
- [7] Cani PD, Amar J, Iglesias MA, Poggi M, Knauf C, Bastelica D, et al. Metabolic endotoxemia initiates obesity and insulin resistance. *Diabetes*. 2007;56:1761-72.
- [8] Amar J, Chabo C, Waget A, Klopp P, Vachoux C, Bermudez-Humaran LG, et al. Intestinal mucosal adherence and translocation of commensal bacteria at the early onset of type 2 diabetes: molecular mechanisms and probiotic treatment. *EMBO Mol Med*. 2011;3:559-72.
- [9] Larrosa M, Yanez-Gascon MJ, Selma MV, Gonzalez-Sarrias A, Toti S, Ceron JJ, et al. Effect of a low dose of dietary resveratrol on colon microbiota, inflammation and tissue damage in a DSS-induced colitis rat model. *J Agric Food Chem*. 2009;57:2211-20.
- [10] Dao TM, Waget A, Klopp P, Serino M, Vachoux C, Pechere L, et al. Resveratrol increases glucose induced GLP-1 secretion in mice: a mechanism which contributes to the glycemic control. *PLoS One*. 2011;6:e20700.
- [11] Etxeberria U, Arias N, Boque N, Macarulla MT, Portillo MP, Martinez JA, et al. Reshaping faecal gut microbiota composition by the intake of trans-resveratrol and quercetin in high-fat sucrose diet-fed rats. *J Nutr Biochem*. 2015;26:651-60.
- [12] Qiao Y, Sun J, Xia S, Tang X, Shi Y, Le G. Effects of resveratrol on gut microbiota and fat storage in a mouse model with high-fat-induced obesity. *Food Funct*. 2014;5:1241-9.
- [13] Bode LM, Bunzel D, Huch M, Cho GS, Ruhland D, Bunzel M, et al. In vivo and in vitro metabolism of trans-resveratrol by human gut microbiota. *Am J Clin Nutr*. 2013;97:295-309.
- [14] Milne JC, Lambert PD, Schenk S, Carney DP, Smith JJ, Gagne DJ, et al. Small molecule activators of SIRT1 as therapeutics for the treatment of type 2 diabetes. *Nature*. 2007;450:712-6.
- [15] Baur JA, Pearson KJ, Price NL, Jamieson HA, Lerin C, Kalra A, et al. Resveratrol improves health and survival of mice on a high-calorie diet. *Nature*. 2006;444:337-42.
- [16] Strimpakos AS, Sharma RA. Curcumin: preventive and therapeutic properties in laboratory studies and clinical trials. *Antioxid Redox Signal*. 2008;10:511-45.
- [17] El-Moselhy MA, Taye A, Sharkawi SS, El-Sisi SF, Ahmed AF. The antihyperglycemic effect of curcumin in high fat diet fed rats. Role of TNF-alpha and free fatty acids. *Food Chem Toxicol*. 2011;49:1129-40.
- [18] Burcelin R, Crivelli V, Dacosta A, Roy-Tirelli A, Thorens B. Heterogeneous metabolic adaptation of C57BL/6J mice to high-fat diet. *Am J Physiol Endocrinol Metab*. 2002;282:E834-42.
- [19] Grasset E, Puel A, Charpentier J, Collet X, Christensen JE, Terce F, et al. A Specific Gut Microbiota Dysbiosis of Type 2 Diabetic Mice Induces GLP-1 Resistance through an Enteric NO-Dependent and Gut-Brain Axis Mechanism. *Cell Metab*. 2017;25:1075-90 e5.

- [20] Amiot MJ, Romier B, Dao TM, Fanciullino R, Ciccolini J, Burcelin R, et al. Optimization of trans-Resveratrol bioavailability for human therapy. *Biochimie*. 2013;95:1233-8.
- [21] Lluch J, Servant F, Paisse S, Valle C, Valiere S, Kuchly C, et al. The Characterization of Novel Tissue Microbiota Using an Optimized 16S Metagenomic Sequencing Pipeline. *PLoS One*. 2015;10:e0142334.
- [22] Chesworth BM, Hamilton CB, Walton DM, Benoit M, Blake TA, Bredy H, et al. Reliability and validity of two versions of the upper extremity functional index. *Physiother Can*. 2014;66:243-53.
- [23] Dubourg G, El Sawi Z, Raoult D. Assessment of the in vitro antimicrobial activity of Lactobacillus species for identifying new potential antibiotics. *Int J Antimicrob Agents*. 2015;46:590-3.
- [24] Martin JC, Maillot M, Mazerolles G, Verdu A, Lyan B, Migne C, et al. Can we trust untargeted metabolomics? Results of the metabo-ring initiative, a large-scale, multi-instrument inter-laboratory study. *Metabolomics*. 2015;11:807-21.
- [25] Dunn WB, Broadhurst D, Begley P, Zelena E, Francis-McIntyre S, Anderson N, et al. Procedures for large-scale metabolic profiling of serum and plasma using gas chromatography and liquid chromatography coupled to mass spectrometry. *Nat Protoc*. 2011;6:1060-83.
- [26] Giacomoni F, Le Corguille G, Monsoor M, Landi M, Pericard P, Petera M, et al. Workflow4Metabolomics: a collaborative research infrastructure for computational metabolomics. *Bioinformatics*. 2015;31:1493-5.
- [27] Martin JC, Canlet C, Delplanque B, Agnani G, Lairon D, Gottardi G, et al. <sup>1</sup>H NMR metabolomics can differentiate the early atherogenic effect of dairy products in hyperlipidemic hamsters. *Atherosclerosis*. 2009;206:127-33.
- [28] Bagul PK, Middela H, Matapally S, Padiya R, Bastia T, Madhusudana K, et al. Attenuation of insulin resistance, metabolic syndrome and hepatic oxidative stress by resveratrol in fructose-fed rats. *Pharmacol Res*. 2012;66:260-8.
- [29] Su Y, Ma L, Wen Y, Wang H, Zhang S. Studies of the in vitro antibacterial activities of several polyphenols against clinical isolates of methicillin-resistant *Staphylococcus aureus*. *Molecules*. 2014;19:12630-9.
- [30] Burcelin R. Regulation of metabolism: a cross talk between gut microbiota and its human host. *Physiology (Bethesda)*. 2012;27:300-7.
- [31] Aman U, Vaibhav P, Balaraman R. Tomato lycopene attenuates myocardial infarction induced by isoproterenol: electrocardiographic, biochemical and anti-apoptotic study. *Asian Pac J Trop Biomed*. 2012;2:345-51.
- [32] Ohnmacht C, Park JH, Cording S, Wing JB, Atarashi K, Obata Y, et al. MUCOSAL IMMUNOLOGY. The microbiota regulates type 2 immunity through ROR $\gamma$  T cells. *Science*. 2015;349:989-93.
- [33] Farkas AM, Panea C, Goto Y, Nakato G, Galan-Diez M, Narushima S, et al. Induction of Th17 cells by segmented filamentous bacteria in the murine intestine. *J Immunol Methods*. 2015;421:104-11.
- [34] Atarashi K, Tanoue T, Ando M, Kamada N, Nagano Y, Narushima S, et al. Th17 Cell Induction by Adhesion of Microbes to Intestinal Epithelial Cells. *Cell*. 2015;163:367-80.
- [35] Furusawa Y, Obata Y, Fukuda S, Endo TA, Nakato G, Takahashi D, et al. Commensal microbe-derived butyrate induces the differentiation of colonic regulatory T cells. *Nature*. 2013;504:446-50.
- [36] Neis EP, DeJong CH, Rensen SS. The role of microbial amino acid metabolism in host metabolism. *Nutrients*. 2015;7:2930-46.
- [37] Tso SC, Gui WJ, Wu CY, Chuang JL, Qi X, Skvora KJ, et al. Benzothiophene carboxylate derivatives as novel allosteric inhibitors of branched-chain  $\alpha$ -ketoacid dehydrogenase kinase. *J Biol Chem*. 2014;289:20583-93.

- [38] Tzounis X, Vulevic J, Kuhnle GG, George T, Leonczak J, Gibson GR, et al. Flavanol monomer-induced changes to the human faecal microflora. *Br J Nutr.* 2008;99:782-92.
- [39] Selma MV, Espin JC, Tomas-Barberan FA. Interaction between phenolics and gut microbiota: role in human health. *J Agric Food Chem.* 2009;57:6485-501.
- [40] Devkota S, Chang EB. Interactions between Diet, Bile Acid Metabolism, Gut Microbiota, and Inflammatory Bowel Diseases. *Dig Dis.* 2015;33:351-6.
- [41] Walker A, Lucio M, Pfitzner B, Scheerer MF, Neschen S, de Angelis MH, et al. Importance of sulfur-containing metabolites in discriminating fecal extracts between normal and type-2 diabetic mice. *J Proteome Res.* 2014;13:4220-31.
- [42] Stenman LK, Waget A, Garret C, Briand F, Burcelin R, Sulpice T, et al. Probiotic B420 and prebiotic polydextrose improve efficacy of antidiabetic drugs in mice. *Diabetol Metab Syndr.* 2015;7:75.
- [43] Pomie C, Blasco-Baque V, Klopp P, Nicolas S, Waget A, Loubieres P, et al. Triggering the adaptive immune system with commensal gut bacteria protects against insulin resistance and dysglycemia. *Mol Metab.* 2016;5:392-403.
- [44] Guasch-Ferre M, Hruby A, Toledo E, Clish CB, Martinez-Gonzalez MA, Salas-Salvado J, et al. Metabolomics in Prediabetes and Diabetes: A Systematic Review and Meta-analysis. *Diabetes Care.* 2016;39:833-46.
- [45] Fuller S, Stephens JM. Diosgenin, 4-hydroxyisoleucine, and fiber from fenugreek: mechanisms of actions and potential effects on metabolic syndrome. *Adv Nutr.* 2015;6:189-97.

#### **Author Contributions**

R.B. and E.S. conceived and designed the study. J.C.M., J.F.L., and L.P. acquired, analyzed and interpreted data of metabolomics. S.K. was responsible for bacterial culture and tests. J.E.C., R.P., V.A., V.B., and P.L. acquired, analyzed and interpreted data of metagenomics. N.S., S.C. and E.S. were responsible for animal and cellular experiments, molecular biology tests and data analysis, and drafted the manuscript. All authors critically revised and approved the final version of the manuscript.

#### **Additional Information**

##### **Competing Financial Interest**

Authors declare that Laurent Pechere has competing interests with Yvery.

#### **Figure legends**

**Figure 1. Curcumin reduce resveratrol effect on glucose tolerance. A, C, E)** Glycemic profiles by oral test glucose tolerance (OGTT) for five weeks of diet: NC (n=7), HFD (n=8), HFD+RSV (n=8), HFD+Cur (n=8), HFD+RSV+Cur (n=8). **A)** NC vs HFD vs HFD+RSV, **C)** NC vs HFD vs HFD+Cur, **E)** NC vs HFD vs HFD+RSV+Cur. **B, D, F)** Area under the curve for glucose (AUC). **B)** NC vs HFD vs HFD+RSV, **D)** NC vs HFD vs HFD+Cur, **F)** NC vs HFD vs HFD+RSV+Cur. Data are presented as mean  $\pm$  S.E.M; Bars not sharing the same letter were significantly different in ANOVA followed by Tukey-Kramer post hoc test  $p < 0,05$

**Figure 2. Relative abundance, diversity, and dimensional reduction plot of cecal content microbiomes. A)** Stacked column bar graphs depicting the dietary group average relative abundances and distribution of the most highly abundant resolved taxa at the phylum and family level for this study. **B)** Dimensional reduction plot (t-distributed stochastic neighbor embedding, t-SNE) depicting the relationships between the microbiomes for each cecal content sample with respect to the five dietary groups. **C)** Plot of microbiome diversity (Shannon index) for each cecal content sample with respect to the five dietary groups. Data are presented as % of total reads  $\pm$  SD; Bars not sharing the same letter were significantly different in ANOVA followed by Tukey-Kramer post hoc test  $p < 0,05$

**Figure 3. Differential abundances of bacterial taxa in cecal contents.** Cladograms derived from pairwise group LEfSe analysis of 16S sequences from cecal contents after 5 weeks of diet: NC (n=7), HFD (n=8), HFD+RSV (n=8), HFD+Cur (n=8), HFD+RSV+Cur. **A)** NC vs. HFD, **B)** HFD vs. HFD+RSV, **C)** HFD vs. HFD+Cur, and **D)** HFD+RSV vs. HFD+RSV+Cur. The cladograms show the taxonomic levels represented by rings with phyla at the innermost ring and genera at the outermost ring, and each circle is a member within that level. Taxa at each level are shaded (green, yellow, blue, red, or purple) according to the dietary group in which it is more abundant ( $P < 0.05$ ; LDA score 2.0). **Microbiome enrichment common between groups.** The taxonomic groups were identified from pairwise group LEfSe analysis of 16S targeted metagenomic sequencing data derived from cecal contents after 5 weeks of diet. **E)** Venn diagram of taxonomic groups enhanced by NC or HFD+RSV diets in comparison to HFD

or HFD+RSV+Cur diets (HFD+Cur modules excluded), and **F**) taxonomic groups enhanced by HFD or HFD+RSV+Cur diets in comparison to NC or HFD+RSV diets. **Commonality of microbiome enrichment results of positively and negatively association with glycemic index by group as identified by regression analysis.** **G)** *Bifidobacterium pseudolongum* and **H)** Peptostreptococcaceae (Clostridiales order) which were identified at the common intersection of the Venn diagram in panel F. Regression analysis of HFD groups for **I)** S24-7 family (Bacteroidales order) **J)** Prevotellaceae (Bacteroidales order), and **K)** *Akkermansia muciniphila* which demonstrate a negative correlation with glycemia area under curve (AUC). Regression analysis of HFD groups for **L)** Peptococcaceae family (Clostridiales order) **M)** Lachnospiraceae Dorea genus (Clostridiales order), and **N)** *Mucispirillum schaedleri* which demonstrate a positive correlation with glycemia area under curve (AUC). Intragroup regression analysis of HFD+RSV for **O)** Lactobacillus genus (Lactobacillales order) and **P)** Prevotella (Bacteroidales order) which demonstrate a negative correlation with glycemia area under curve (AUC), while **Q)** Peptococcaceae family (Clostridiales order) and **R)** *Mucispirillum schaedleri* demonstrate a positive correlation with glycemia area under curve (AUC). The data points in the regression plots are differentially highlighted for HFD (yellow), HFD+RSV (blue), HFD+Cur (pink), and HFD+RSV+Cur (violet). **S)** RSV effect on *Alistipes putredinis*. DGGE profiles generated from the caecal content of mice fed normal chow (NC), high fat diet (HFD), HFD+RSV, HFD+Cur, and HFD+RSV+Cur for 5 weeks. The arrow denotes a subset of band, which have disappeared with the RSV treatment. This band, was cloned and sequenced. **T)** Antibiotic effect of RSV, Cur and RSV+Cur on *Alistipes putredinis*. 100  $\mu$ M RSV, 50  $\mu$ M Cur and 100  $\mu$ M RSV + 50  $\mu$ M Cur were used in this susceptibility test.

**Figure 4. Predicted gene enrichment of pathways.**

Cladograms derived from pairwise group LEfSe analysis of PICRUSt data derived from sequencing of cecal contents after 5 weeks of diet: NC (n=7), HFD (n=8), HFD+RSV (n=8), HFD+Cur (n=8), HFD+RSV+Cur. **A)** NC vs. HFD, **B)** HFD vs. HFD+RSV, **C)** HFD vs. HFD+Cur, and **D)** HFD+RSV vs. HFD+RSV+Cur. The cladograms show the pathway hierarchy represented by rings with pathway modules at outermost ring. Pathway hierarchies at each level are shaded (green, yellow, blue, red, or purple) according to the dietary group in which the PICRUSt analysis predicted higher gene abundance ( $P < 0.05$ ; LDA score 2.0). **Pathway enrichment common between groups.**

Commonality of KEGG pathway module enrichment results positively and negatively associated with glycemic index by group. The pathway modules were predicted from pairwise group LEfSe analysis of PICRUSt data derived from sequencing of cecal contents after 5 weeks of diet. **E)** Venn diagram of KEGG pathway modules enhanced by NC or HFD+RSV diets in comparison to HFD or HFD+RSV+Cur diets (HFD+Cur modules excluded), **F)** KEGG pathway modules enhanced by HFD or HFD+RSV+Cur diets in comparison to NC or HFD+RSV diets, and **G)** regression analysis for dissimilatory sulfate reduction module.

**Figure 5. Predicted gene enrichment of structural complexes.**

Cladograms derived from pairwise group LEfSe analysis of PICRUSt data derived from sequencing of cecal contents after 5 weeks of diet: NC (n=7), HFD (n=8), HFD+RSV (n=8), HFD+Cur (n=8), HFD+RSV+Cur. **A)** NC vs. HFD, **B)** HFD vs. HFD+RSV, **C)** HFD vs. HFD+Cur, and **D)** HFD+RSV vs. HFD+RSV+Cur. The cladograms show the structural complex hierarchy represented by rings with modules at outermost ring. Structural complex hierarchies at each level are shaded (green, yellow, blue, red, or purple) according to the dietary group in which the PICRUSt analysis predicted higher gene abundance ( $P < 0.05$ ; LDA score 2.0). **Structural complex enrichment common between groups.** Commonality of KEGG structural complex module enrichment results positively and negatively associated with glycemic index by group. The structural complex modules were predicted from pairwise group LEfSe analysis of PICRUSt data derived from sequencing of cecal contents after 5 weeks of diet. **E)** Venn diagram of KEGG structural complex modules enhanced by NC or HFD+RSV diets in comparison to HFD or HFD+RSV+Cur diets (HFD+Cur modules excluded), and **F)** KEGG structural complex modules enhanced by HFD or HFD+RSV+Cur diets in comparison to NC or HFD+RSV diets.

**Figure 6. Characterization of plasma metabolic changes induced by HFD alone (red) or supplement with RSV (green), Cur (yellow) or RSV+Cur (blue) comparing to NC (black).** **A)** Tri-dimensional PLS-DA score plot showing group discrimination according to dietary treatment. **B)** Clustering analysis of summarized metabolome score for each dietary with degree of dissimilarity. **Characterization of plasma metabolic changes induced by HFD supplemented with RSV comparing to HFD alone or HFD+RSV+Cur.** **C)** Di-dimensional PLS-DA score plot

showing the discrimination between HFD supplemented RSV (green) and HFD (red). **D**) Di-dimensional PLS-DA score plot showing the discrimination between HFD supplemented RSV (green) and HFD+RSV+Cur (blue). **E**) **Venn plot showing the shift metabolites of polyphenol supplemented comparing with HFD.** 5 of 7 metabolites from mice group treated with RSV were identified (**Right side**); 3 of 7 metabolites from mice group treated with Cur were identified (**Left side**); and 4 of 5 common metabolites from mice group treated with Cur and from mice group treated with RSV were identified (**in the middle**).

**Figure 1**

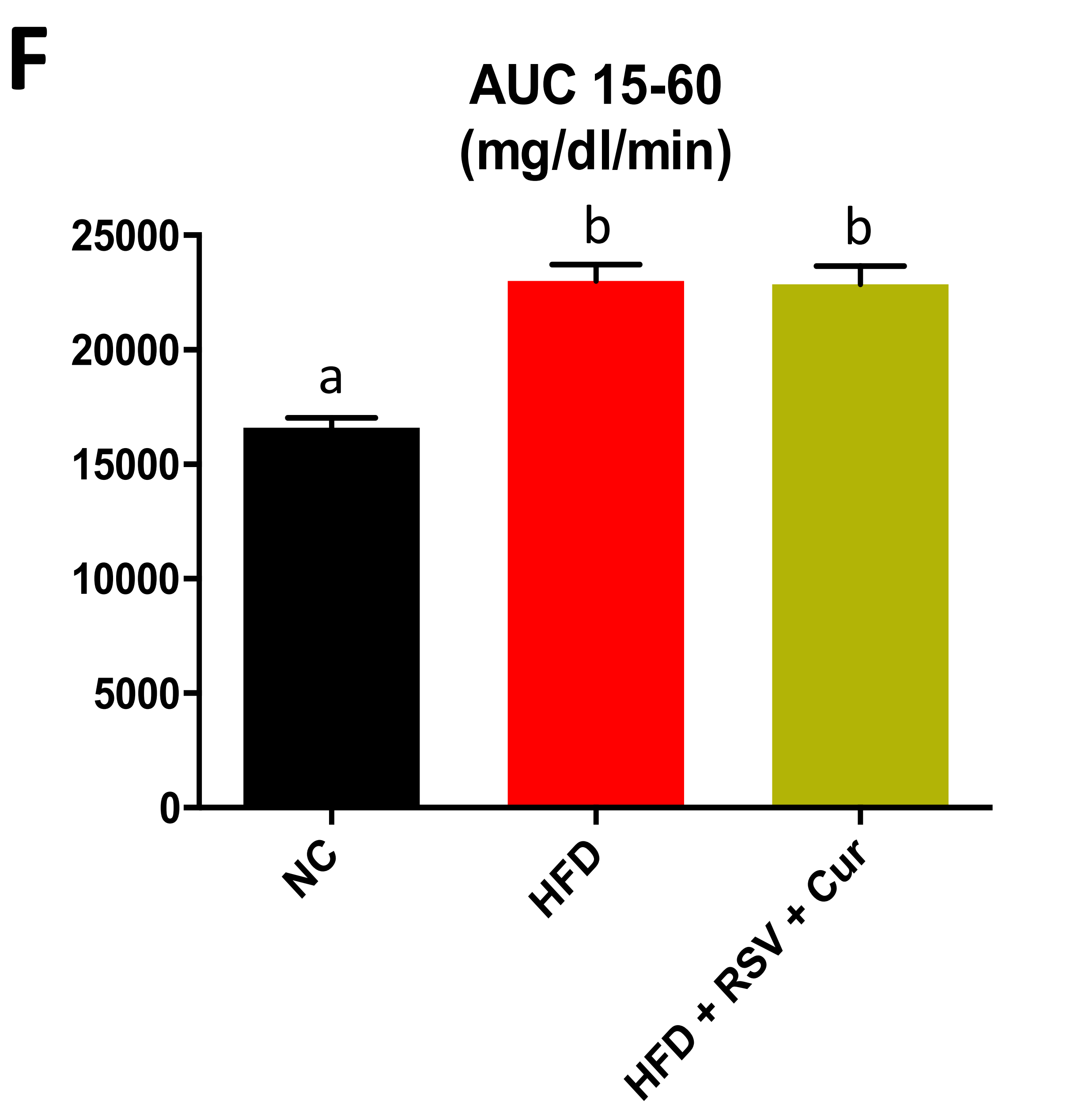
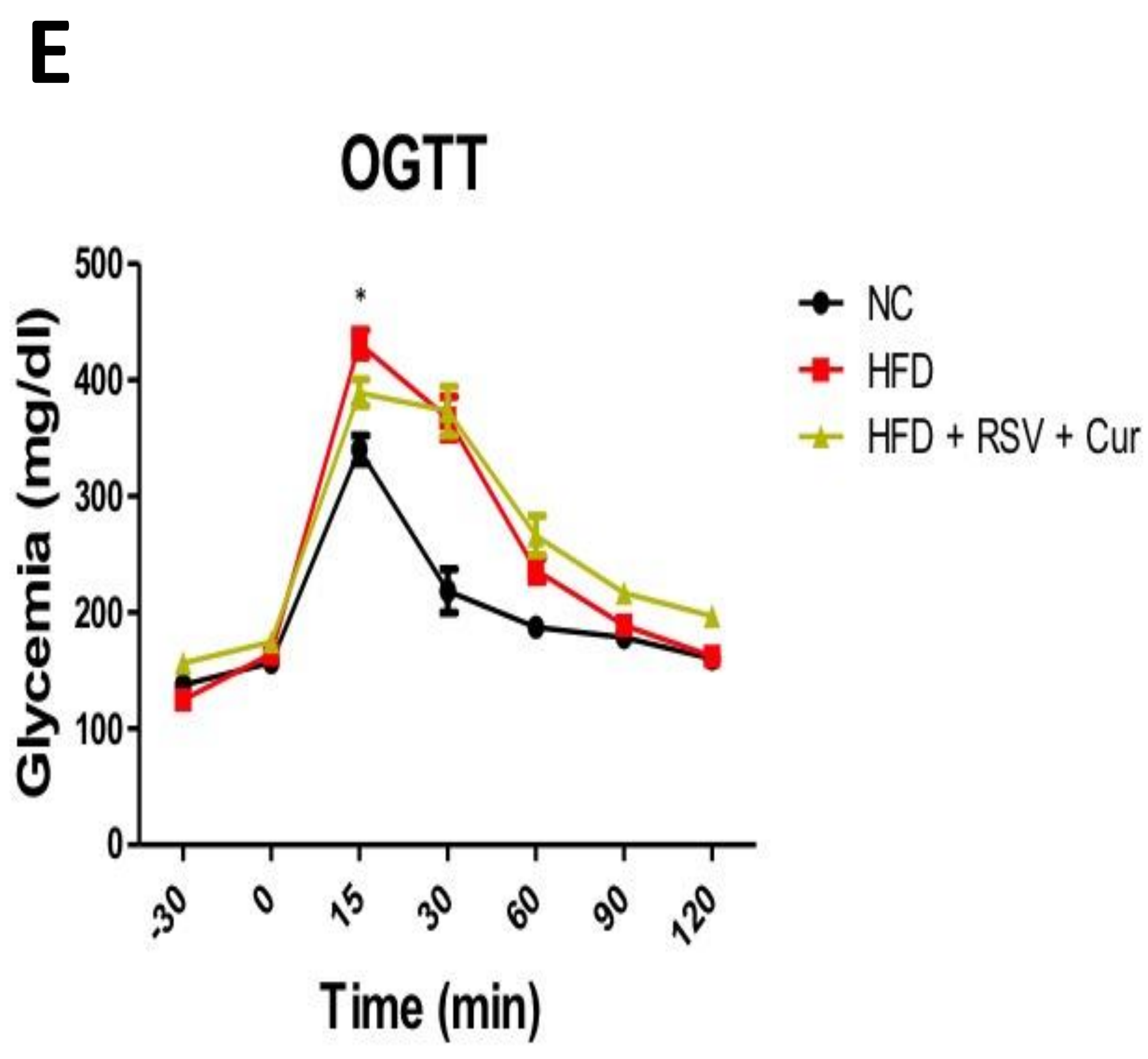
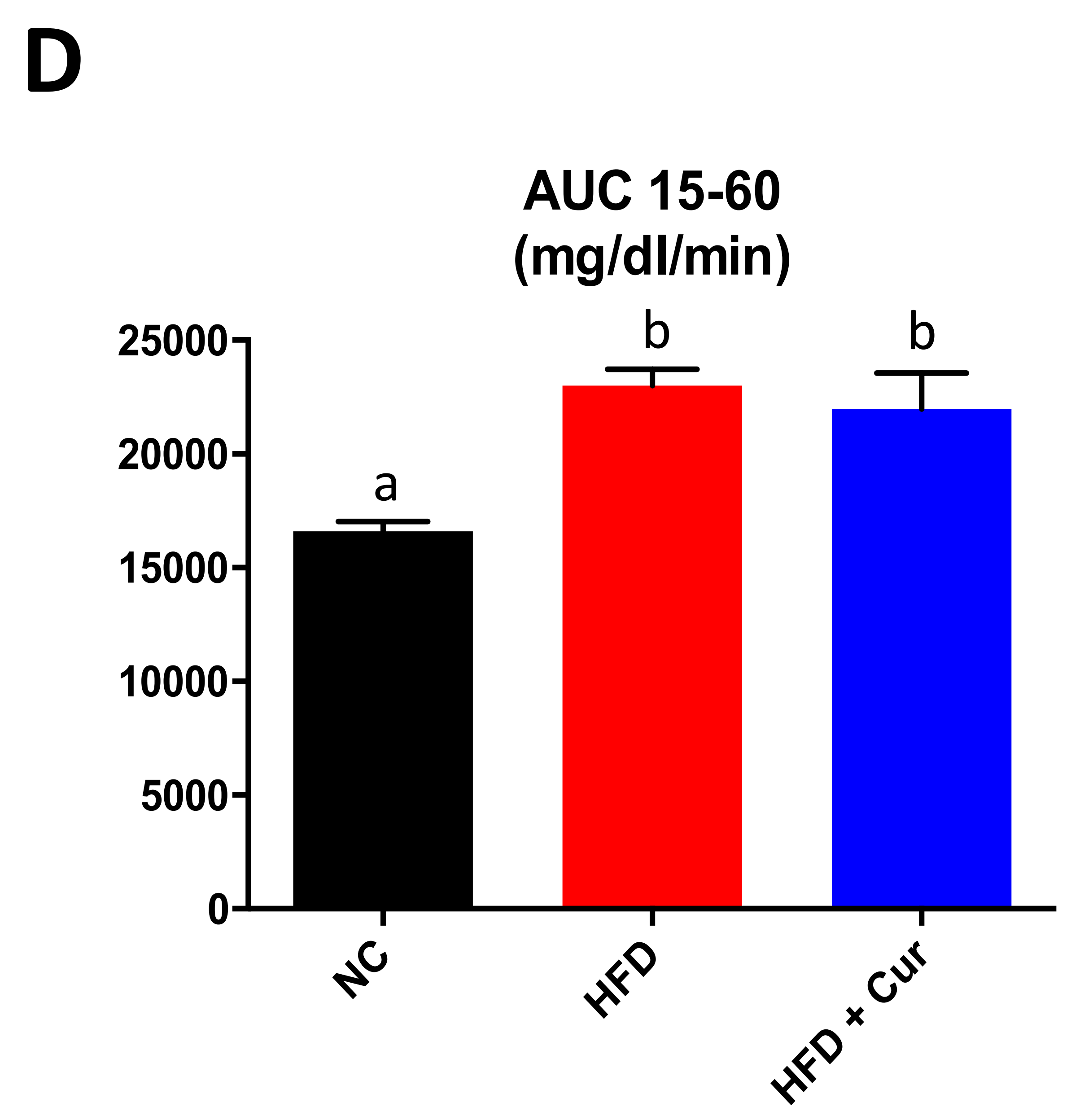
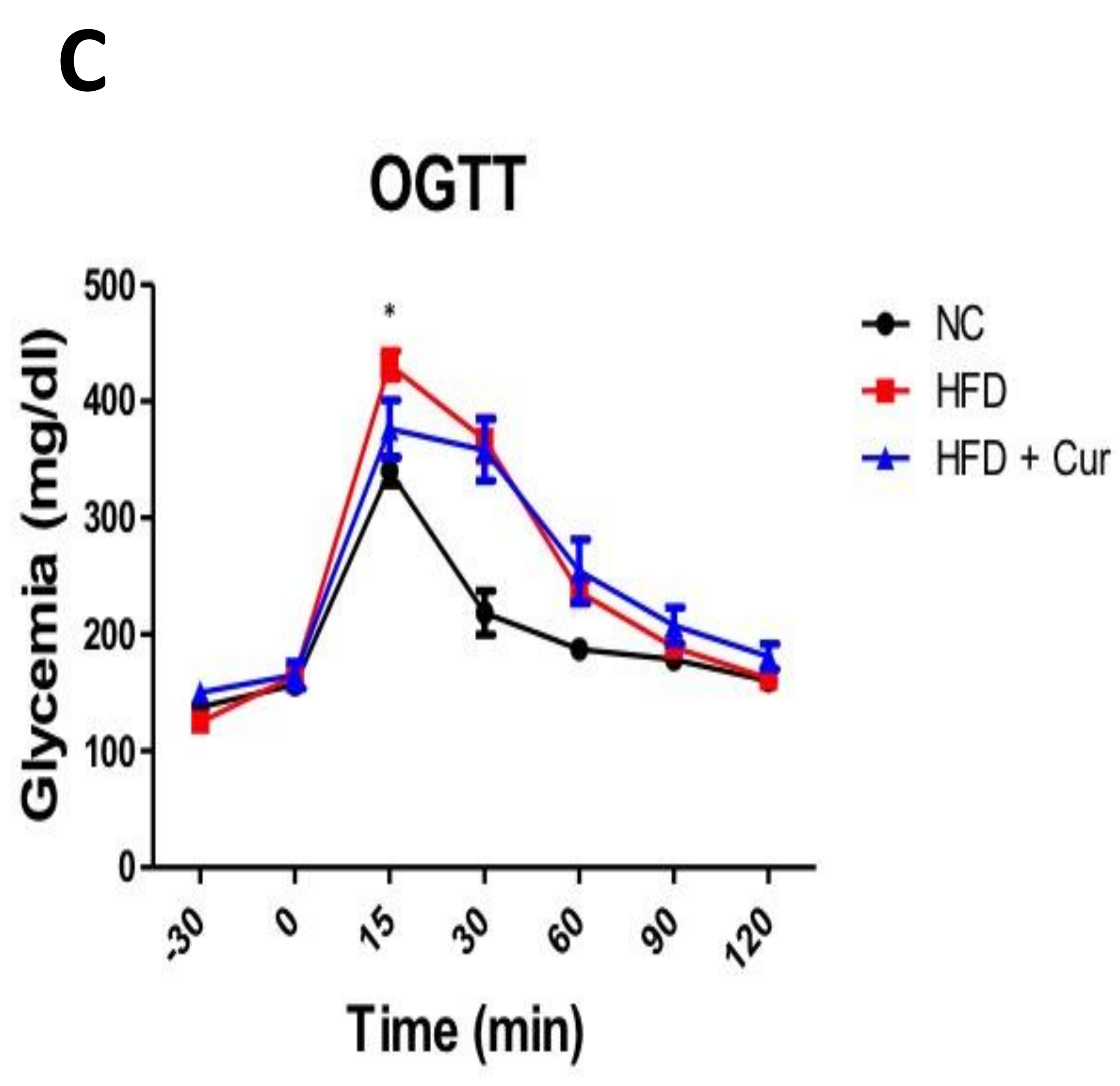
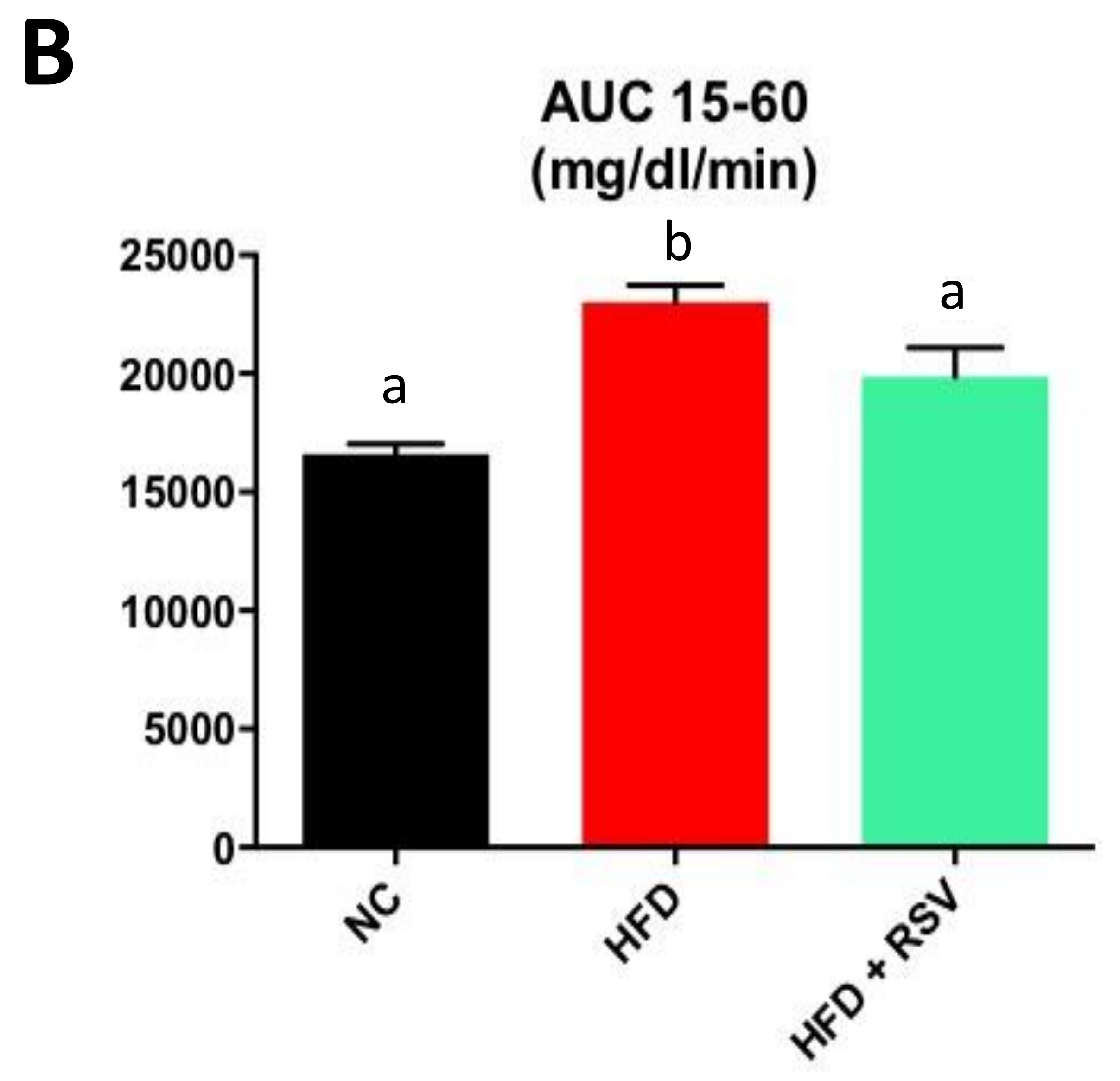
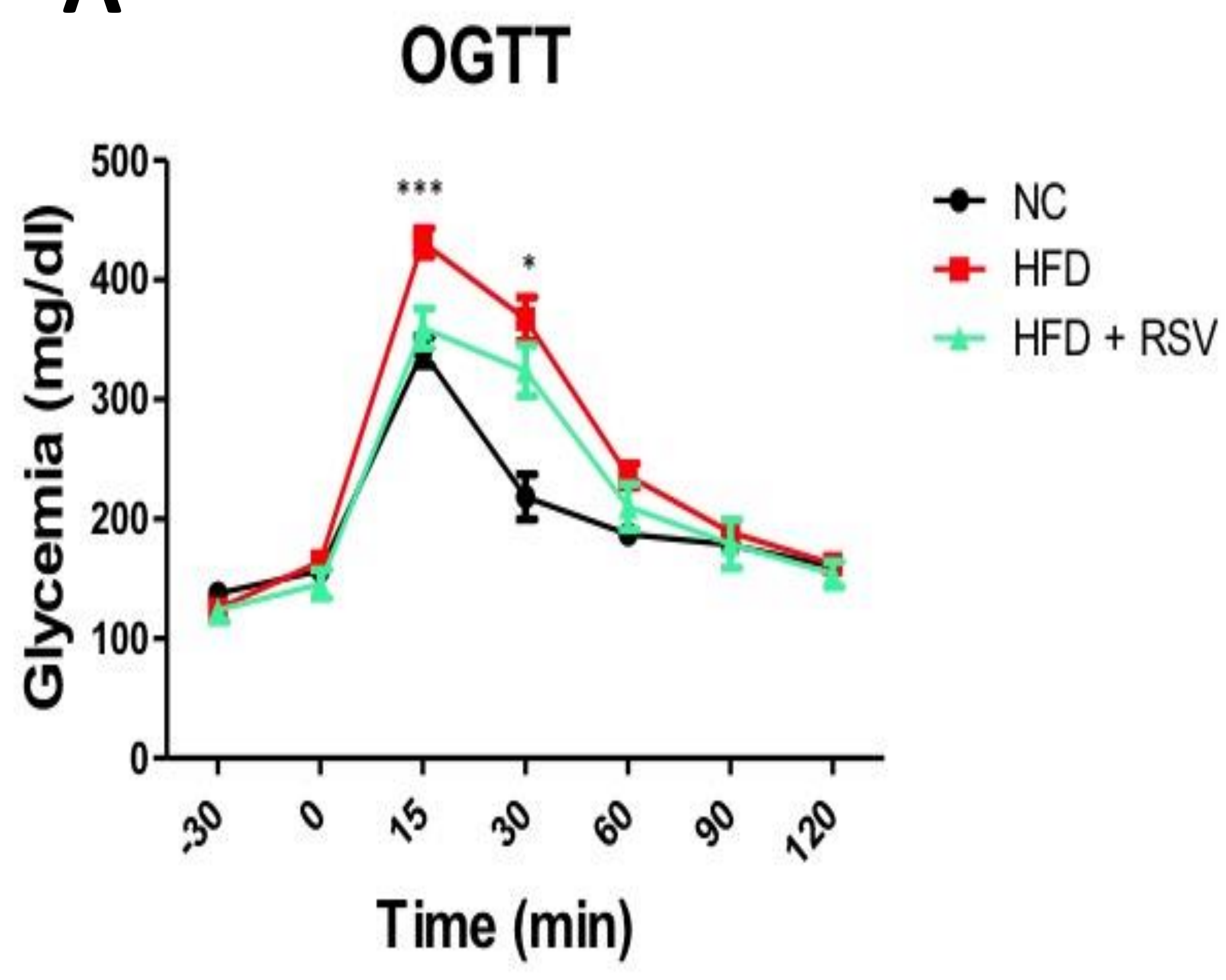




Figure 2

B

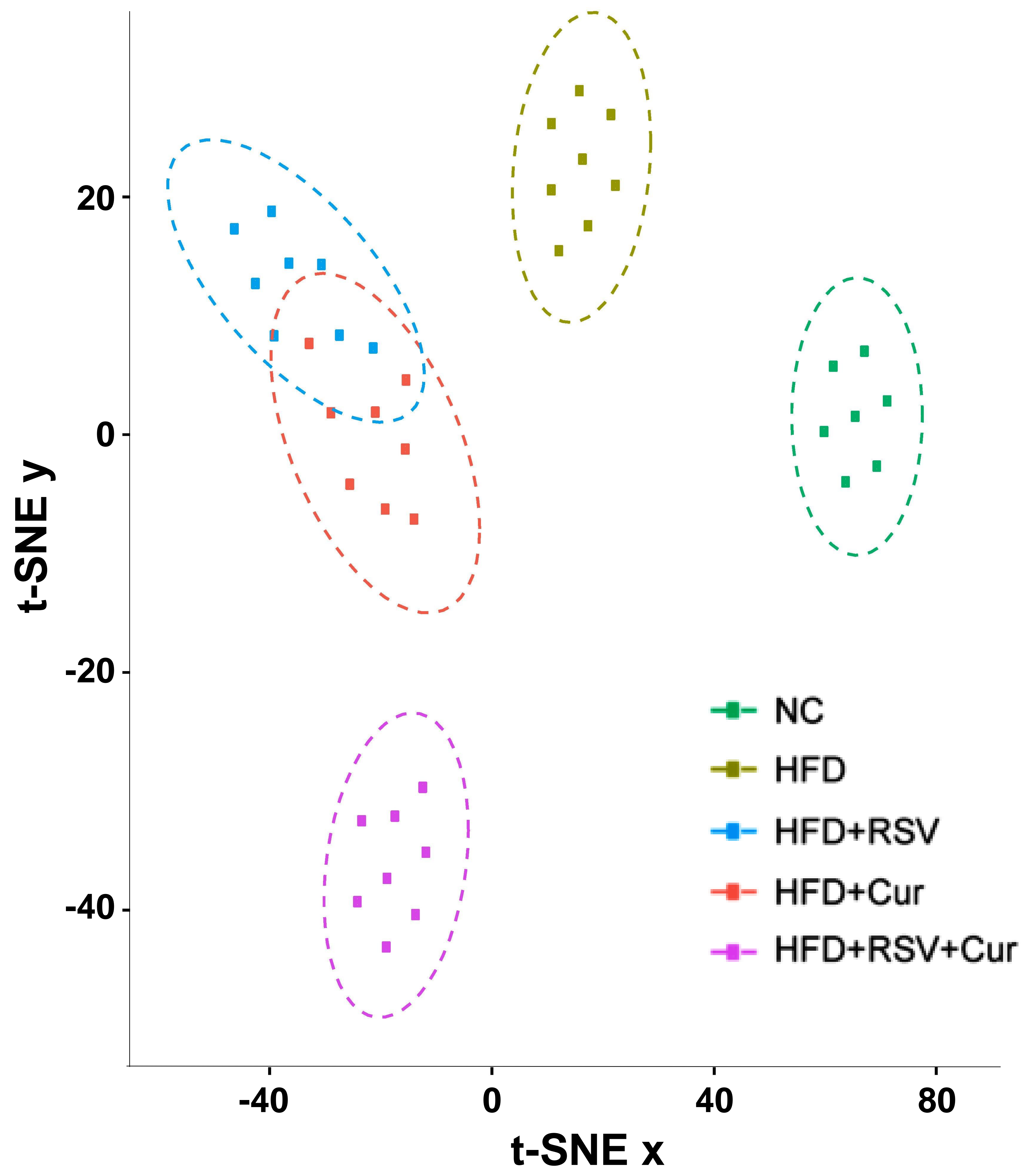
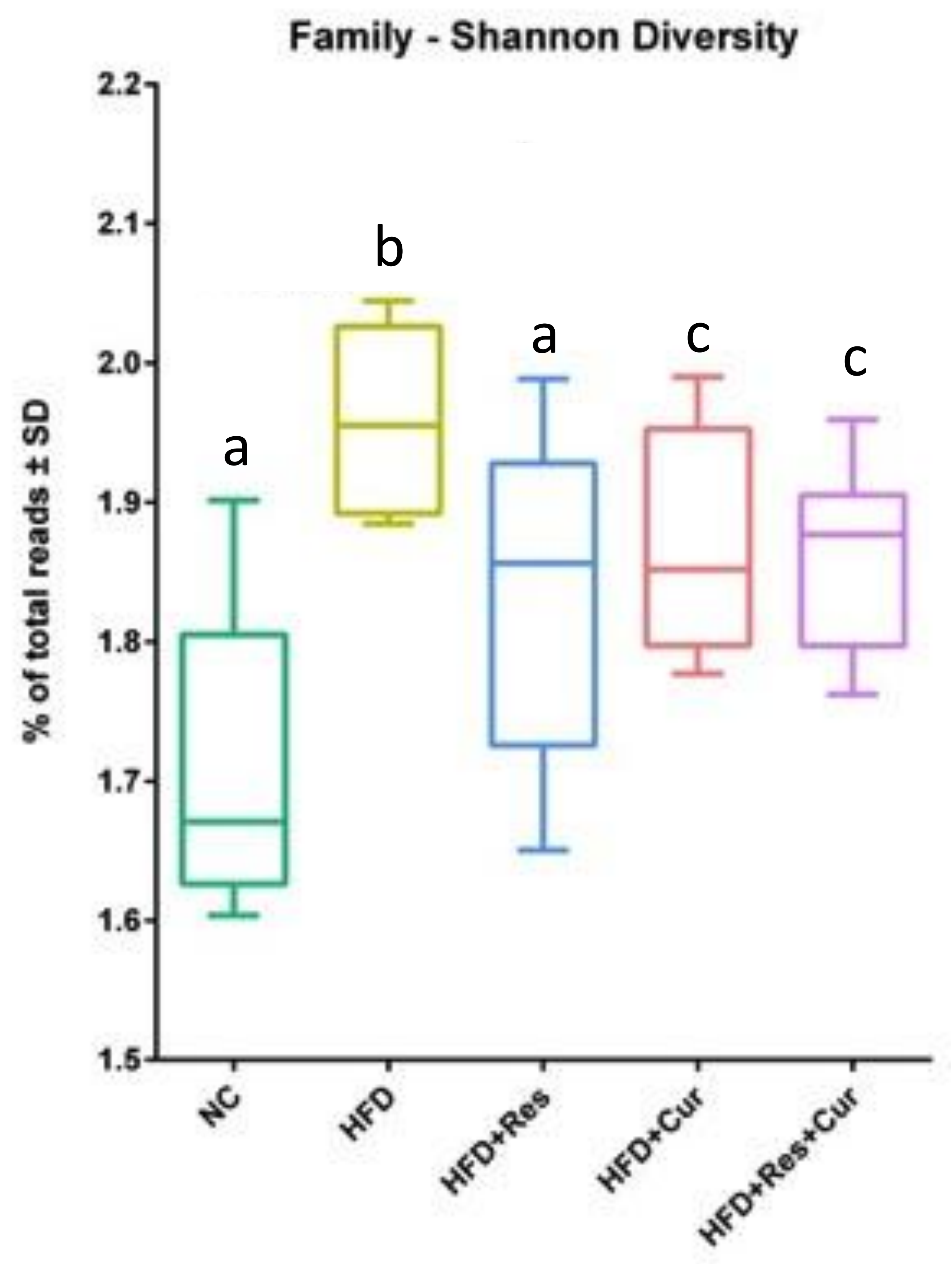
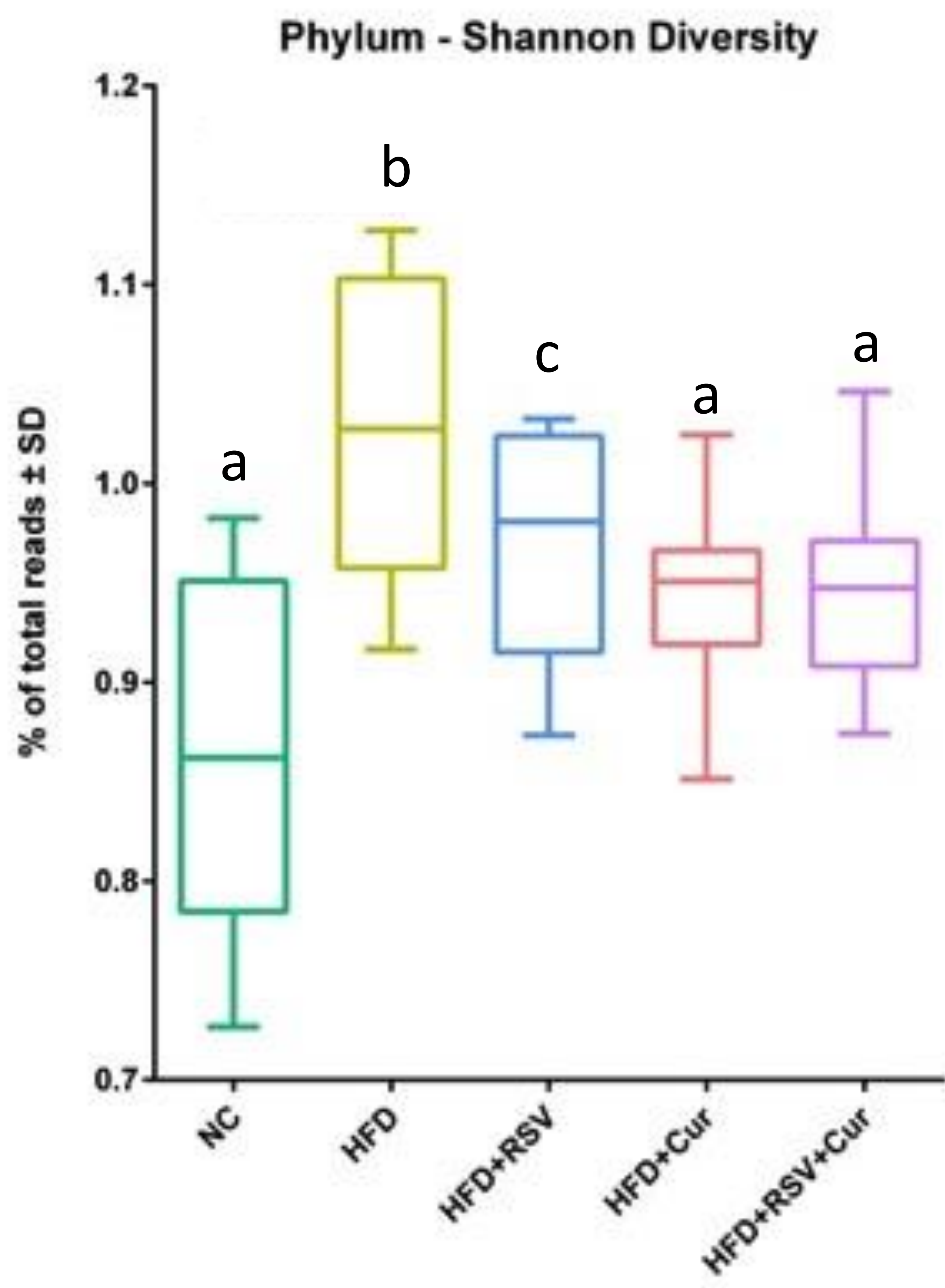


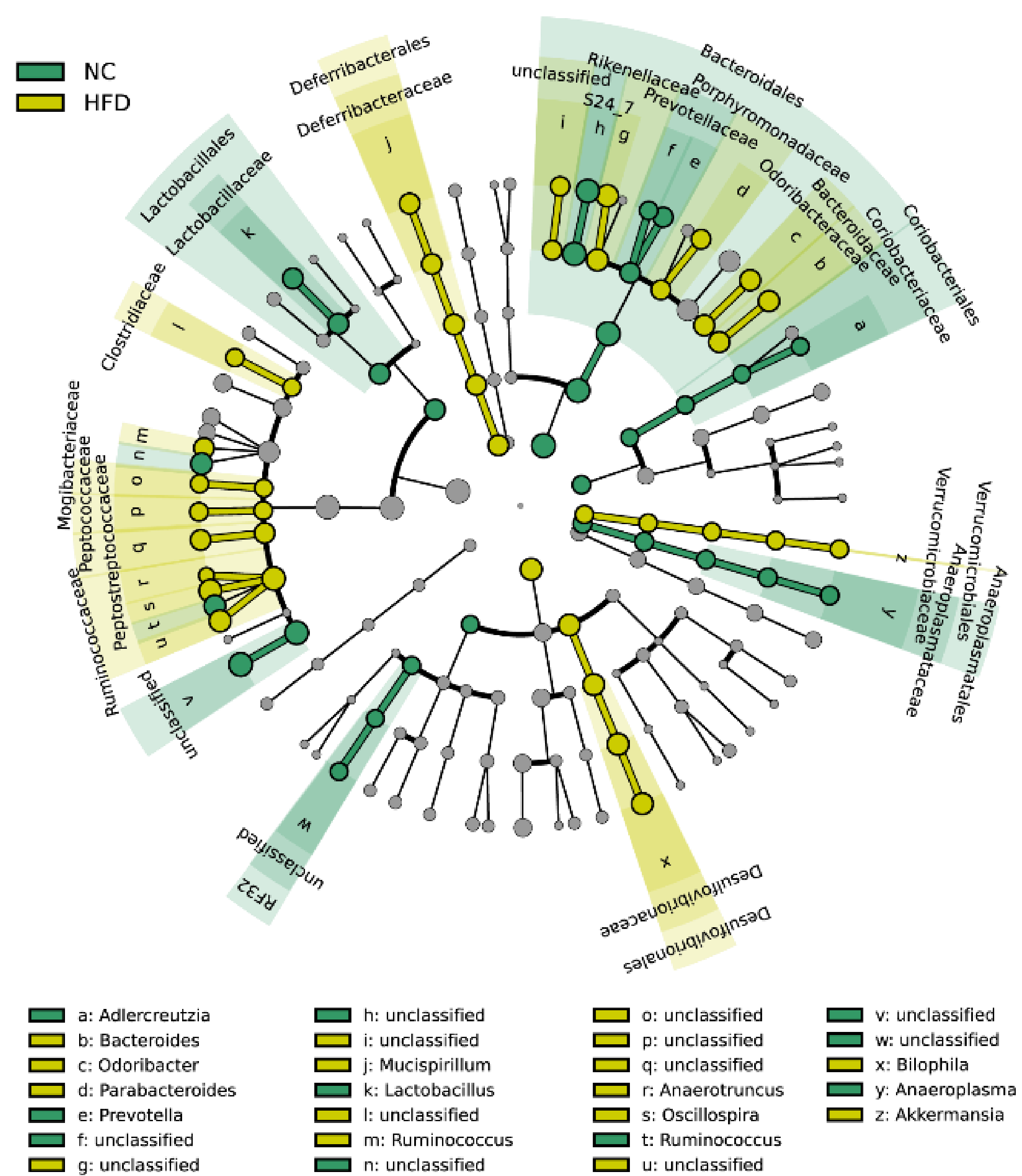
Figure 2

C

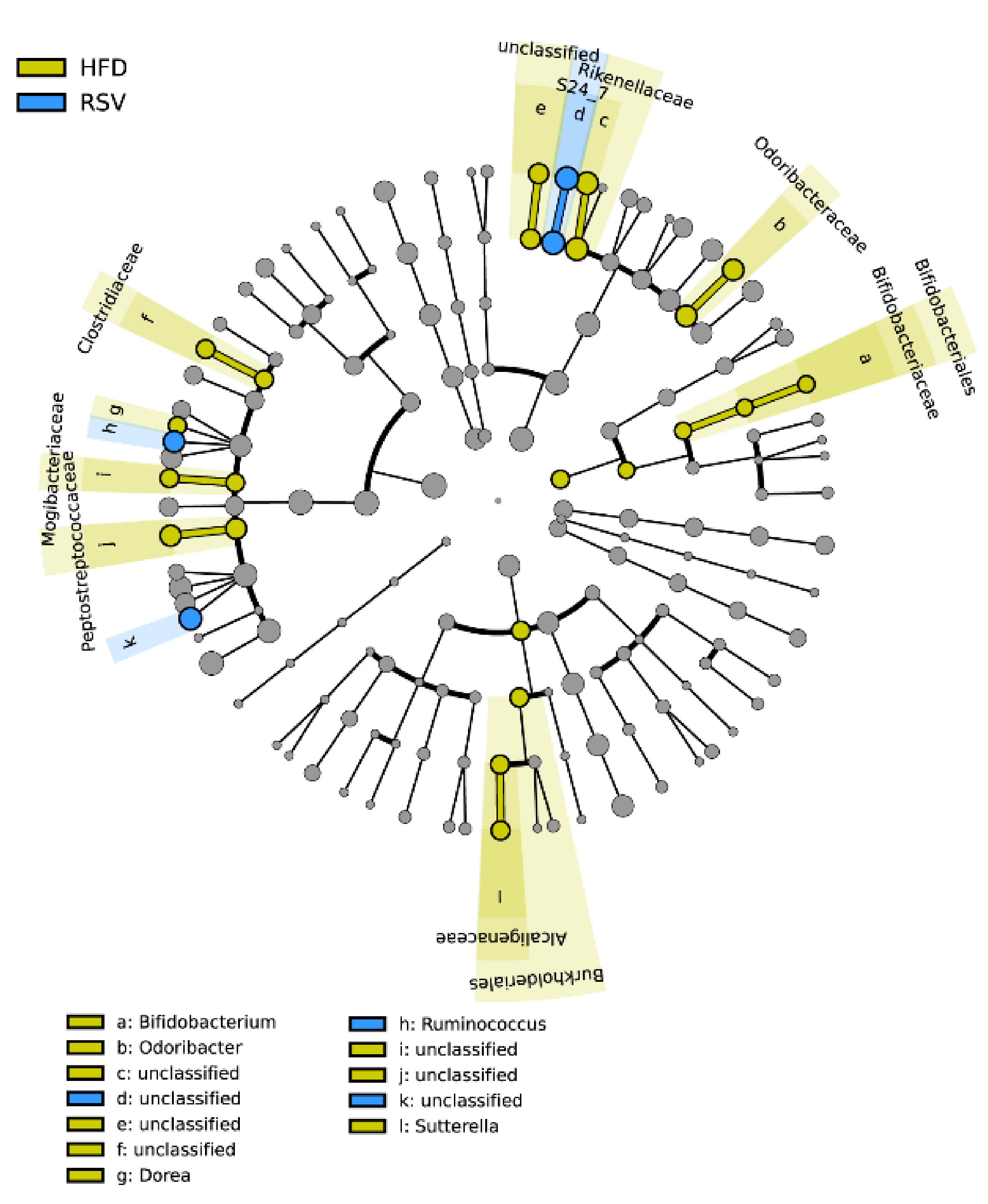


# Figure 3

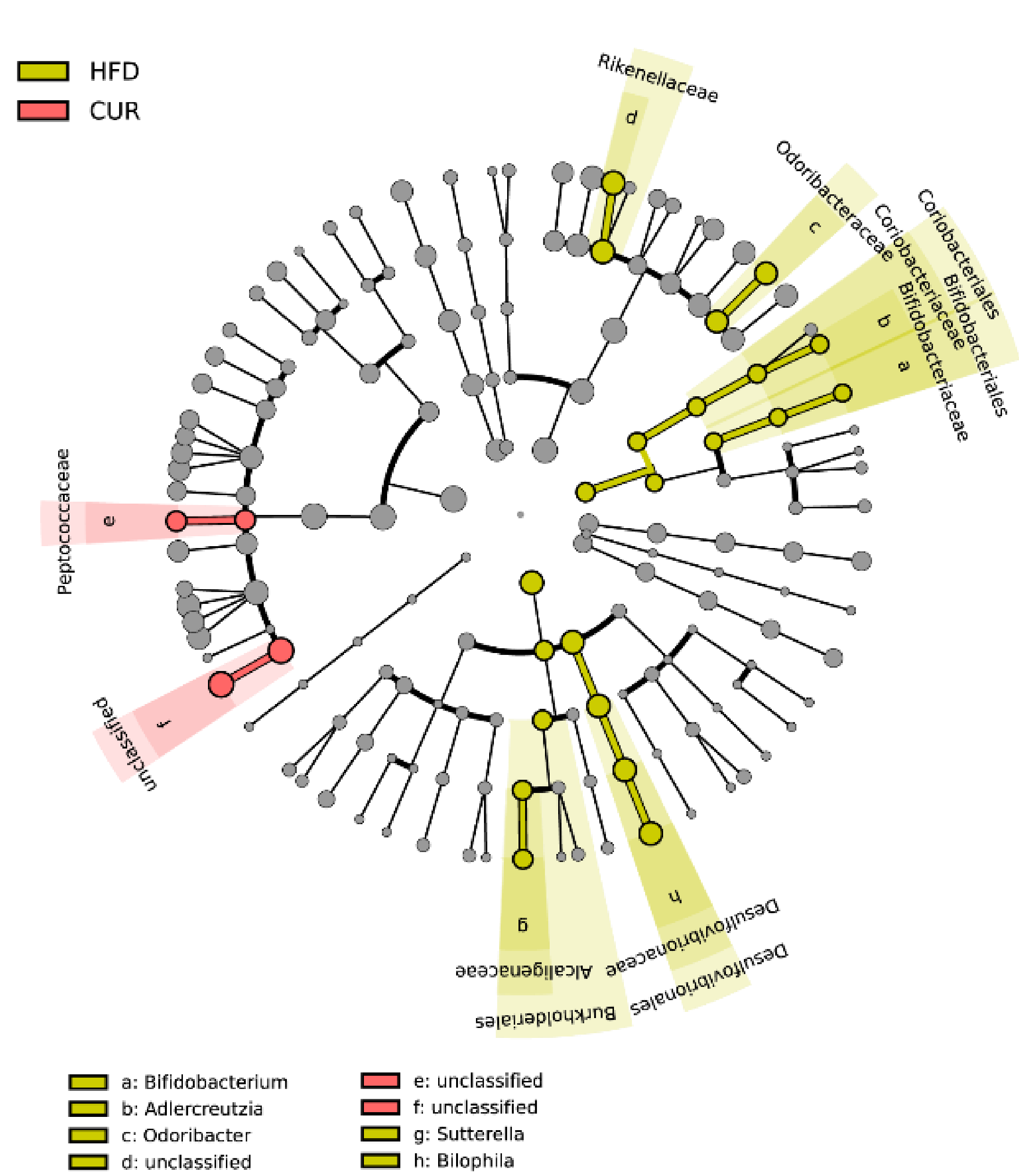
## A



## B



## C



## D

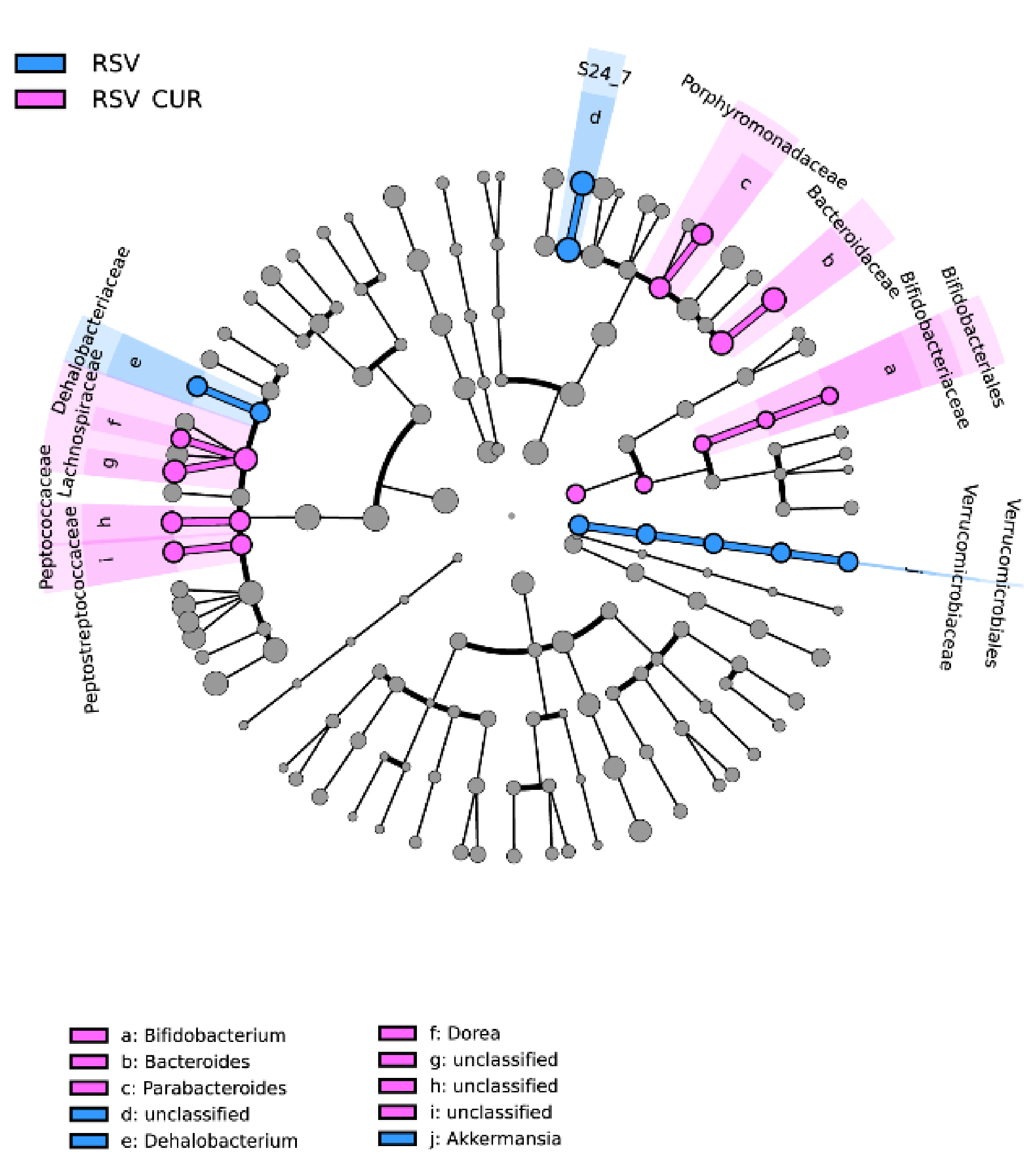
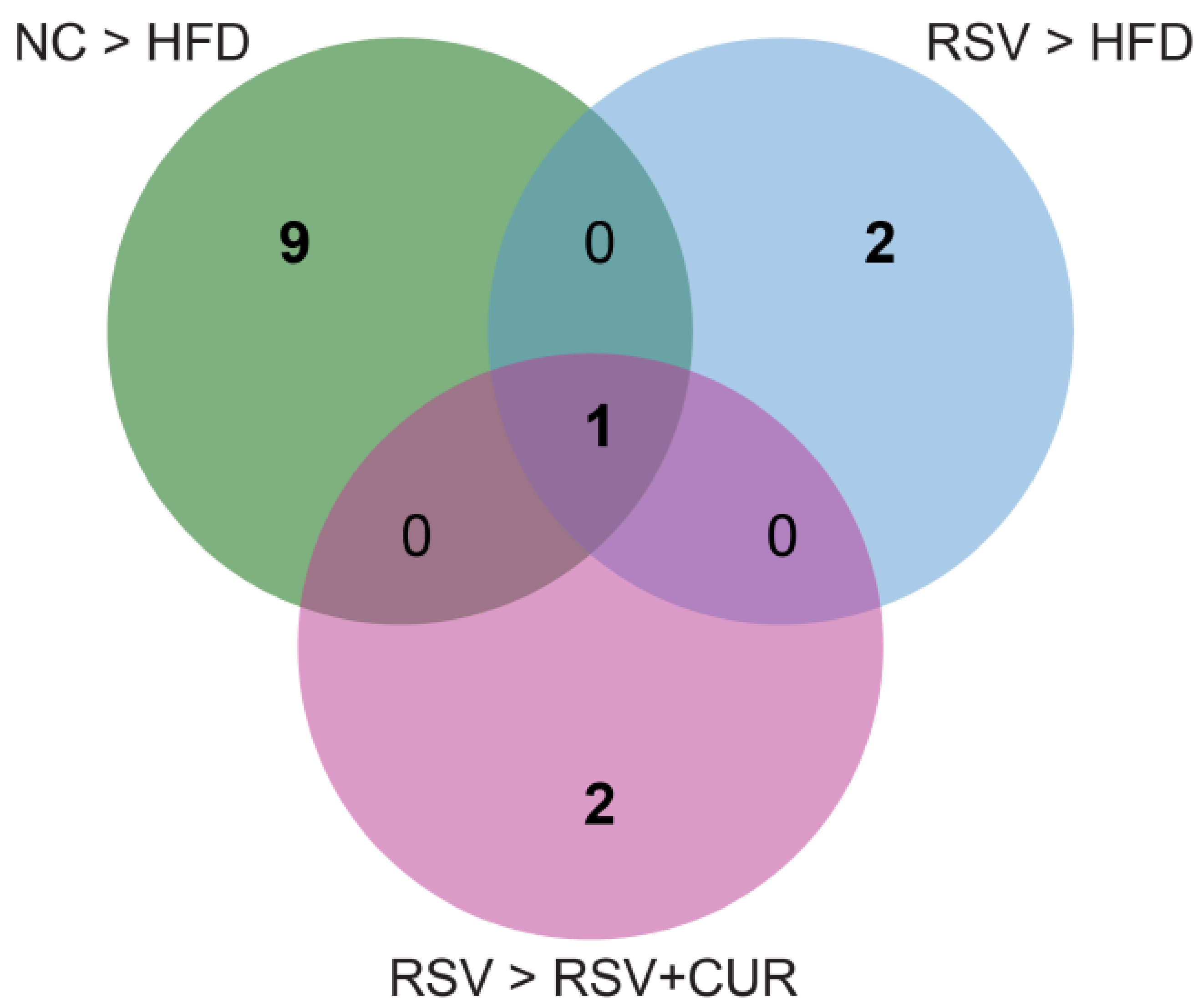
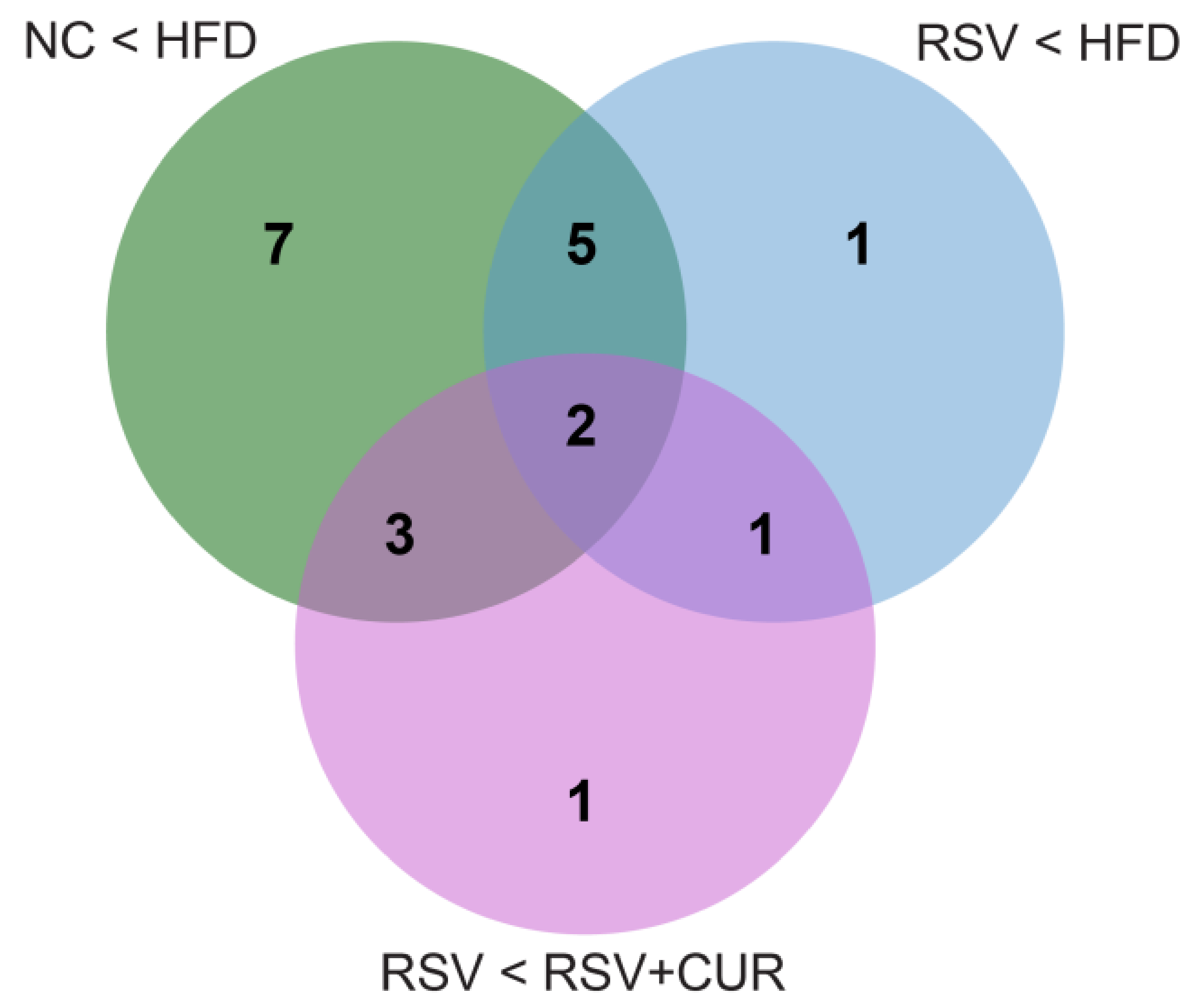


Figure 3

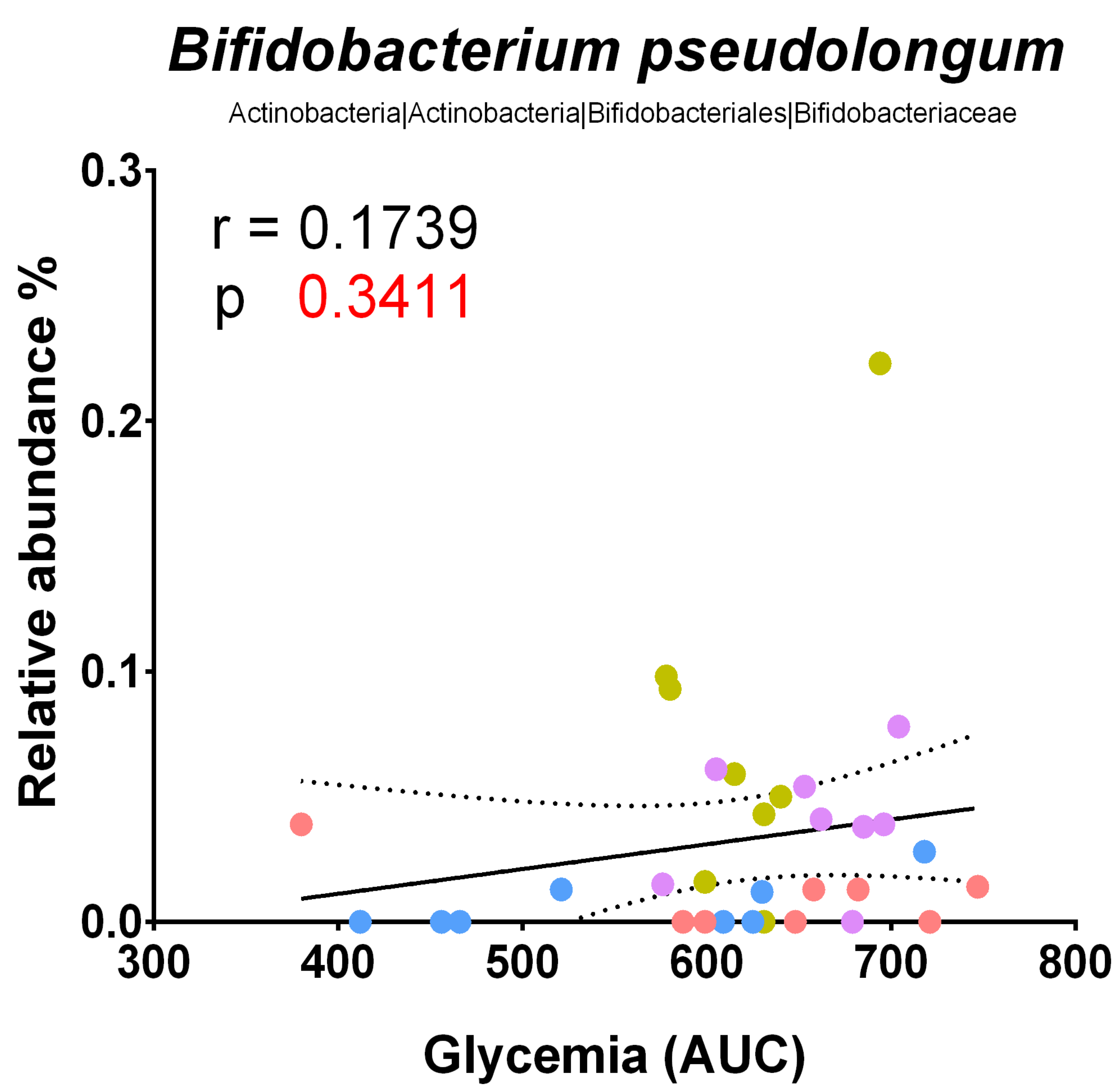
E



F



G



H

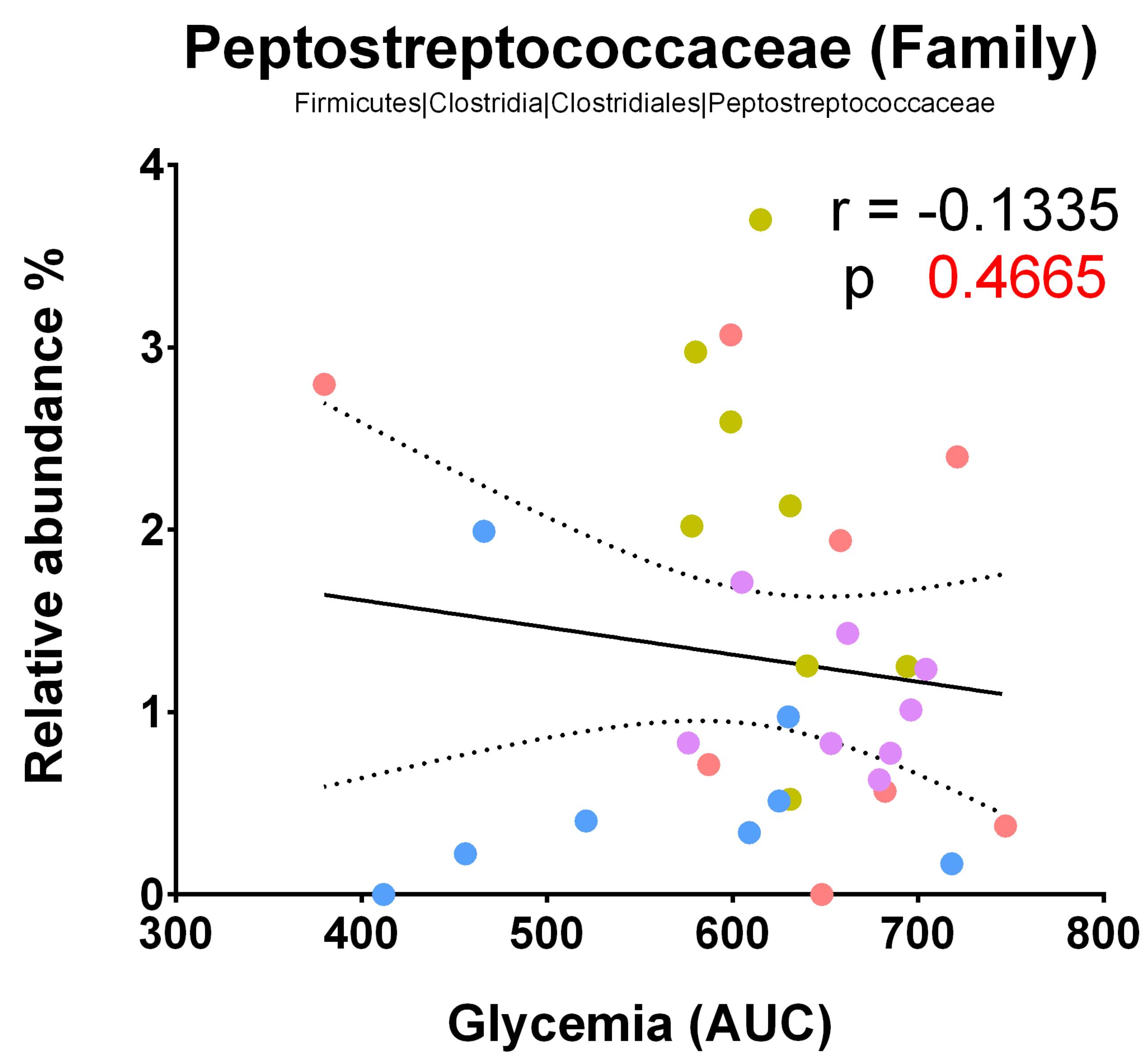


**Figure 3**

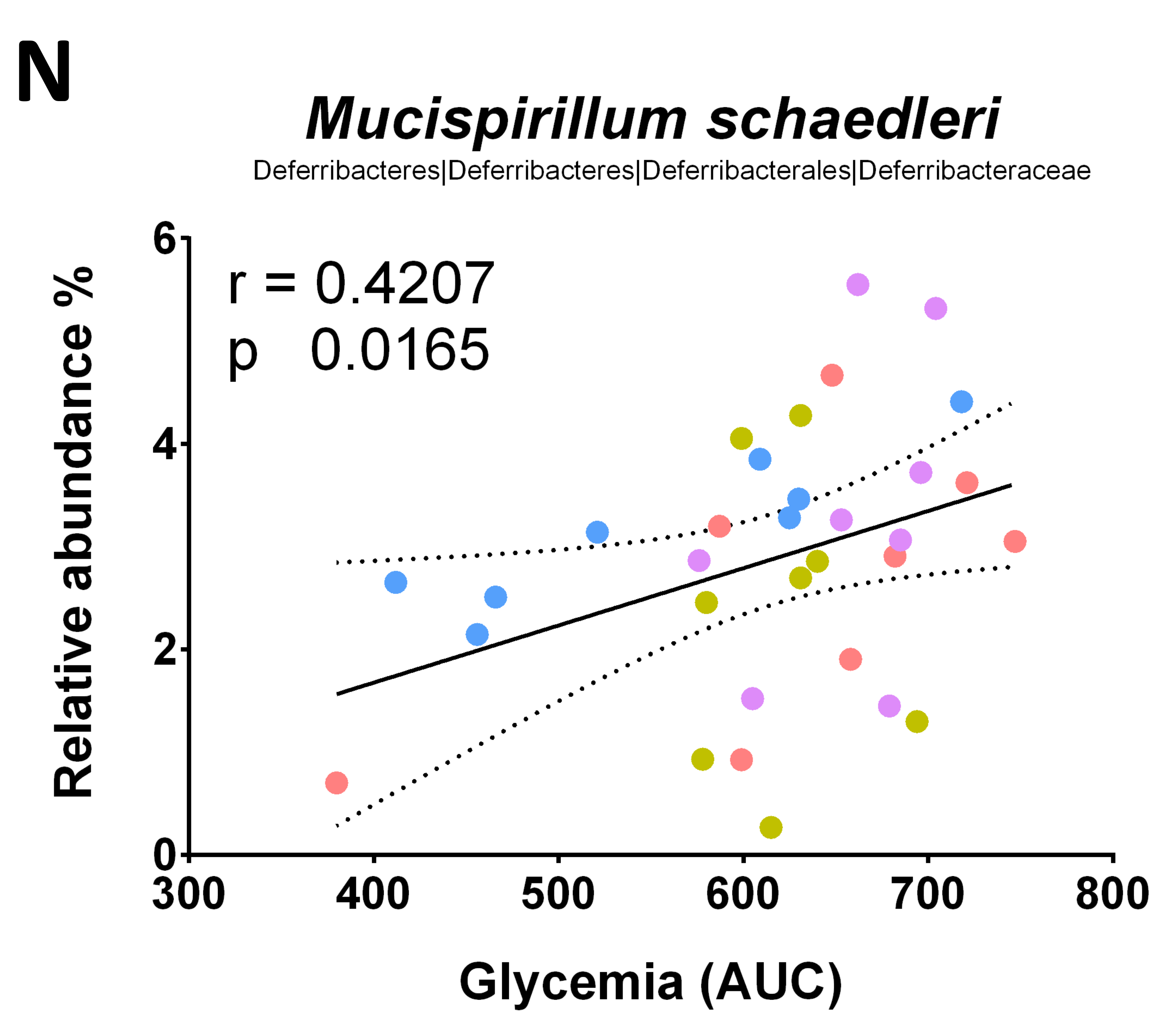
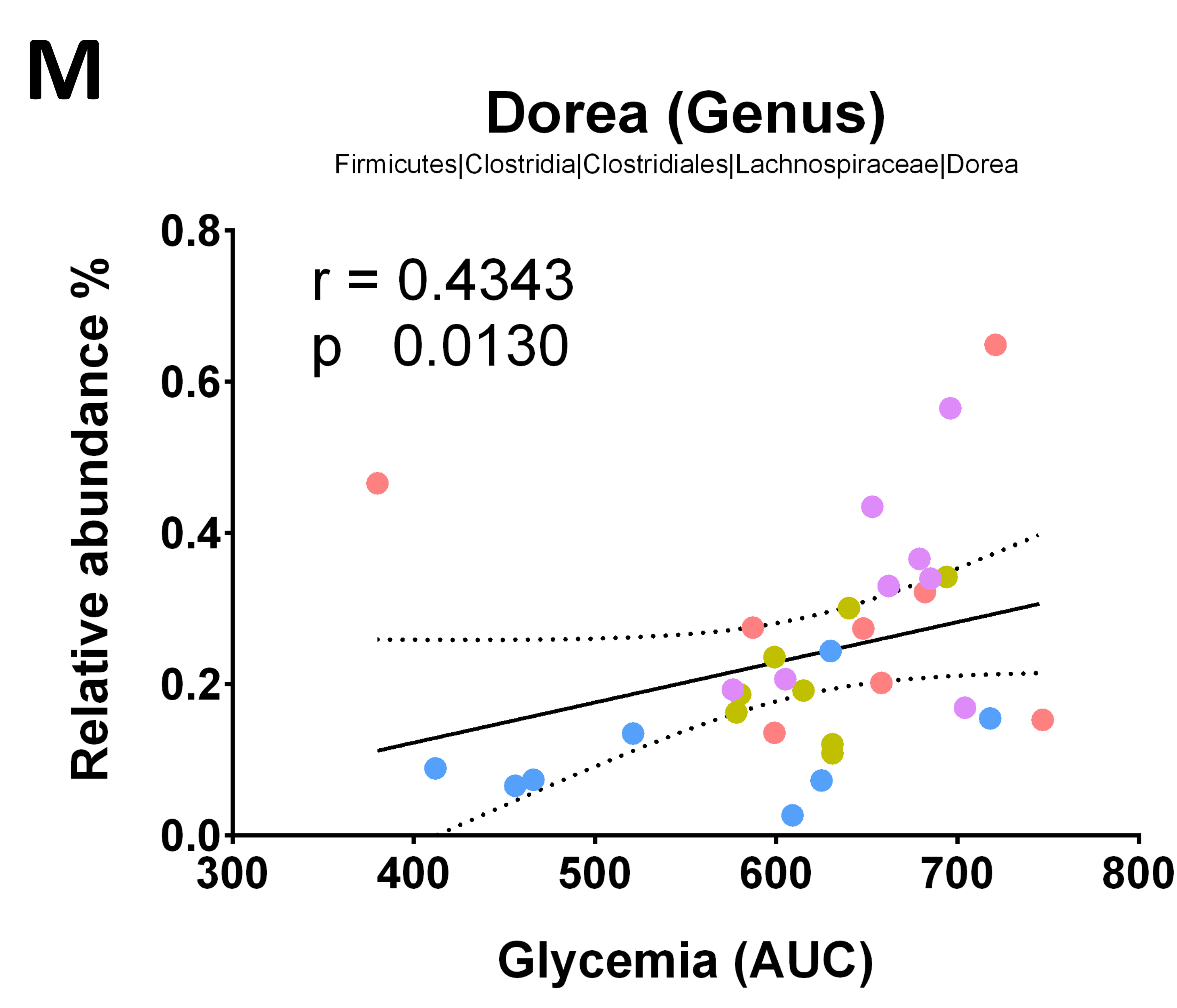
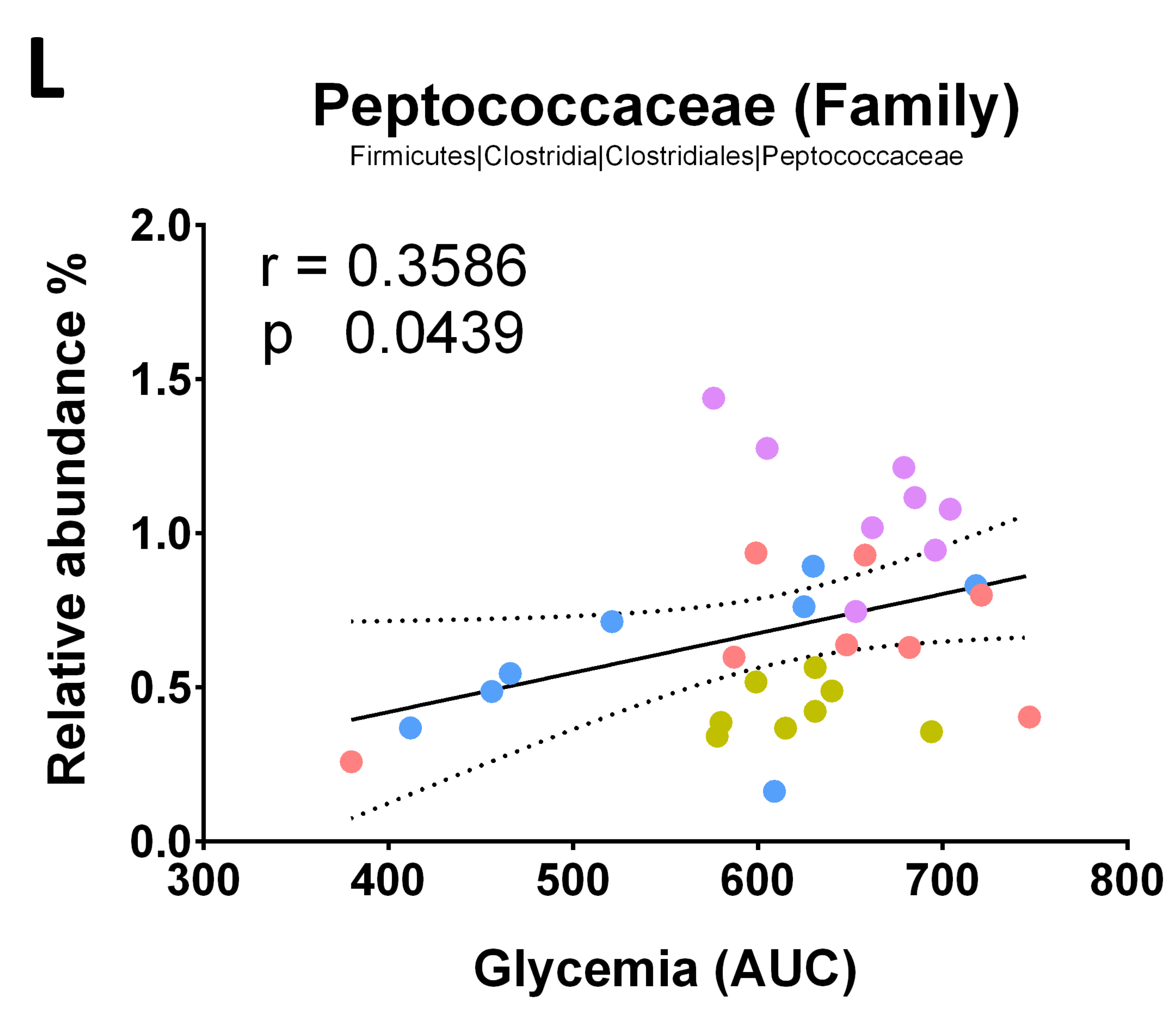
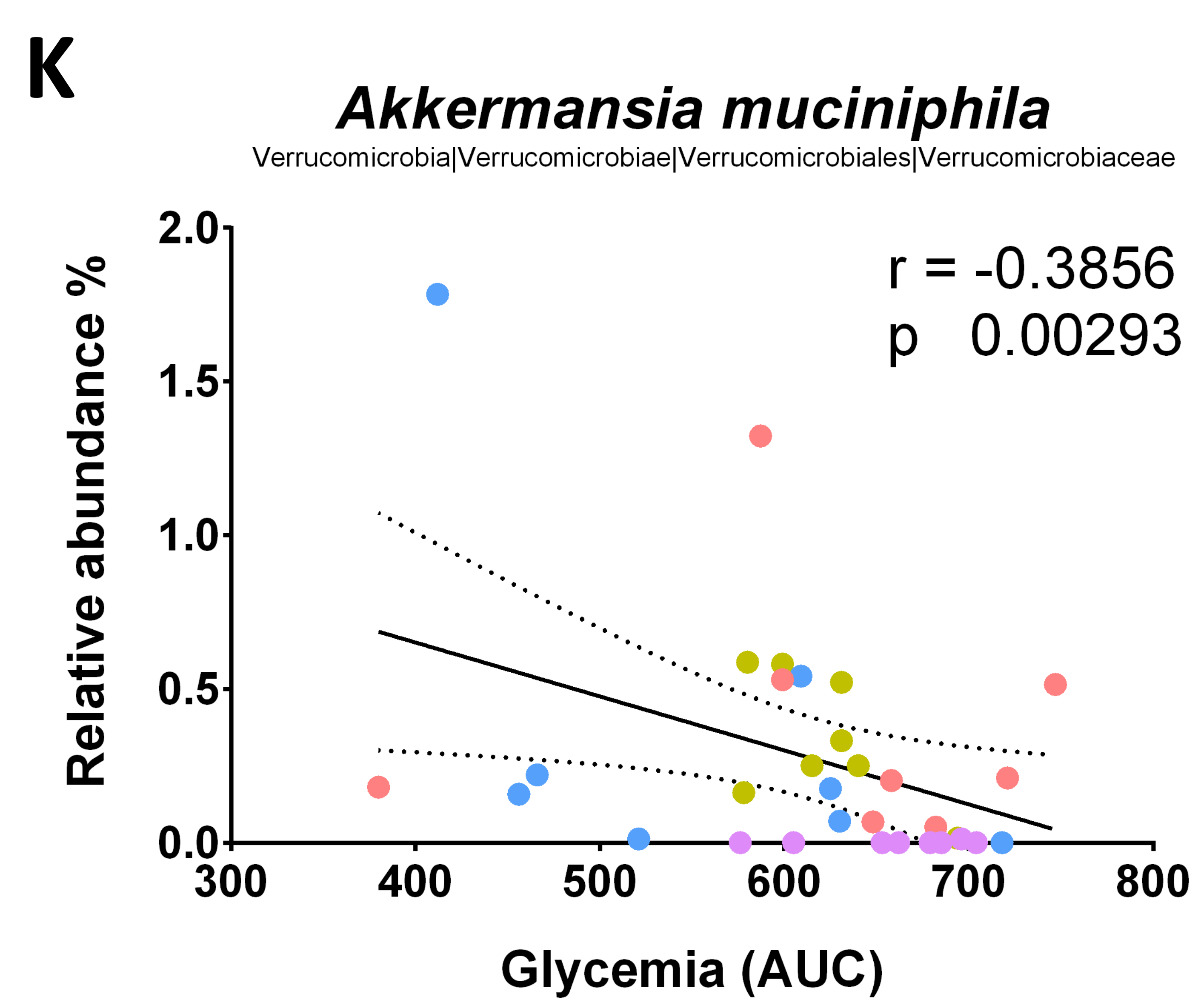
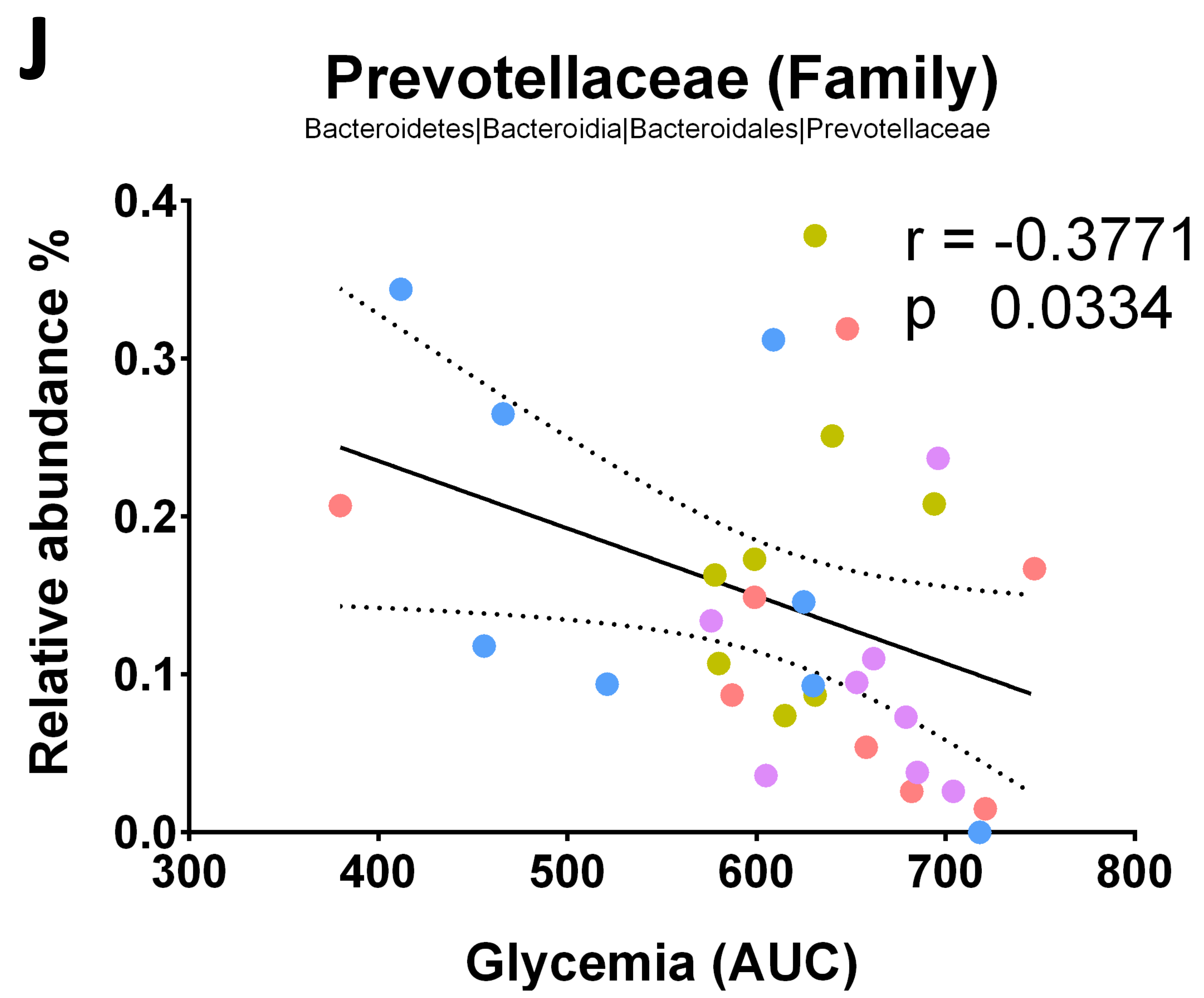
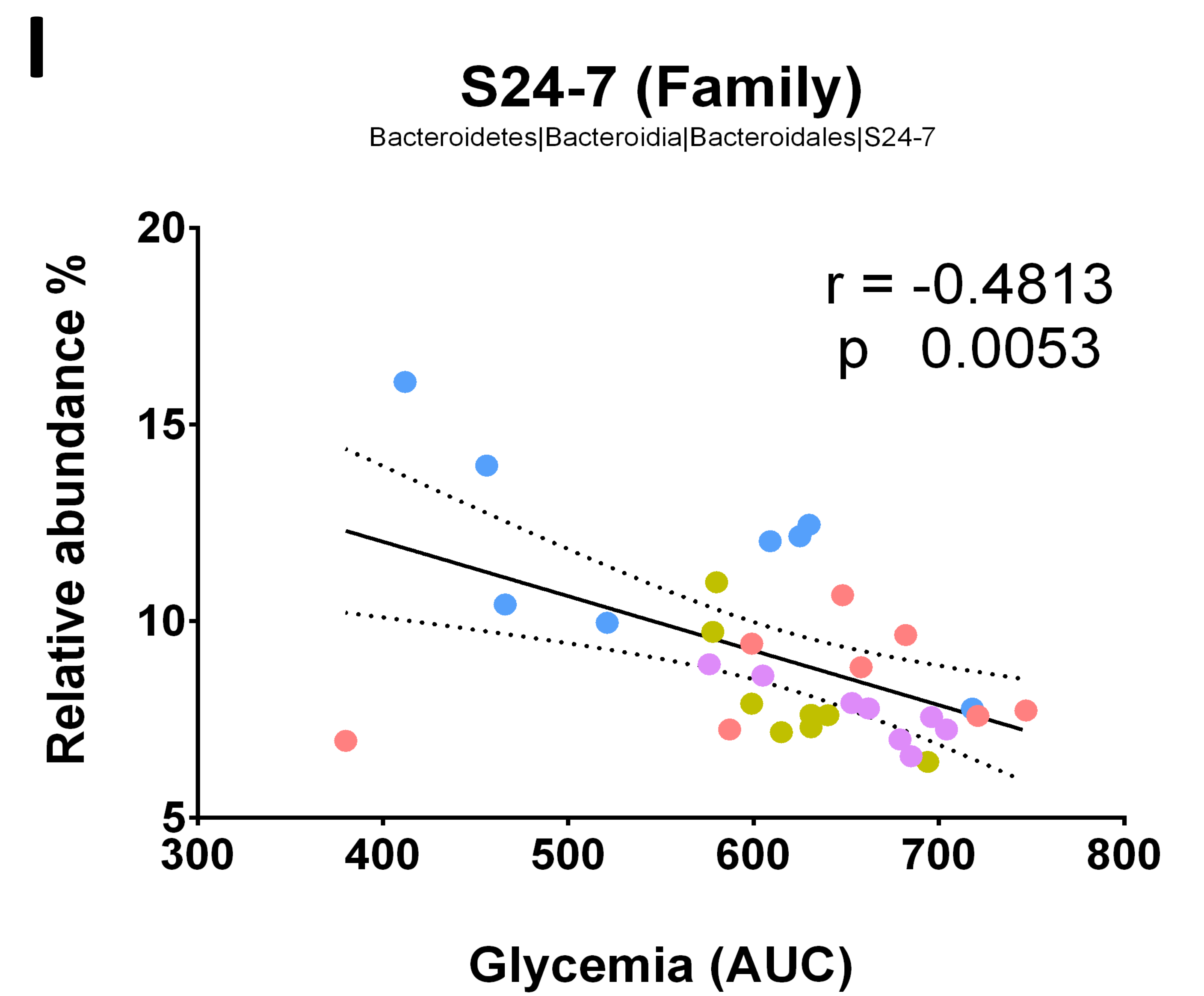


Figure 3

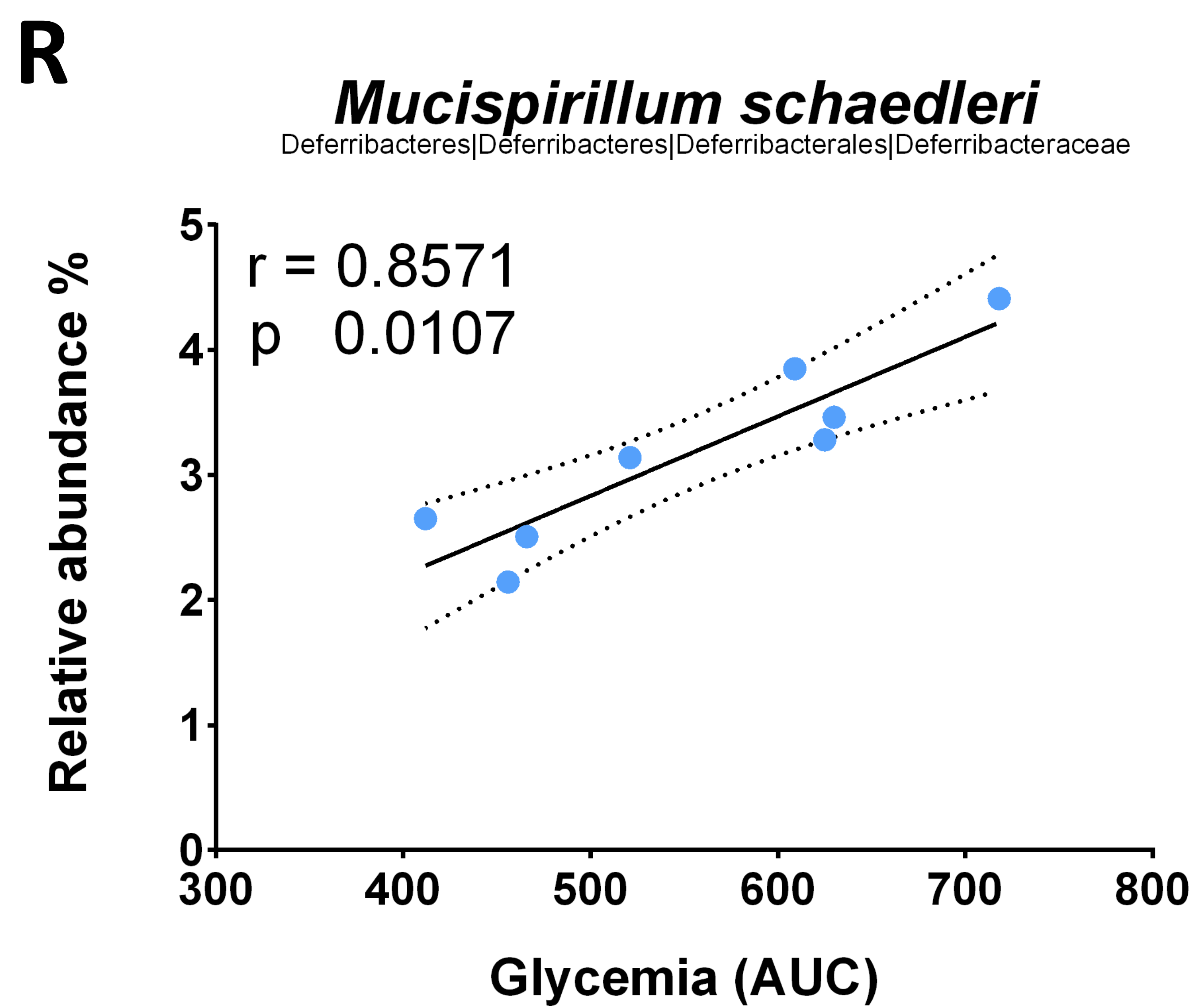
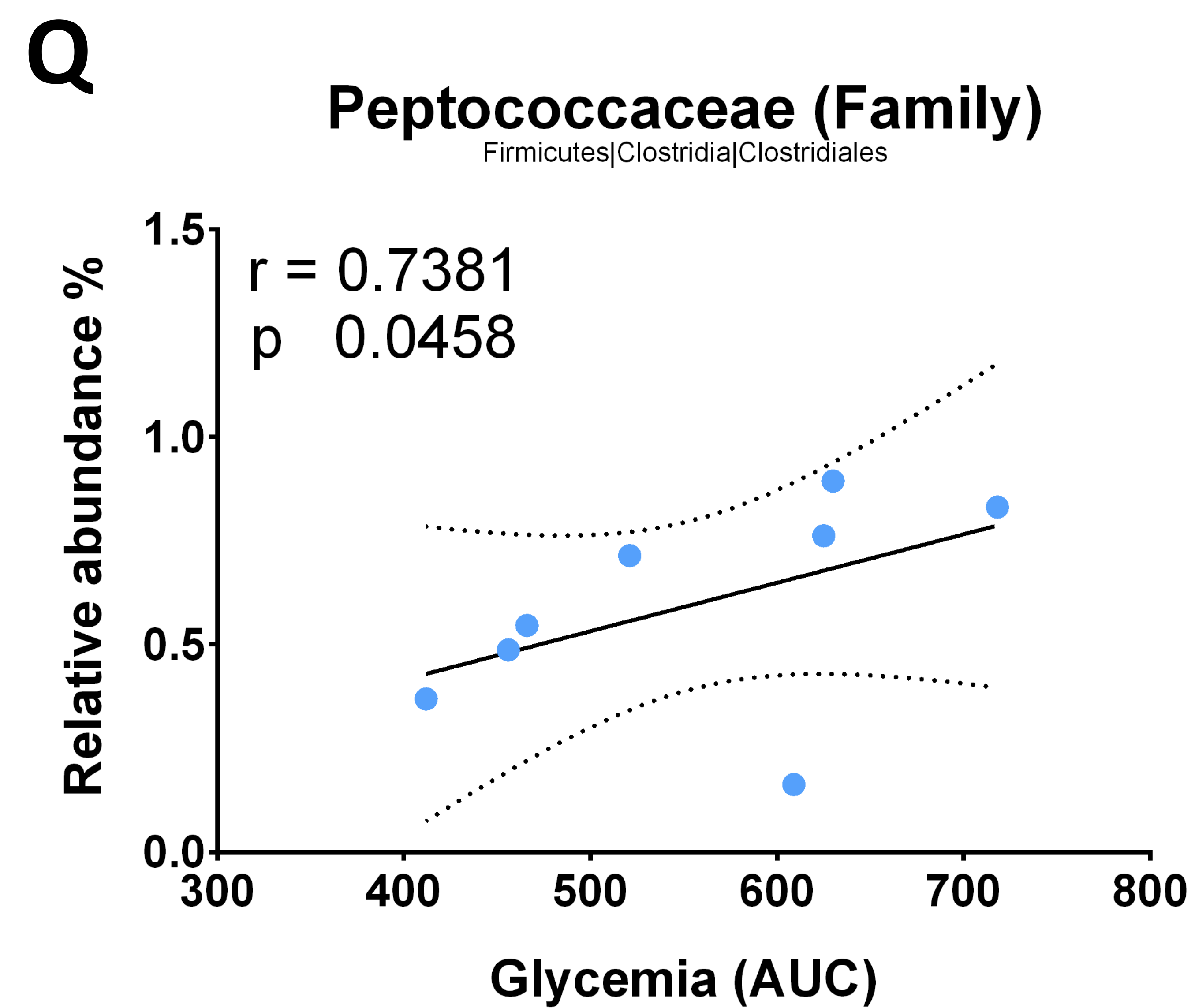
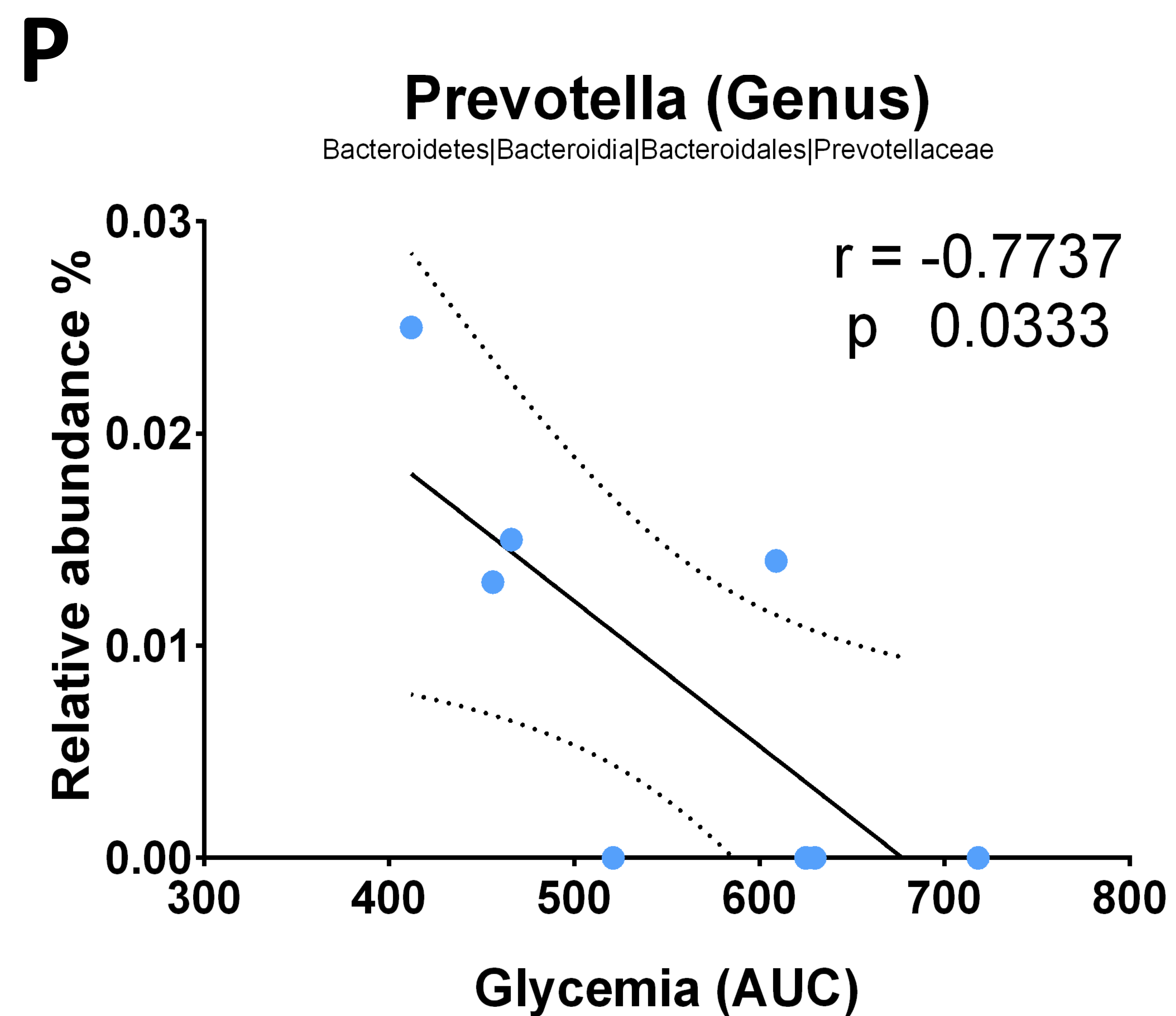
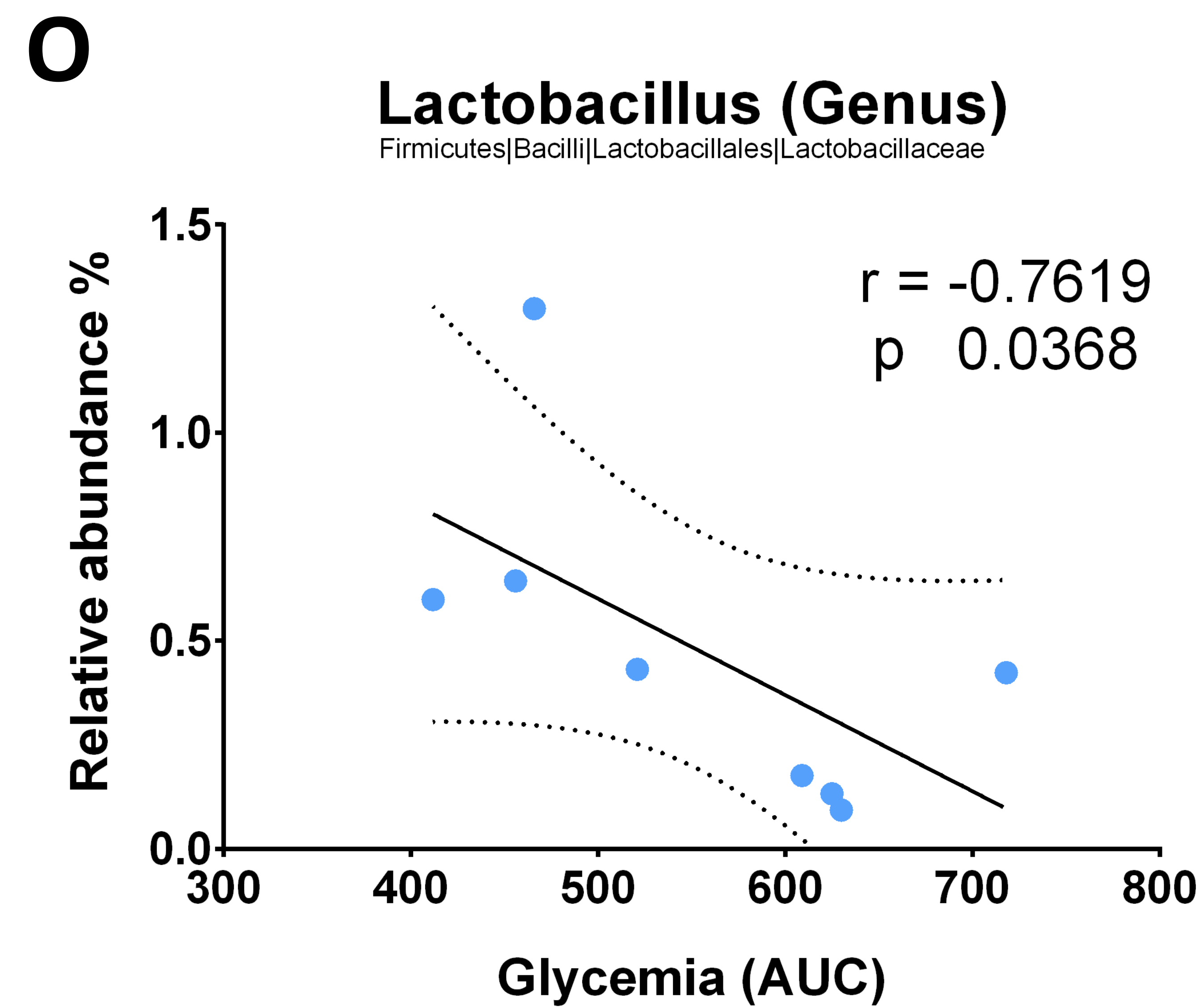
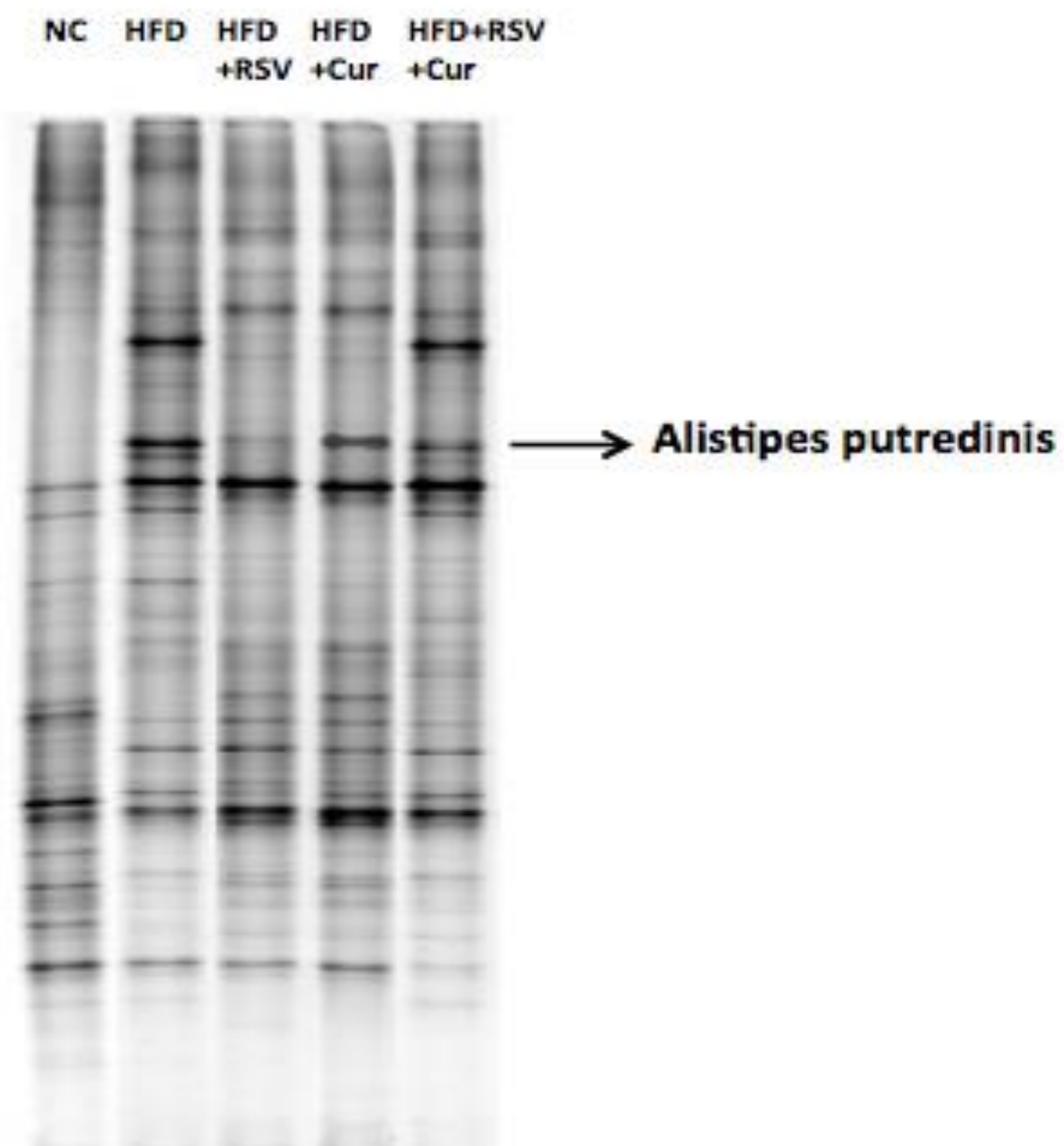
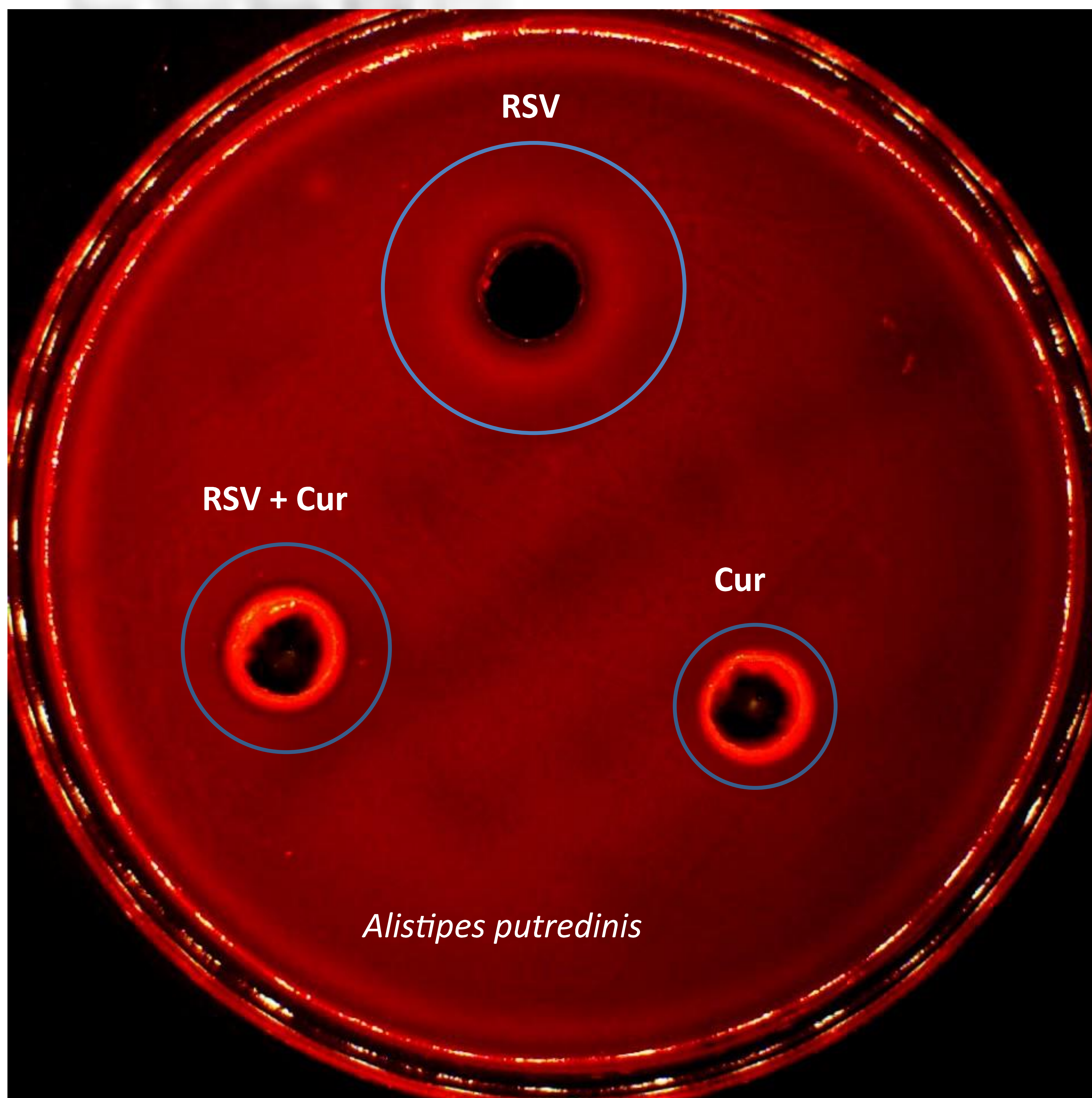


Figure 3

S

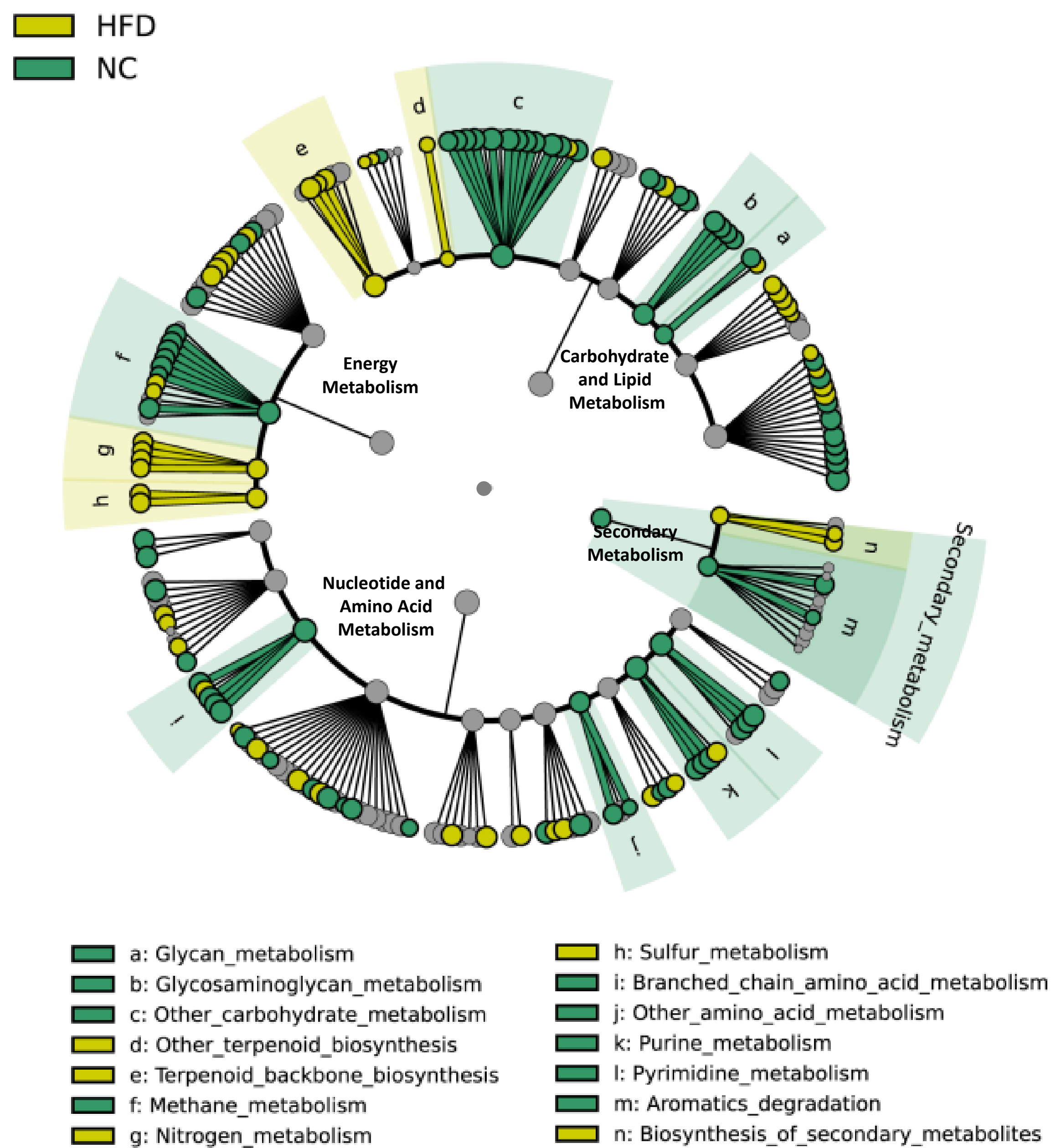


T

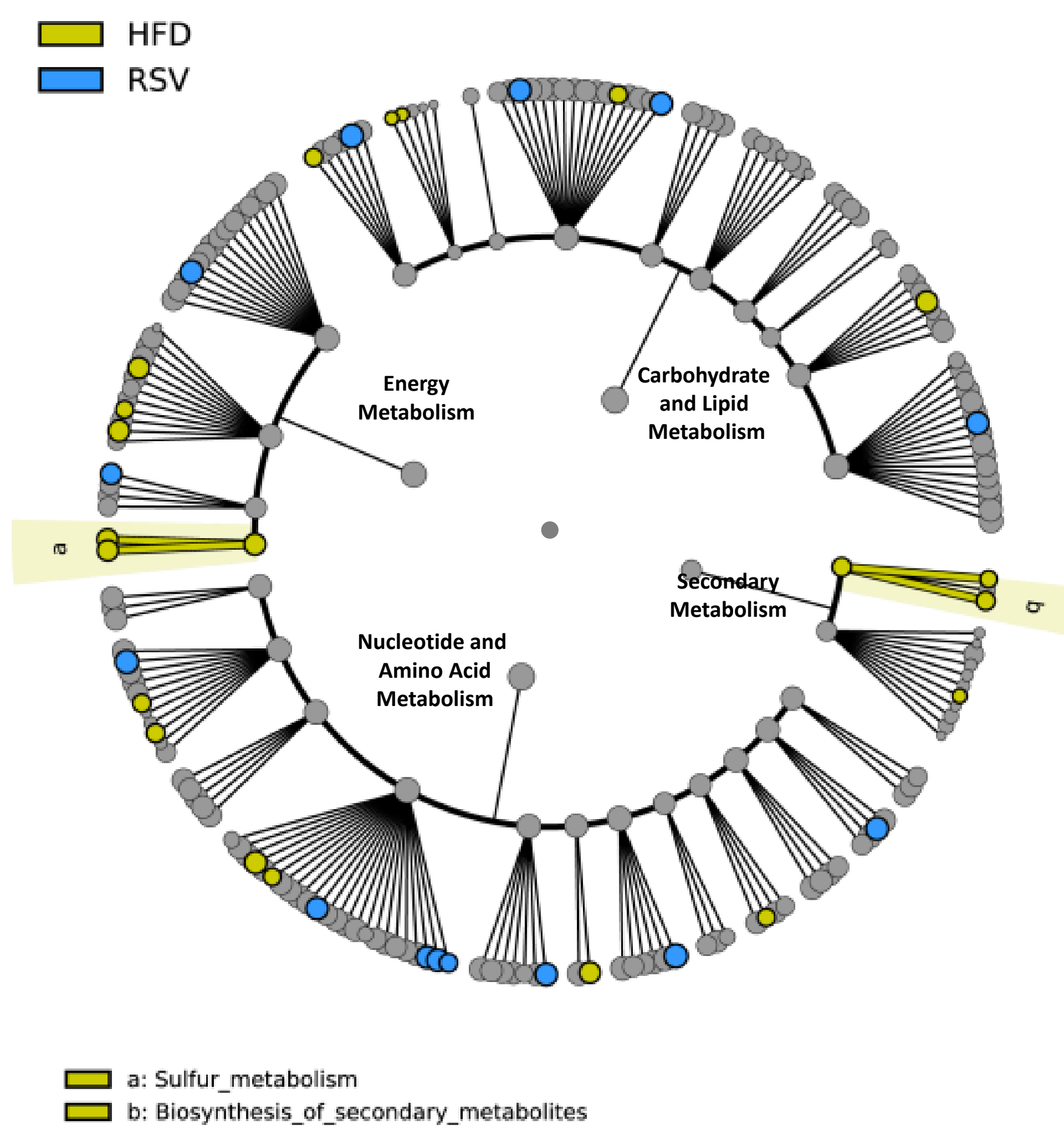


# Figure 4

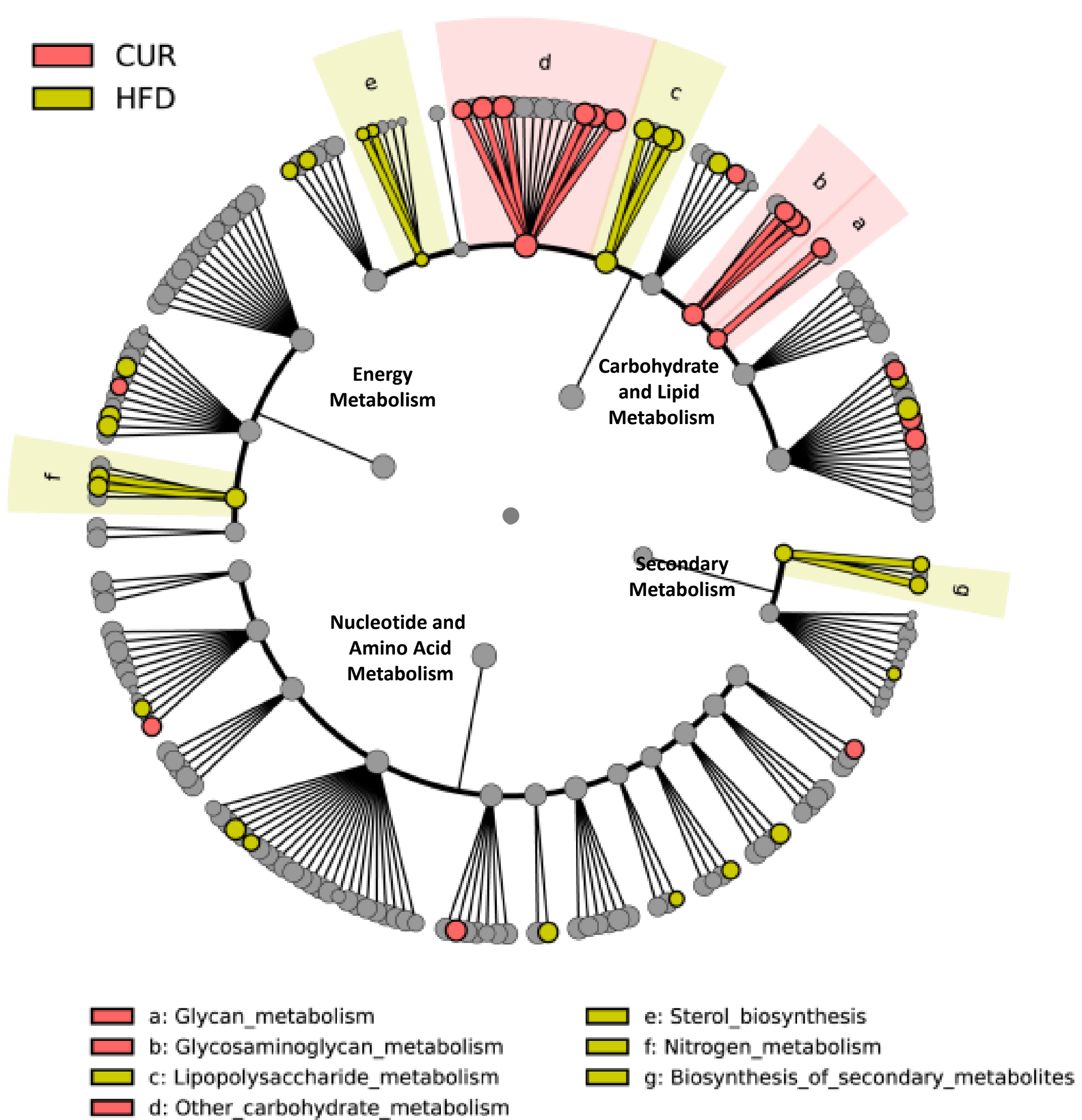
## A



## B



## C



## D

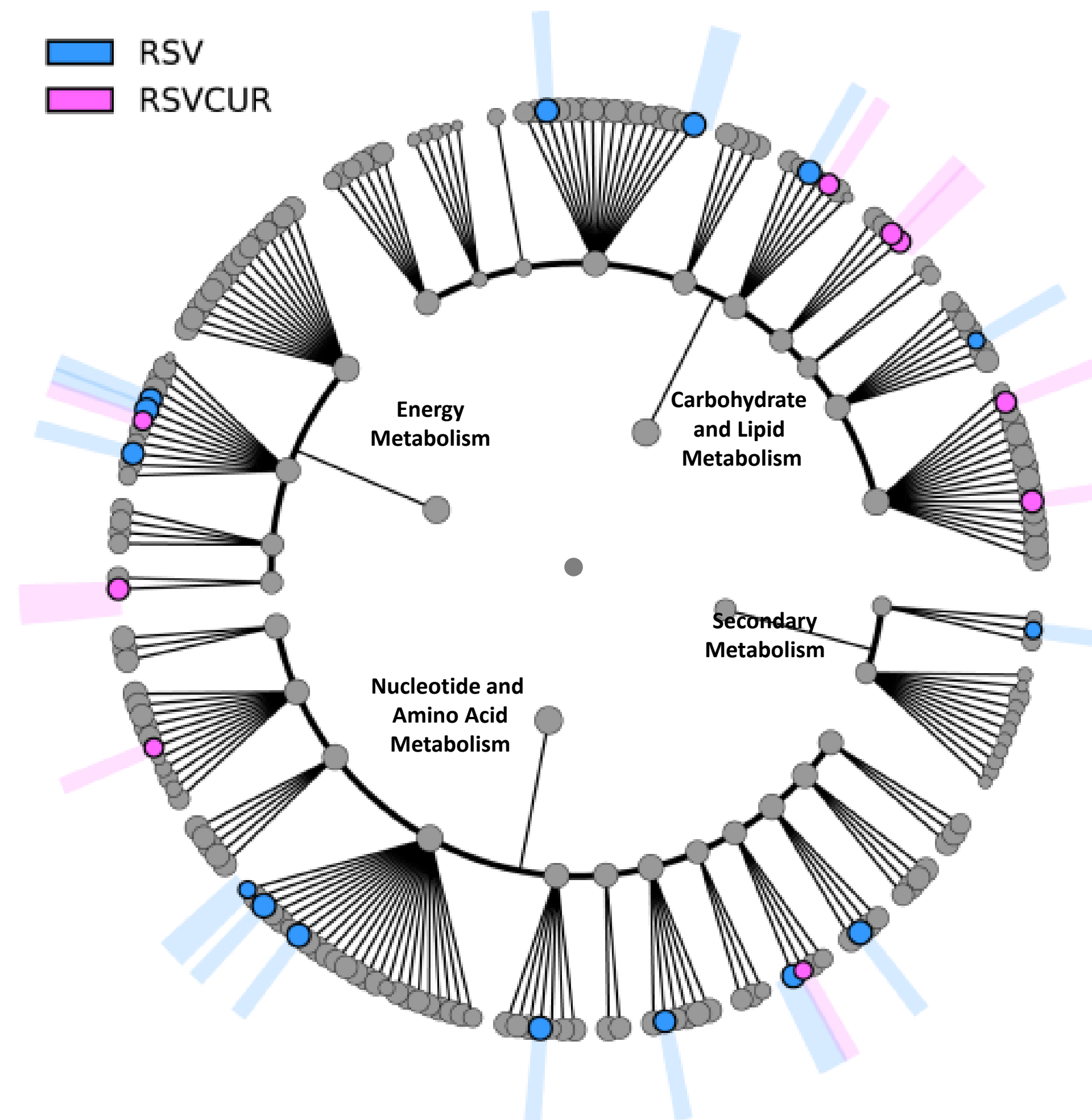
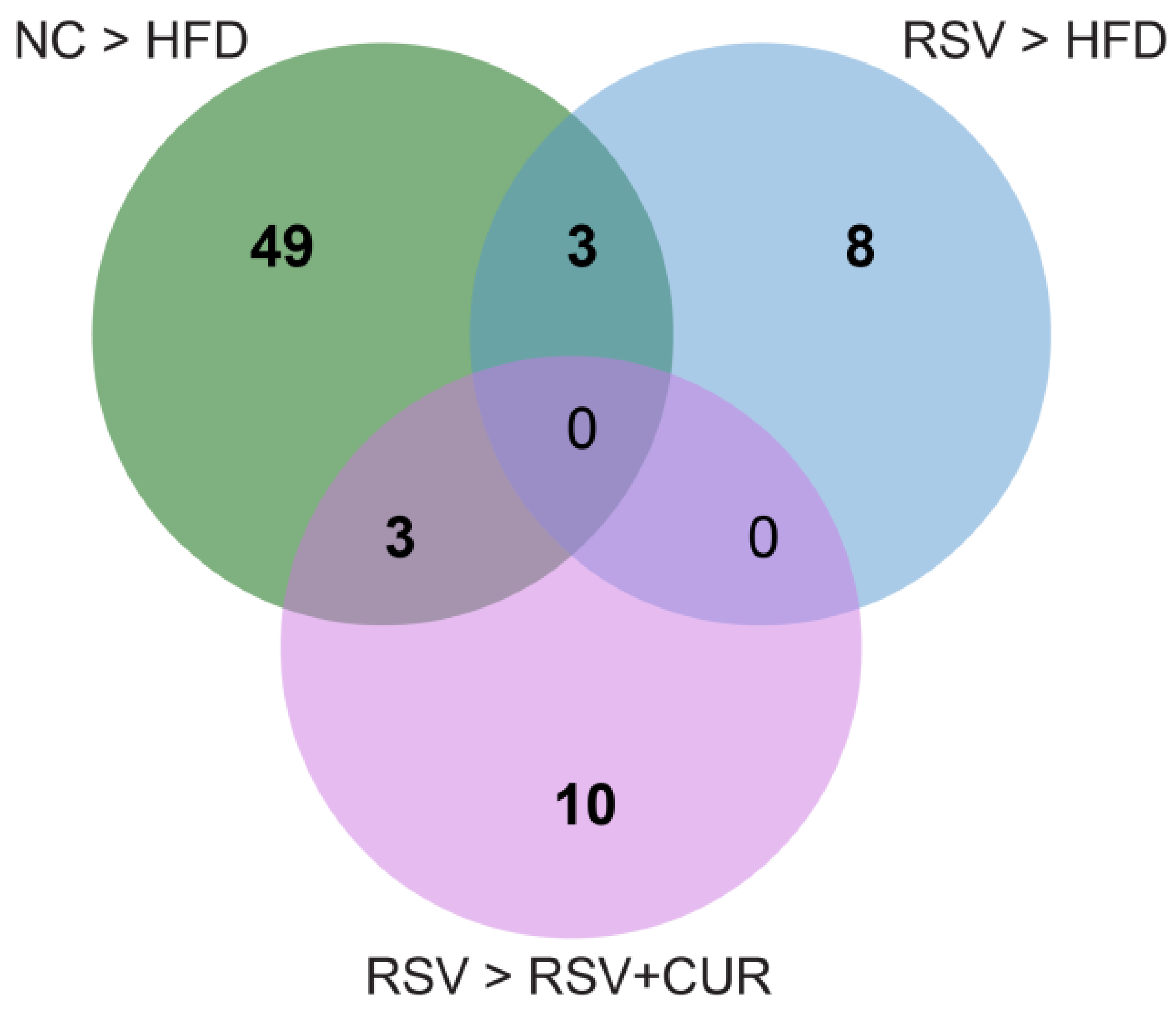
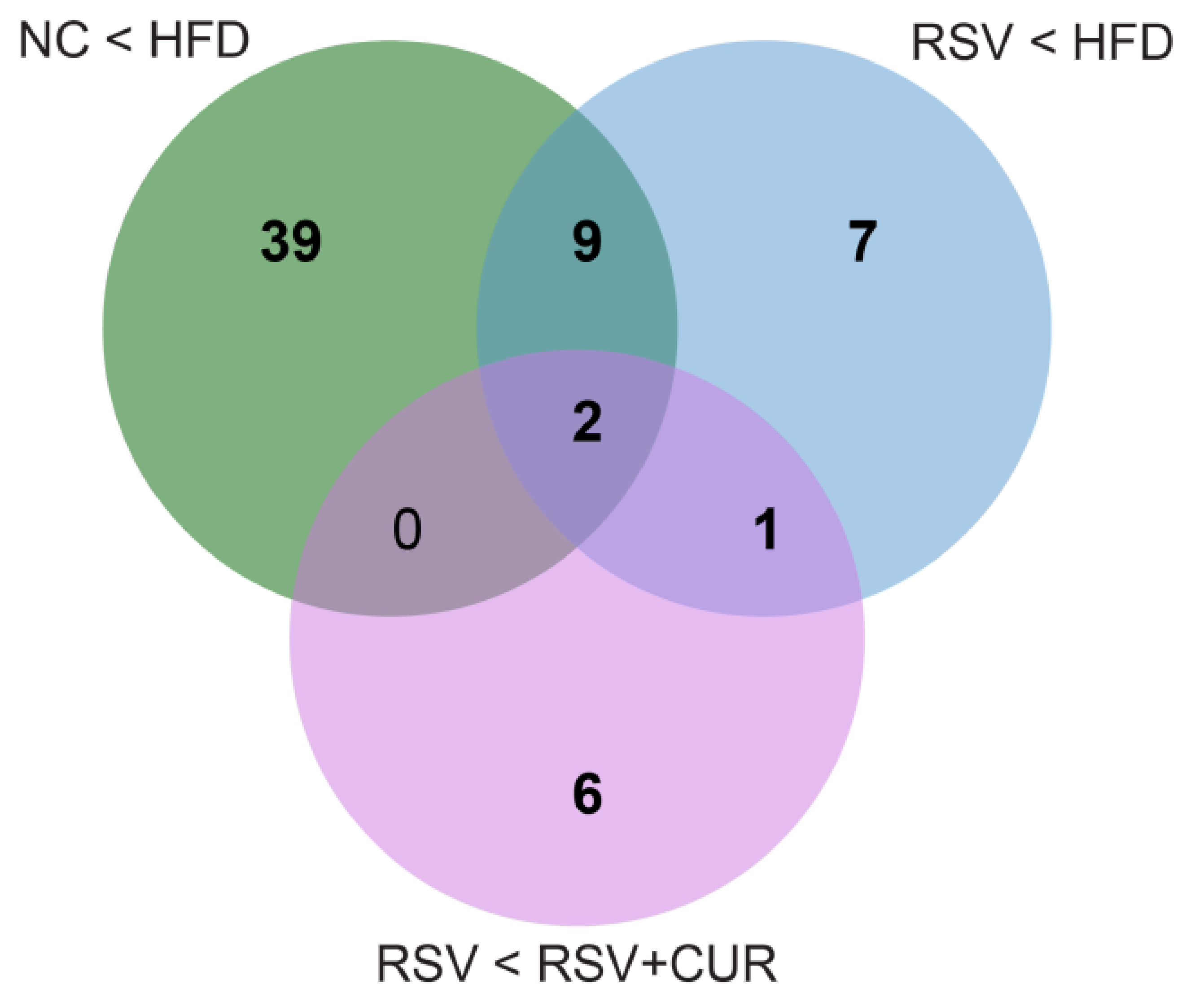


**Figure 4**

**E**



**F**



**G**

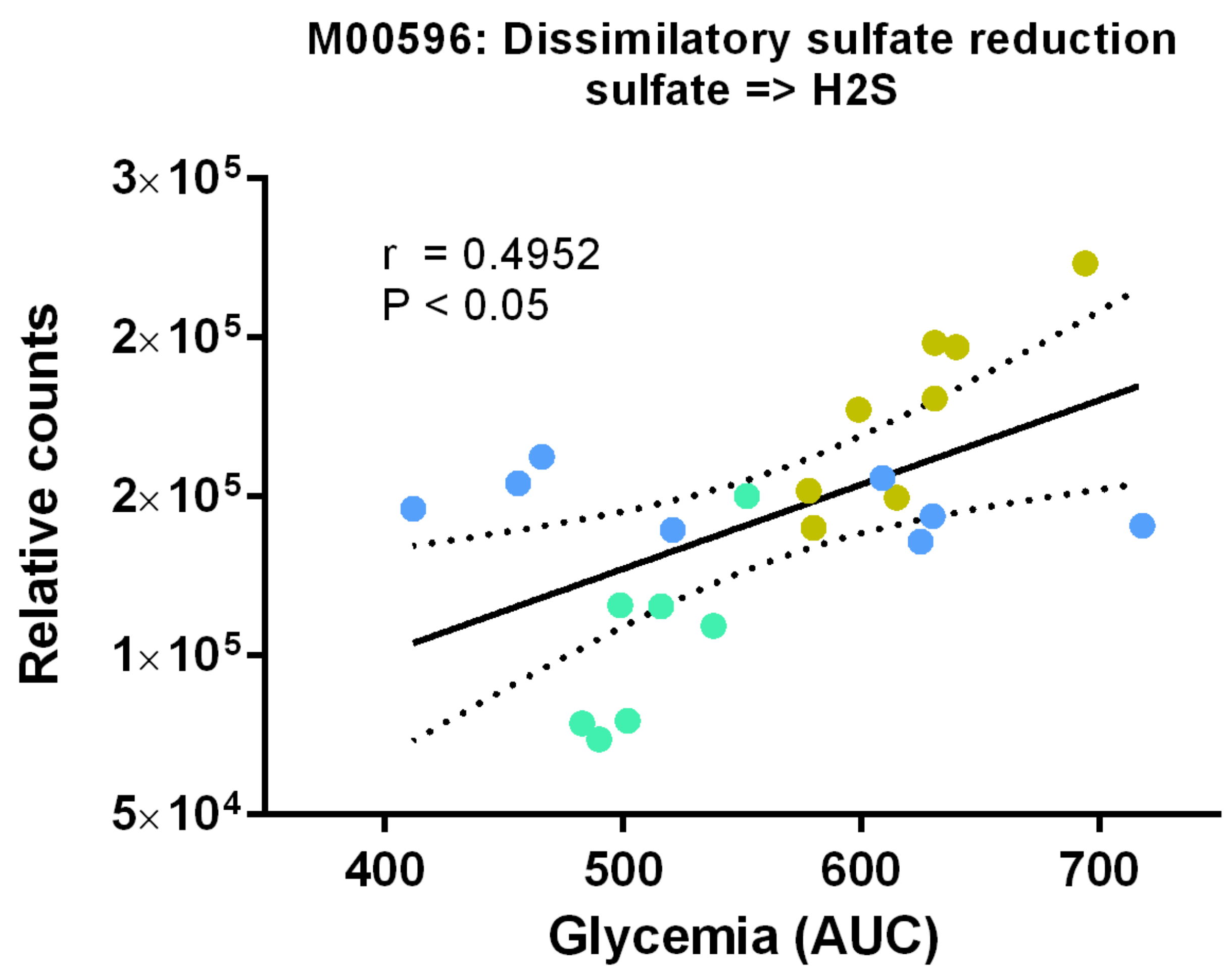
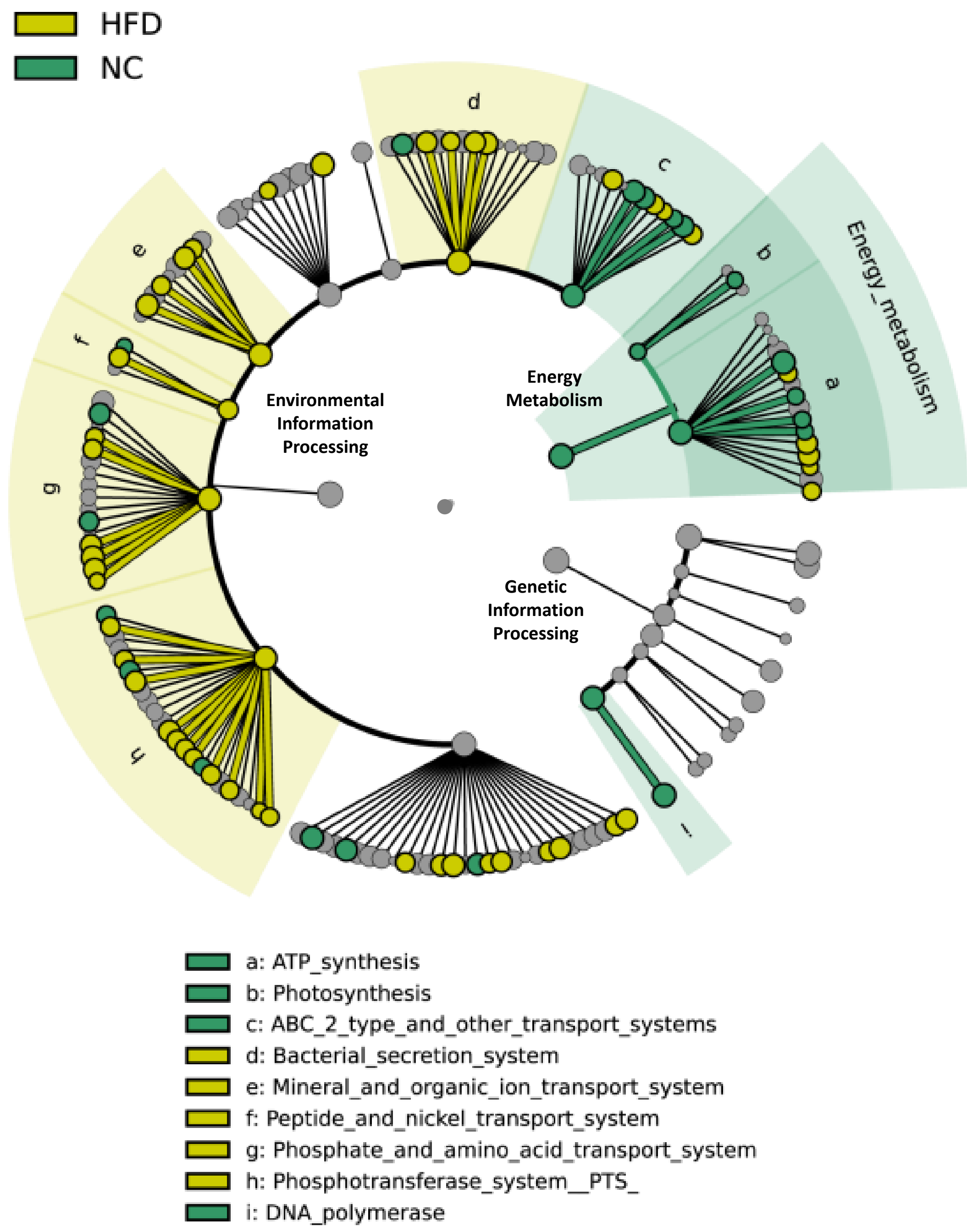
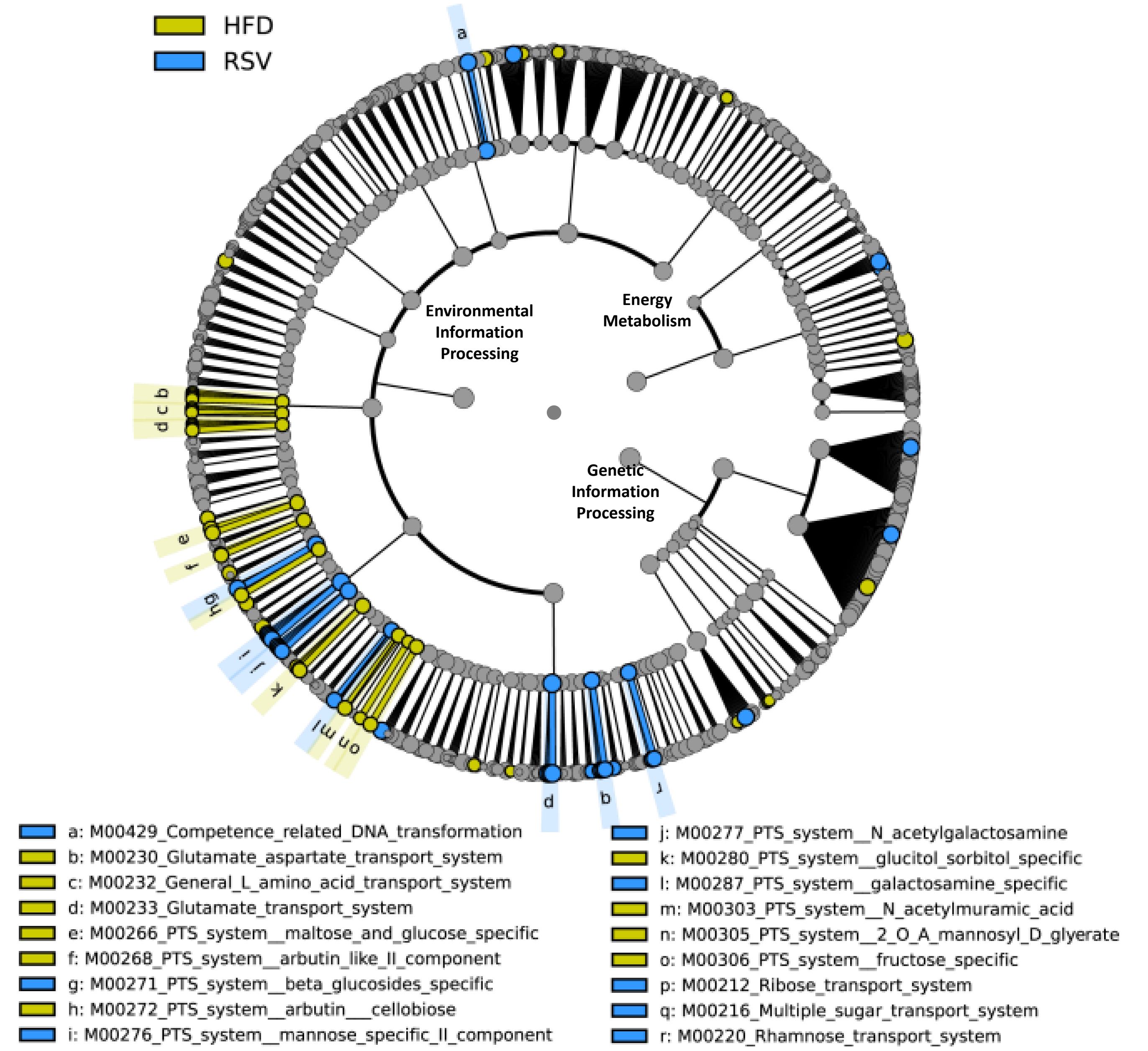


# Figure 5

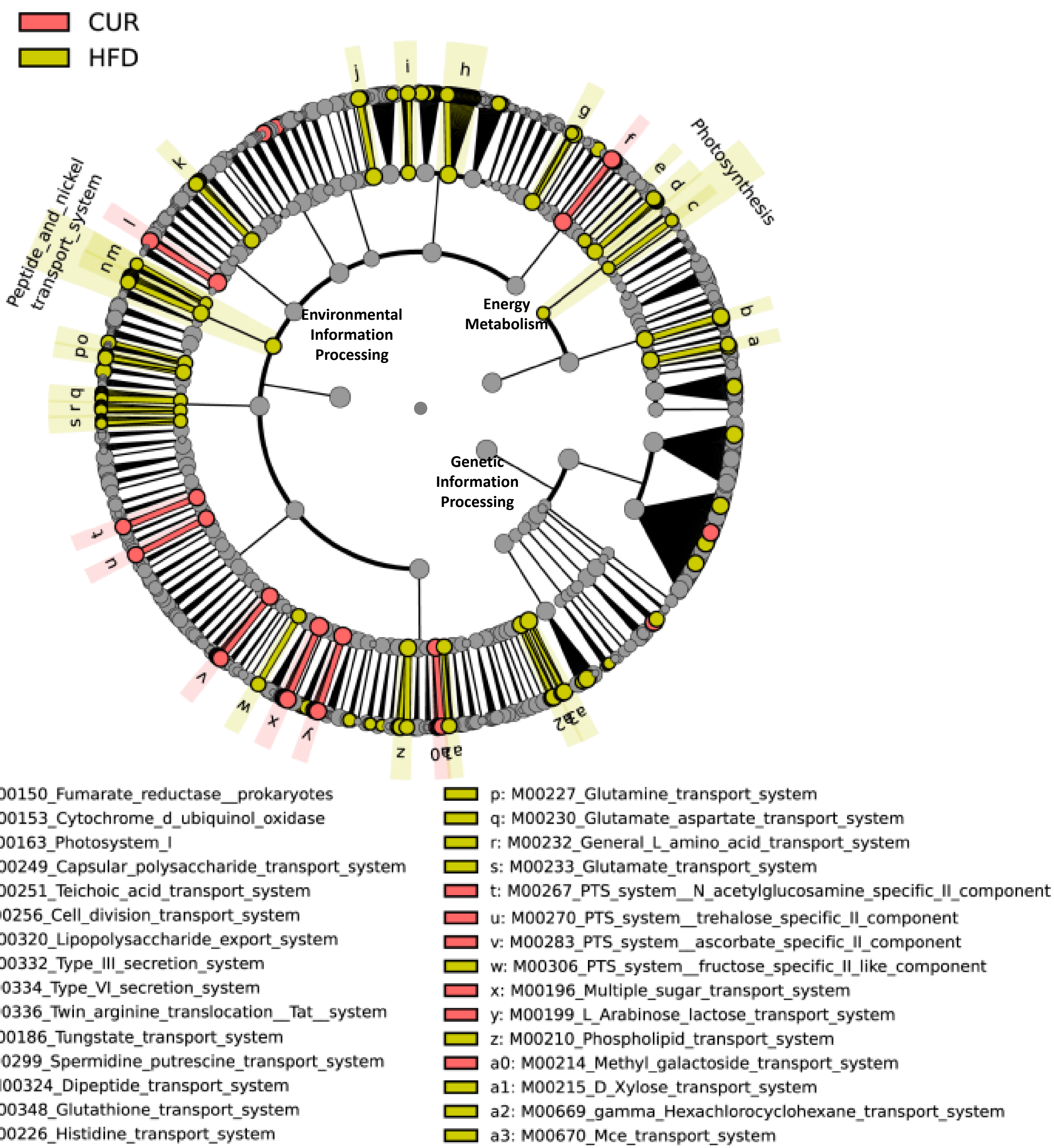
## A



## B



## C



## D

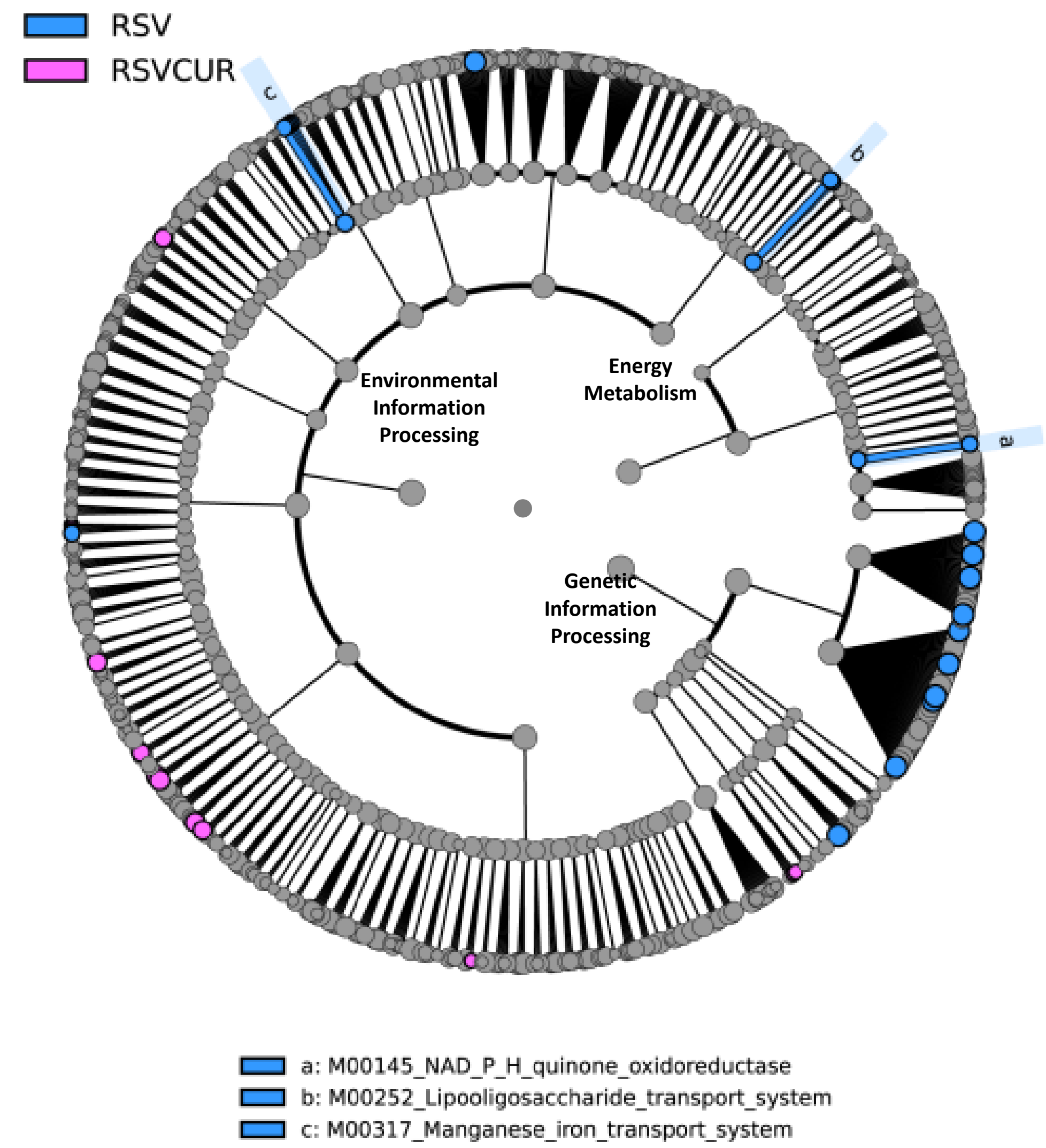
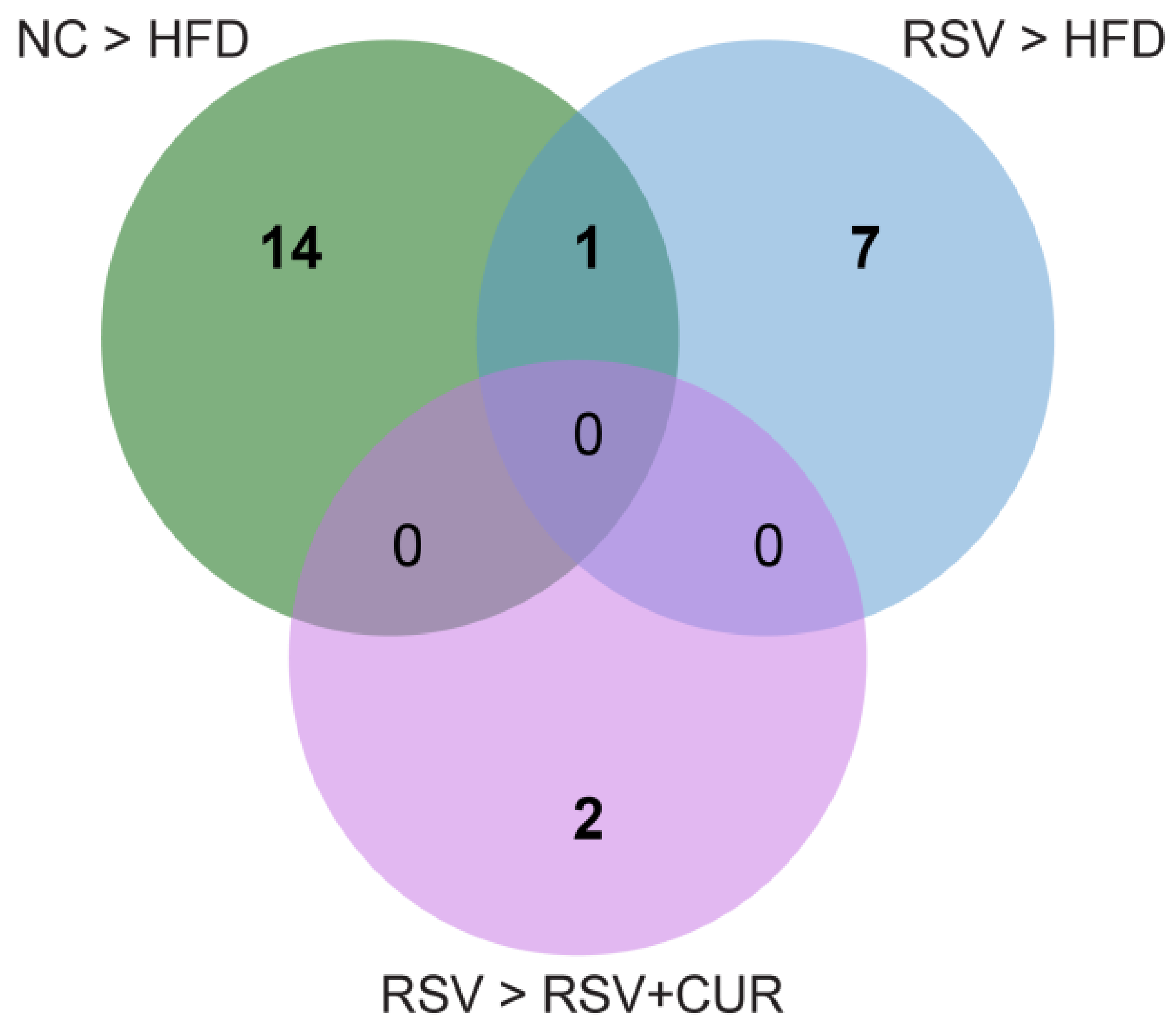


**Figure 5**

**E**



**F**

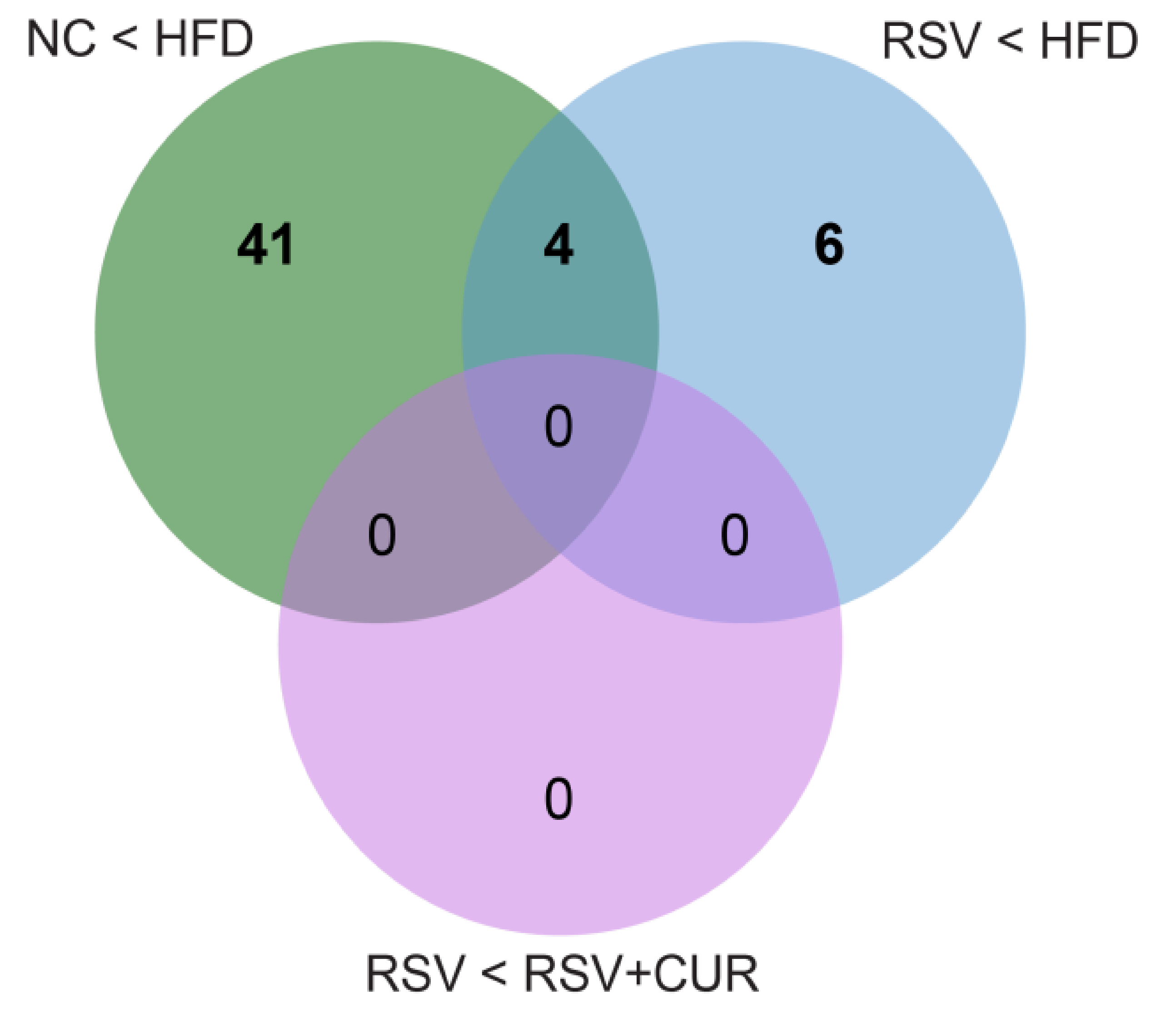
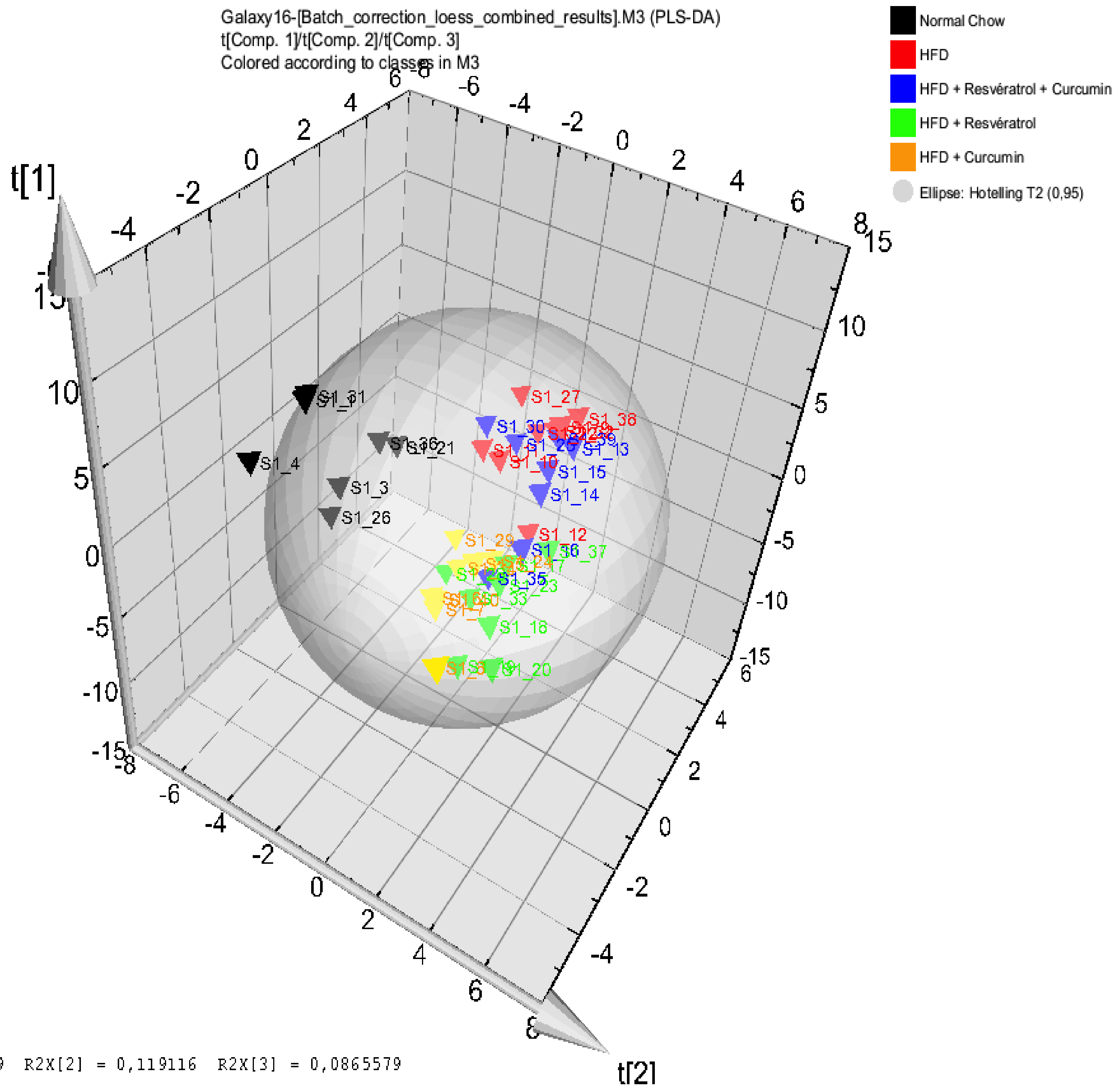


# Figure 6

## A



## B

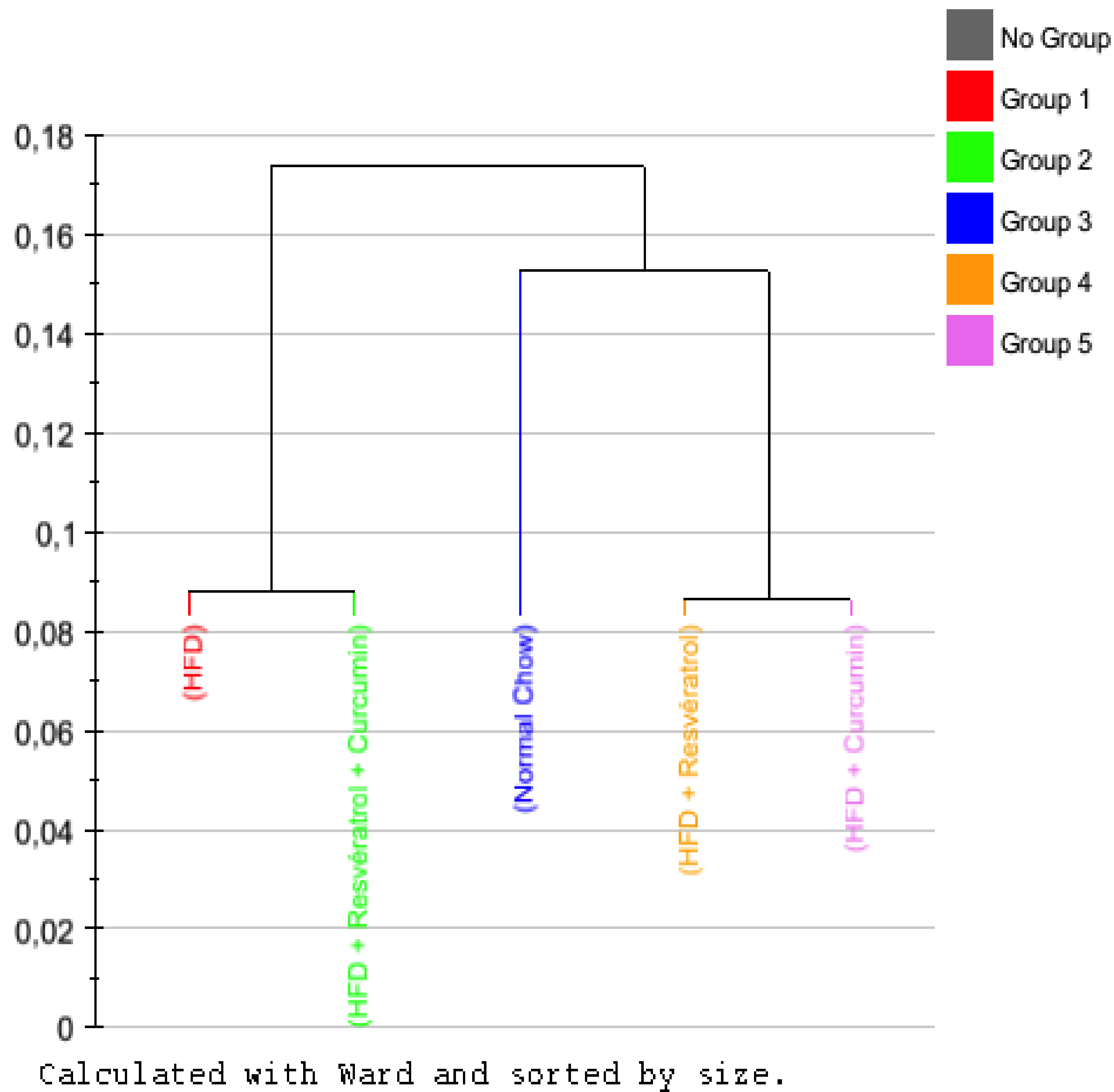
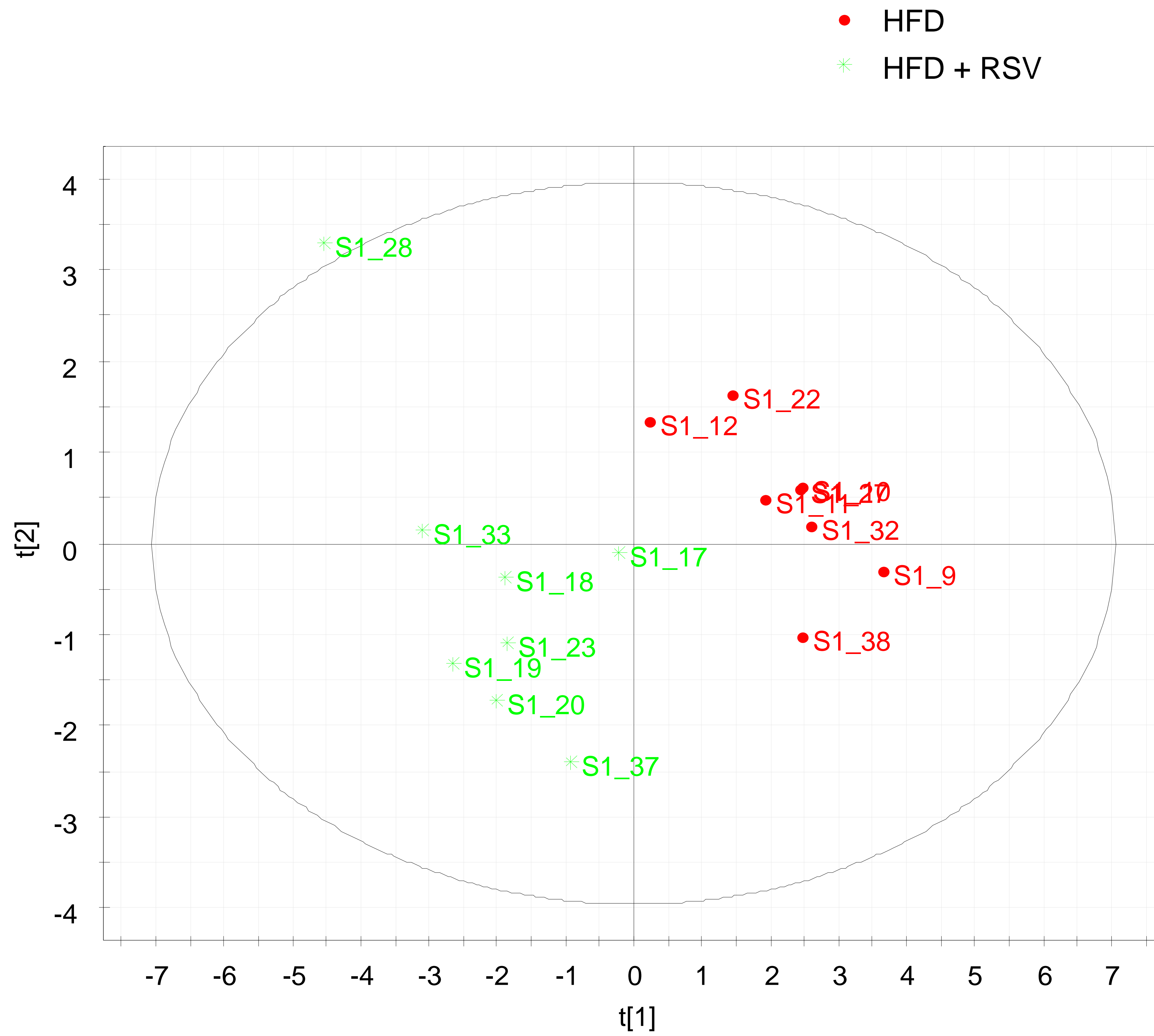


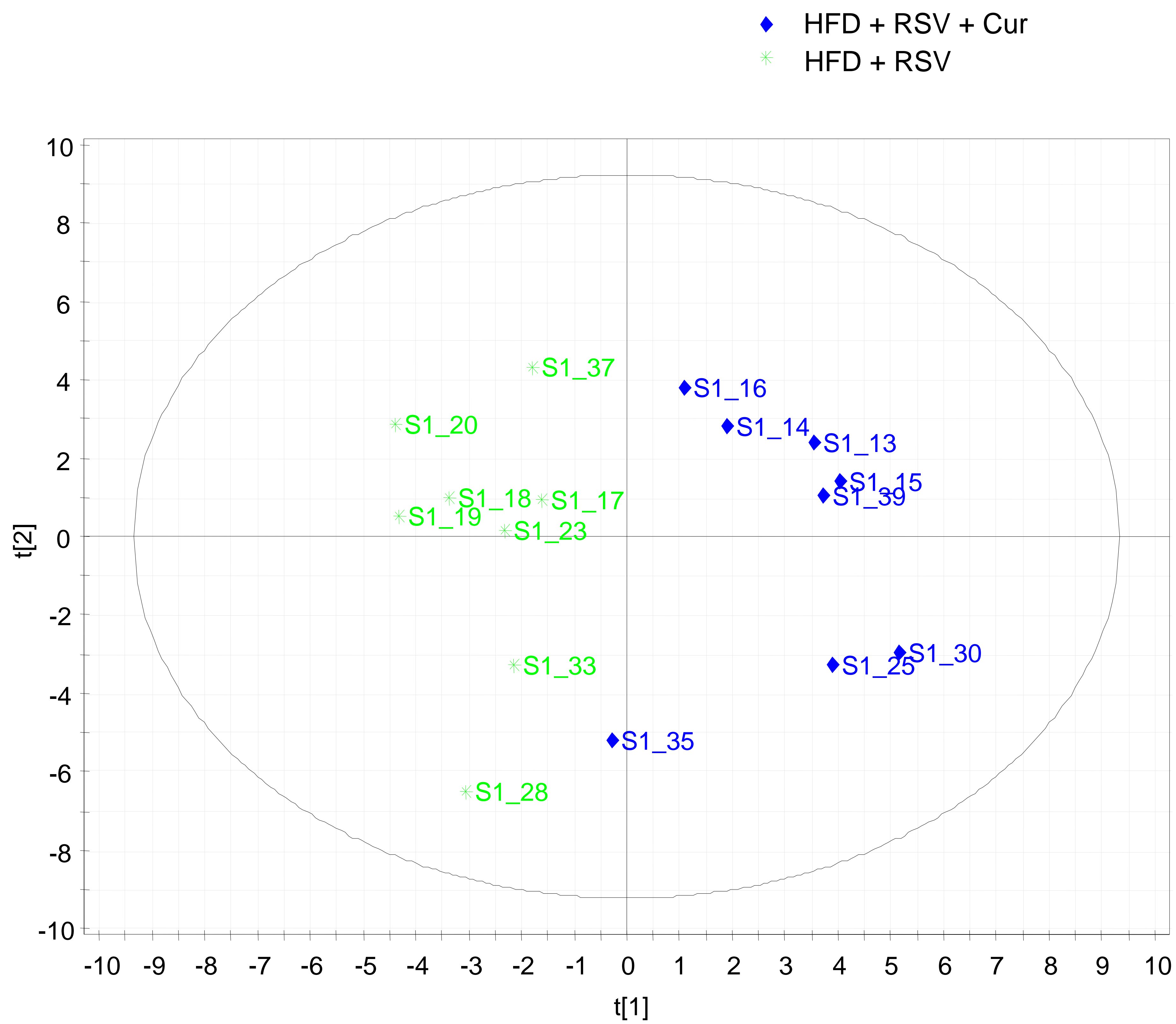
# Figure 6

## C



R2X[1] = 0,541353 R2X[2] = 0,170963 Ellipse: Hotelling T2 (0,95)

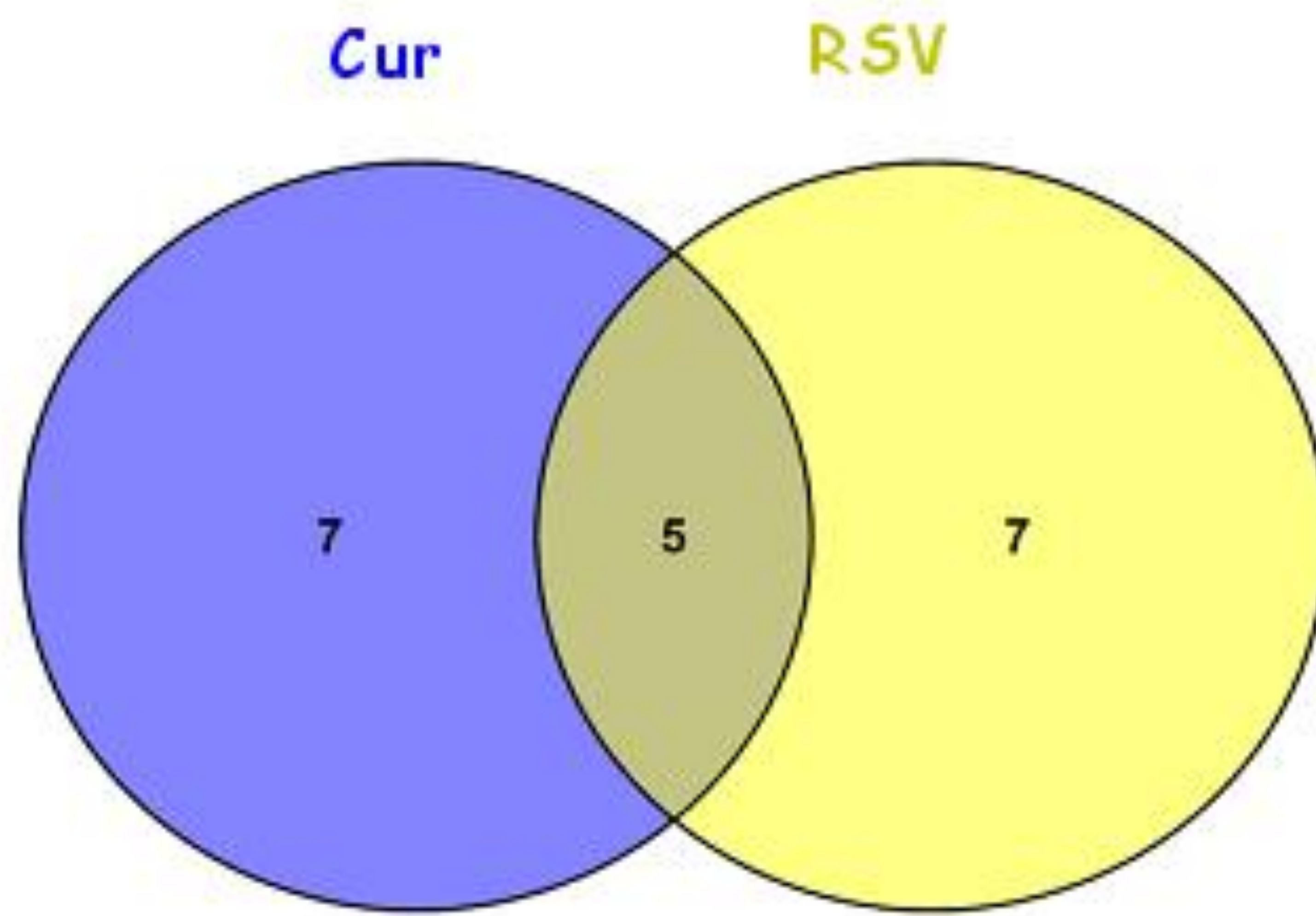
## D



R2X[1] = 0,202656 R2X[2] = 0,337946 Ellipse: Hotelling T2 (0,95)

Figure 6

E



urea (up in C)  
proline (down in C)  
tri-hydroxy-butyric acid (down in C)  
glucuronic acid (up in C)  
cholesterol (down in C)

acetic acid (up in R and C)  
butanoic acid (up in R and C)  
serine (down in R and C)  
gluconic or butanedioic acid (down in R and C)

isoleucine (up in R)  
glucose (down in R)  
glucitol (down in R)